UNIVERSITY OF TWENTE.

Sediment transport under irregular waves

CEM MSc. Thesis

Institute:
University of Twente, Enschede
Faculty of Engineering Technology
Water Engineering and Management

Date:
November 12, 2013

Author:
S.S. Helmendach BSc

Supervisors:

Dr. Ir. J.S.	(Jan)	Ribberink	(University of Twente)
Dr. Ir. W.M.	(Wouter)	Kranenburg	(University of Twente)
Dr. Ir. J.J.	(Jebbe)	Van der Werf	(Deltares & University of Twente)

Colophon

Title:	Sediment transport under irregular waves
Description:	Thesis for the degree of Master in Science in Civil Engineering and Management
Author:	S.S. Helmendach BSc
Institute:	University of Twente
Faculty:	Faculty of Engineering Technology
Departement:	Water Engineering and Management
Supervisors:	Dr. ir. J.S. (Jan) Ribberink University of Twente Departement of Water Engineering and Management
	Dr. ir. W.M. (Wouter) Kranenburg University of Twente Departement of Water Engineering and Management
	Dr. ir. J.J. (Jebbe) Van der Werf Deltares and University of Twente Departement of Water Engineering and Management
Date:	November 12, 2013

Cover photo: "Irregular waves approaching coast",
S.S. Helmendach at Koh Phi Phi, Thailand, 2012

Summary

There is an increasing desire to understand and successfully model nearshore processes, especially in the nearshore zone where many different hydrodynamic and sediment transport processes take place. Different wave conditions and bed shapes for example can cause sediment to move at the bottom, the place where the largest sediment transport often occurs (Malarkey & Davies, 2012). In order to simulate and gain knowledge, about the processes that occur in the nearshore area, mainly regular, sinusoidal, waves have been used for experiments and irregular, realistic, waves have been left aside. This study is focused on the improvement of the knowledge of these irregular waves. Therefore, the main objective of this research is: *to increase the understanding of the nearshore sediment transport processes occurring under irregular non-breaking wave conditions, with the use of the boundary layer model.* To obtain a better understanding of the irregularity processes and its effects on sediment transport, a regular wave that represents an irregular wave would be easier to implement in existing morphological models that simulate sediment transport. Therefore, the second objective of this research is: *to develop, or to approach, a representative regular wave for an irregular wave signal.*

An analysis on regular wave knowledge of today showed that hydrodynamic processes, such as wave propagation and orbital motions, could cause and have influences on the streaming (progressive- and wave shape streaming) near the seabed, in the boundary layer. The processes also contribute to friction and bed shear stresses at the seabed, causing sediment to move and be brought into suspension. Asymmetry in the wave shape, velocity skewed waves, can contribute to the sediment transport by transporting the remaining sediment that is in suspension, after it was entrained during one part of the flow cycle and did not settle down prior to the following half-cycle, in the opposite direction during the following half-cycle, which is also called the phase lag effect (Grasso et al., 2011; Van der A et al., 2010).

In this study, the boundary layer model of Kranenburg (2013) is first validated on net sediment transports of irregular wave flume experiments. Subsequently, research is done to which extent the net sediment transports of irregular and regular waves differ for wave flume- and oscillatory flow tunnel simulations and how these can be explained by hydrodynamic and sediment transport related processes. Finally, research is done on the influence of skewed wave groups on the net sediment transport in oscillatory flow tunnel simulations.

Firstly, using fine and medium sediment irregular wave-flume experiments, of Schretlen (2012) and Dohmen-Janssen (2002) respectively, for the boundary layer model wave-flume simulations, the net sediment transport results were considered a good quantitative reproduction for net sediment transports, despite of a slight overestimation in the net sediment transport of a few experiment condition runs.

Secondly, for the indication of differences in net sediment transport between irregular and regular waves, two representative regular wave approaching methods for an irregular wave were introduced, the “full signal influence approach” and the “partial signal influence approach”. For both methods, Stokes second order solution for the horizontal velocity is used to create the representative regular wave and the original, irregular wave, wave peak period, wave energy and velocity skewness are retained. However, in the latter principle the two methods differ. Where for the full signal influence approach the entire irregular wave signal is used to define the velocity skewness, for the partial signal influence approach only the highest one-third of the peaks (positive/onshore) is used to define the velocity skewness. Irregular wave simulations (thirteen in total), with fine sediment, of the boundary layer model showed that for flume simulations, both the representative regular waves have equal onshore net sediment transports as their irregular waves, only a slight overestimation occurs. For the oscillatory flow tunnel simulations however, the irregular waves show an offshore net sediment transport, while both the representative regular waves show onshore net sediment transports. Furthermore, between the two representative regular waves there was no significant difference noticeable and therefore a new representative regular wave approaching method is introduced first, before explaining the difference between irregular and regular

waves in net sediment transport, according to hydrodynamic and sediment transport related processes. In the new "high wave, signal influence approach" method, only the wave energy of one-third of the highest waves in the irregular wave signal is used to define the velocity amplitudes (u_1 and u_2) and the velocity skewness.

Thirdly, the difference in net sediment transport between the irregular and regular wave, is found in the wave-related component of the intra-wave horizontal sediment flux where phase lag effects after each single irregular wave, and in case the irregular wave contains a sequence of high irregular waves a accumulation of these phase lag effects (pumping effect) occurs. The influence of velocity-skewed waves brings the sediment offshore. For the difference in net sediment transport between oscillatory flow tunnel and flume simulations for irregular waves, the vertical momentum advection is becoming less important with an increasing wave energy (third method) or when the wave signal is irregular. But the vertical sediment advection and the horizontal momentum advection do get more important with more wave energy in a regular wave and with an irregular wave (both including phase lag), and decrease the amount of phase lag effect and also the contribution to the pumping effect occurring for irregular waves (amount of sediment concentration due to offshore flow), resulting in more onshore-directed sediment transport.

Finally, net sediment transport simulations, in the oscillatory flow tunnel, showed that three different skewed wave groups, with single irregular waves, have no influence on (the direction of) the net sediment transport.

Preface

After finishing my Bachelor Civil Engineering at the University of Twente, I started with the Water Engineering and Management track of the Master Civil Engineering and Management. The Master consists of several theoretical subjects within water engineering and is finished with the completion of the Master thesis. After completion of all master courses I participated in the ConcepT study tour throughout Singapore and Java, Indonesia where we visited multiple water engineering related projects. After traveling trough several other Asian countries I started with my master thesis research at the University of Twente.

I have chosen to do my master thesis internal at the University of Twente due to the fact that beside my study I am also a professional baseball athlete in the "Dutch Major League Baseball" and the University allowed me to schedule my time more freely.

During one of my last master courses, Marine Dynamics, the, for me new, in depth information of wave propagation and sediment transports at the coast drew my attention. This eventually led to my decision to do research on "sediment transport under irregular waves". During my research I have learned a lot and I am proud of the final result. This would not have been possible without the support I received from my supervisors. Therefore I would like to thank Wouter Kranenburg for being my daily supervisor. I could walk into his office at every moment of the workday for explanation of his Boundary Layer Model and for discussing research related plans and results. He also reminded me to focus on the relevant point of the research and provided me with enough feedback to learn from. I am grateful to Jebbe van der Werf for providing me feedback on my draft versions, for the help he gave adjusting some Matlab scripts which I had to use during my research and for reminding me to stay within the scope of my research. I also would like to thank Jan Ribberink for providing me feedback on my research proposal, half way report and concept final report, and for helping me to define the scope of my research.

I would like to thank the other graduate students of the WEM graduation room for the moments of fun and the discussions. Last but definitely not least; I would like to thank my parents, René and Ingrid, for their unconditional support during my entire education.

Sander Helmendach

Apeldoorn, November 2013

Contents

Appendices

List of Figures

List of Tables

1. Introduction

There is an increasing desire to understand and successfully model nearshore processes, especially in the nearshore zone where many different hydrodynamic and sediment transport processes take place. Different wave conditions and bed shapes for example can cause sediment to move at the bottom, the place where the largest sediment transport often occurs (Malarkey & Davies, 2012). In order to simulate and gain knowledge about the processes that occur in the nearshore area, mainly regular, sinusoidal, waves have been used for experiments and irregular, realistic, waves have been left aside. This research can contribute to the improvement on the knowledge of these irregular waves. The next section provides a brief description on the background of this research; regular waves studies. Section 1.2 presents the context and relevance of this research, followed by the research objectives and questions in section 1.3. Finally, in section 1.4, the research strategy and the thesis outline are presented.

1.1 Theoretical background

Over time a lot of research has been done to create sediment transport formulas and incorporate newly investigated conditions and processes. Most of the formula are based on a quasi-steady assumption (see section 2.4 for explanation) between the transport and velocity or bed shear stress. These are therefore not able to predict sediment transport rates that are affected by phase differences between the velocity and concentration fields (Van der A et al., 2010) and do not account for effects related to progressive surface waves that further influence the net transport (Ribberink et al., 2010). In order to expand the knowledge of the interaction between wave motion and net sediment transport, more experimental studies were carried out which show influences of the wave shape on bed shear stress, flow velocity and the sediment transport. The focus of these studies was either on regular velocity skewed waves (occur under waves with amplified crests), regular acceleration skewed waves (occur under waves with steep fronts) or a combination of both (Ruessink et al., 2009).

The experimental studies on the influence of wave shape (Ribberink and Al-Salem, 1995 and Van der A et al., 2010), grain size effects (Dibajnia and Watanabe, 1992, Dohmen-Janssen et al., 2002, O'Donoghue and Wright, 2004 and Van der A et al., 2009) and on the sediment transport with rippled bed conditions (Van der Werf et al., 2007) were often done in oscillating flow tunnels. From the oscillatory flow tunnel experiments in the sheet-flow regime it was observed that for regular velocity skewed waves the net sediment transport in case of coarse sediment is directed onshore. However, with an increasing percentage of fine sand in the bed the offshore sediment transport will become increasingly more dominant with the result that the net sediment transport decreases and ultimately can become offshore (negative) (O'Donoghue & Wright, 2004). The studies on grain size and ripple effects showed that sediment concentration and sediment transport do not always react instantaneously to changes of the flow velocity and in case of ripples and fine sand sheet flow the concentration and the transport show a phase lag with respect to the free stream velocity. To account for these phase lag effects on the net sediment transport, semi-unsteady transport formulas have been developed (e.g. Dibajnia and Watanabe, 1998, Dohmen-Janssen et al., 2002 and Van der A et al., 2013).

For accelerated skewed waves in an oscillatory flow tunnel, Silva et al. (2011) showed that a net sediment transport is produced in the direction of the highest acceleration and that in presence of an opposing current the net sediment is negative, against the direction of the highest acceleration, and reduces with an increase in flow acceleration.

Experimental, regular wave studies have also been carried out with flume experiments. Dohmen-Janssen & Hanes (2002) and Schretlen (2012) showed that for their wave flume experiments on sediment transport with waves in the sheet flow regime, the net sediment transport is onshore directed for fine sediments under 2nd order Stokes, velocity skewed, waves compared to offshore directed transport in oscillatory flow tunnel experiments. Flume experiments with medium sediment showed an even larger onshore-directed net sediment transport compared to the net sediment transport results of medium sediment conditions in oscillatory flow tunnel experiments.

In order to explore the net sediments transport rate Uittenbogaard et al. (2001) developed an (numerical) intra-wave net sediment transport model (Point-Sand model), which aims to eventually include irregular waves and wave-induced streaming to determine the net sediment transport of more *realistic* coastal conditions. The model simulates time-dependent vertical profiles of horizontal flow, turbulence quantities, and sediment concentration by solving the 1DV Reynolds-averaged Navier-Stokes and advection-diffusion equations in conjunction with a k- ε turbulence model under the assumptions of horizontal uniform conditions, a flat bed and a single grain size (Ruessink et al., 2009). Ruessink et al. (2009) neglected all variations in the horizontal direction and considered fully developed "u tube" flows only to explore the net sediment transport under combined skewed asymmetric waves. Kranenburg (2013) boundary layer model is an extension of the hydrodynamic model described in Kranenburg et al. (2012) for which the sediment formulations correspond to those in the previous model version used by Ruessink et al. (2009). The boundary layer model has an addition of a horizontal and vertical advection of momentum in the flow velocity, sediment concentration and turbulence equations, and some turbulence properties additions to get a better sediment balance and feedback of sediment on the flow through stratification effects.

1.2 Research context and relevance

Aimed at developing predictive capability for sand transport under waves (O'Donoghue et al., 2011), researchers of the University of Twente, the University of Aberdeen and the University of Liverpool, have set up a Dutch – UK joint project, the SINBAD project. Researchers of this project will be investigating sediment transport near the seabed in the coastal marine environment by conducting large-scale wave experiments, in a large wave-flume in Barcelona, Spain, and in an oscillatory flow tunnel in Aberdeen, Scotland. The primary aim is to establish a new semi-empirical model for sediment transport near the seabed, accounting for wave irregularity and wave breaking in a way that is well founded on experimental data and the understanding of the fundamental processes (O'Donoghue et al., 2011). The second aim is to improve the understanding of the near bed hydrodynamics and sand transport processes occurring under real scale irregular non-breaking and regular breaking wave conditions. Therefore, the project will include multiple experimental studies with respect to sediment transport under breaking waves and sediment transport under irregular waves.

This master thesis research is part of the SINBAD project in such a way that it will help to understand and clarify the hydrodynamic and sediment transport process principles of the differences between sediment transport by irregular and regular waves. During this research, the boundary layer model of Kranenburg (2013) will be, after validation for irregular waves, used to explain process differences occurring between regular and irregular waves. Indirectly, the capabilities of the boundary layer model will be tested with irregular, non-breaking, waves during the model validation, which may expand the possibilities of application.

Additionally, net sediment transports results for certain wave conditions are provided to the SINBAD department in Aberdeen, Scotland, which may contribute to design good experimental irregular non-breaking wave conditions for the large scale wave-flume-and oscillatory flow tunnel experiments in Barcelona, Spain, and Aberdeen, Scotland, respectively.

1.3 Research objectives and questions

Recent studies were mainly focusing on regular waves and their wave shape effects on the sediment transport. The focus on irregular waves is increasing, but explanation of the processes that take care of the differences between regular and irregular waves is not done extensively, and when attempts are done, these are not satisfactory yet. Therefore, the main objective (*objective 1*) of this research is: to increase the understanding of the nearshore sediment transport processes occurring under irregular non-breaking wave conditions, with the use of the boundary layer model.

To obtain a better understanding of the irregularity processes (objective 1) and its effects on sediment transport, a regular wave that represents an irregular wave would be easier to implement in existing morphological models that simulate sediment transport. Therefore, the second objective (*objective 2*) of this research is: to develop, or to approach, a representative regular wave for an irregular wave signal.

The following main research question and its sub research questions serve to accomplish the research objectives:

Main research question (M): "*What are the main differences between irregular and regular waves in terms of sediment transport and what processes can explain the differences?*"

Sub research questions (S):

S1. Which hydrodynamic and sediment transport related processes are known for regular waves and when irregularity is involved; which models are developed that incorporate these processes?
S2. How is the numerical boundary layer model of Kranenburg (2013) specified; and how can it be used to simulate net sediment transport rates?
S3. How well do the boundary layer model results for irregular wave conditions compare with measured data from flume experiments?
S4. How do sediment transport rates for irregular waves and representative regular waves compare, for both flume and oscillatory flow tunnel simulations, with the boundary layer model?
S5. How can differences in the net sediment transport between irregular and regular waves in oscillatory flow tunnel simulations, and differences in the net sediment transport between oscillatory flow tunnel and flume simulations for irregular waves, be explained in terms of hydrodynamic and sediment transport processes?
S6. To which extent does a skewed wave group, with single irregular velocity skewed waves, has influence on the net sediment transport, for both fine and medium sediment, in oscillatory flow tunnel simulations?

1.4 Research strategy and thesis outline

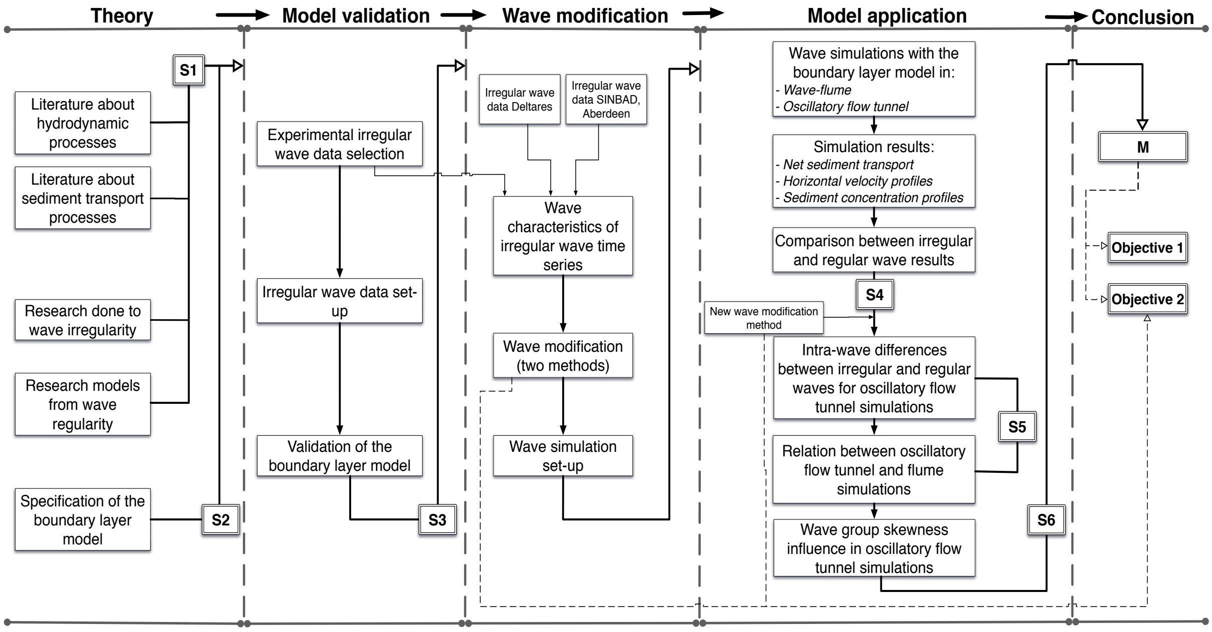

Figure 1: Research strategy defined in four stages in the thesis. The consistency of the subjects studied and the sub research questions answered with it is shown. Final result is to achieve the two objectives and answering the main question.

In order to answer the above described research questions and to achieve the objectives a research strategy of a certain amount of steps is followed. Figure 1 presents a schematic overview of this research strategy and shows how the research questions are related to the conducted research and how the objectives are reached.

The thesis is divided into five stages: Theory, Model validation, Wave modification, Model application and Conclusion. Each stage is described in one or more chapters, for which each chapter will answers one sub research question (S). By answering the main research question, by answering the sub research questions, in the conclusion, the first objective will be reached. The second objective will be reached by using different approaches to represent an irregular wave in a regular wave.

In the *first stage* of the research (Theory), literature is consulted first to gain knowledge about known hydrodynamic and sediment transport processes for regular waves and also for when irregularity is involved. Developed regular wave formulas that include results of completed experiments on sediment transport and new established models (numerical) are also listed. (Chapter 2 and S1) The first stage also contains the specification of the boundary layer model of Kranenburg (2013) and its boundary conditions (Chapter 3, and S2).

In the *second stage* (Model validation), irregular wave data sets of flume experiments, conducted by Dohmen-Janssen (2002) (medium sediment) and Schretlen (2012) (fine sediment), are used to simulate the net sediment transport rates with the boundary layer model and are compared with the measured net sediment transport data. To check if turbulence in irregular wave data would result in significant different net sediment transport rates, it is checked at the same time whether ensemble-averaged wave signals fit the measured net sediment transport results better than the original wave signals (including turbulence) of the experiments. (Chapter 4 and S3)

In the *third stage* (Wave modification), two representative regular wave methods are introduced and are used to develop a representative regular wave signal for irregular wave signals, which are ensemble- averaged timeseries of Schretlen (2012), an irregular wave signal provided by the SINBAD project department in Aberdeen, Scotland, and an irregular wave signal provided by Deltares. (Chapter 5)

In the *fourth stage* (Model application), the irregular and regular wave signals are simulated in both the flume and the oscillatory flow tunnel version of the boundary layer model. The net sediment transport results are then compared and discussed. (Chapter 5 and S4)
The results show that there is no significant difference in net sediment transport between the two used regular wave methods and therefore a new third representative regular wave method is introduced. The observed differences between the net sediment transport results of the irregular and regular waves, within oscillatory flow tunnel simulations, and between the oscillatory flow tunnel and flume simulations for irregular waves however, are examined closer using intra-wave horizontal sediment fluxes. (Chapter 6 and S5)
From the explanation of the differences between the net sediment transport results of the irregular and regular waves, within oscillatory flow tunnel simulations, the questions emerged if the sequence of (higher) waves in a wave group contributes to determination of the final net direction of the sediment transport. This was examined by carrying out research on the influence of skewed wave groups. (Chapter 7 and S6)

In the *fifth stage* (Conclusion), a brief discussion is held (Chapter 8), followed by answering the main research question, which is done by answering the sub research questions, and a brief recommendation for further research (Chapter 9).

2. Cross-shore coastal processes

Sediment transport in the cross-shore direction is the motion of sediment perpendicular to the coast. Since the sediment can be transported in the entire water column the main responsible processes that produce this transport will be discussed in two separate sections. Section 2.1 will elaborated the hydrodynamic processes, while section 2.2 will elaborate the sediment transport related processes closer to the bed. Section 2.3 will briefly give results of research done on irregularity. Section 2.4 will briefly discuss the definition and observed influences on sediment transport by quasi-steady and semi-unsteady models. It will also include the origin and definition of the numerical boundary layer model used in this research.

2.1 Hydrodynamics

In this section the hydrodynamic processes will be discussed by going from the top of the water column towards the region where sediment transport is predominant.

2.1.1 Wave propagation

There are two different types of waves that approach a coast, which are capillary waves and gravity waves, for which the latter can be divided in wind waves, long-period waves and ordinary tide waves (Park, 2008). From these the wind waves are one of the most common waves. The other common and noticeable waves are swell, which can be classified as a combination of capillary waves and wind waves with small wavelengths. They have been generated elsewhere and have travelled far from their place of origin. Their wave periods are between 1 and 25 seconds and their wave heights vary. These waves mostly travel in wave groups, which propagate with the wave group velocity. In deep water the group speeds is half of phase speed of the individual waves. But when waves propagate into more shallow water the wave velocity (c) decreases to become equal to the group speed (Park, 2008). During this process of waves entering shallower water the wave height is increasing, which is called shoaling. It is caused due to the fact that the group velocity, which can also be seen as the wave energy transport velocity, is decreasing with the decrease of the water depth (h). With stationary conditions the transport speed decrease must be compensated by an increase in energy (E) to maintain a constant energy flux. E.g. from point one, deeper water, to point two, shallower water, the energy flux remains the same $E_2/E_1 = c_1/c_2 = h_2^2/h_1^2$ (1), with the energy proportional to the square of the wave height included. During this shoaling the wave firstly becomes velocity skewed, which can be seen by an increasing crest and a flattening trough (see section 2.2.3). Followed by larger accelerations between trough and crest compared to smaller accelerations between crest and trough (acceleration skewness). The final result is a change of the waveform from a more symmetric shape to an asymmetric shape with sharp wave crests and shallow troughs. Hereby the front of the wave will become steeper until the point the wave will finally break because the water depth is to shallow or the front is to steep.

2.1.2 Orbital motion

Under progressive waves water particles move along elliptic orbits (Park, 2008; Hulscher & Ribberink, 2012), which are generally not completely closed. At the surface, the orbital diameter corresponds with the wave height, but the diameter is decreasing with increasing depth, until at a depth roughly equal to half the wavelength, the orbital diameter is negligible, and there is virtually no displacement of the water particles. During the propagation there is a small net displacement component in the forward motion caused by further forward movement of the particle in the crest than the backward movement in the trough, and is called wave drift (Park, 2008).

In deep water (h>1/2L, with h being the water depth and L the wavelength) the seabed does not influence the waves and the waves are mostly sinusoidal. The underlying water particles follow the orbital motion with a small forward motion displacement component. In the top figure of Figure 2 the decrease of the horizontal diameter with increasing depth is shown. In the intermediate depth (L/20<h<1/2L) and in shallow water (h<L/20) the asymmetry of the wave changes due to the wave propagation and change of water depth (see section 2.1.1) and subsequently the asymmetric of the orbital motion changes. With a decreasing water

depth the waves are getting more influenced by the seabed and the orbits become progressively flattened (middle and bottom figure in Figure 2).

With the decrease of the water depth a horizontal velocity in the bottom layer will still be noticeable. However, *at* the seabed the vertical water velocity will always be zero, because no vertical mass flux can exist at the seabed (Dohmen-Janssen C. M., 1999).

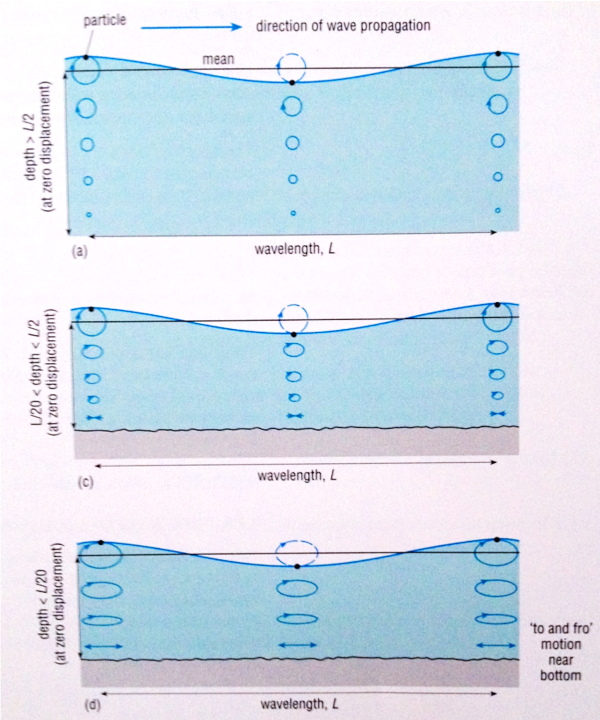

Figure 2: Motion of water particles; *Top:* deep water, *Middle:* intermediate depth and *Bottom:* shallow water (Park, 2008).

2.1.3 Boundary layer

With this study focusing on the sediment transport in the boundary layer by irregular waves it should be clear first what the boundary layer is and how it is defined. As mentioned in the previous section there will be a horizontal velocity noticeable at the bottom. However, exactly at the bottom (seabed) the horizontal velocity will be zero. Since just above this seabed there is a small horizontal velocity, a shear force will occur and due to the viscosity and turbulence water can transfer these shear forces. The small subsequent layers above will slightly less be influenced by the shear forces and the horizontal velocity increases, also resulting in small shear force. This continuous until the free-stream where there is no influence by the bed anymore. This transition region of zero horizontal velocity at the seabed to the free-stream is the boundary layer, Figure 3.

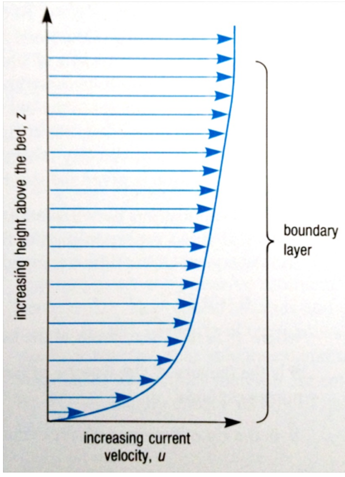

Figure 3: Boundary layer and velocity profile just above the bed (Park, 2008).

The boundary layer thickness depends on three things, the viscosity, the bed roughness (height) and the wave period. If the viscosity is increasing it means that the layers above the bed can transfer larger shear forces and thus results in a larger boundary layer thickness. For the bed roughness height the boundary layer will also increase since an increase in roughness height will also increase the shear force. The influence of the wave period is slightly more difficult. With a large wave period the onshore motion continuous until the wave reverses to an offshore motion. During this time the boundary layer keeps on increasing and might finally cover the entire water column. With a small wave period the time period of the onshore motion is much shorter, deceleration has more influence and the velocity becomes zero long before the boundary layer could fully be developed. At the point of zero horizontal velocity the boundary layer changes direction and has to start growing again (offshore directed). Therefore the wave period has a lot of influence on the thickness of the boundary layer.

An estimate of the boundary layer thickness can be defined with the following equation of Sleath (1987):

$$\frac{\delta_s}{k_N} = 0.27\left(\frac{A}{k_N}\right)^{0.67} \qquad (2)$$

, with A being the orbital excursion ($A = \frac{u_{max}}{\omega}$; $\omega = \frac{2\pi}{T}$ and umax the maximum horizontal velocity) and k_N the Nikuradse roughness height (k_n=2*D_{50}, with D_{50} the median grain size).

2.1.4 *Wave-current/streaming boundary layer interaction*

The interaction of wave-current/streaming and the boundary layer can be split up in three different interaction processes. The first interaction, current-only, is already described in section 2.1.3. A second interaction is the wave-only interaction and the third is a conjunction of both, current-wave interaction.

The wave-only interaction creates two different streamings; prograssive wave and wave shape-streaming. Allthough indicated that the vertical velocity at a certain level in the boundary layer is very small it is not completely zero due to convergence or divergence of the horizontal flow beneath the certain level. Due to the fact that the horizontal flow inside the boundary layer has a phase lead (Kranenburg, 2013) the vertical velocity at the edge of the boundary layer will also develop a phase lead. As a result the horizontal and vertical orbital motion will be more than ninety degrees out of phase. Longuet - Higgins (1953) demonstrated this and shows that the vertical, w, and horizontal, u, velocities in the wave boundary layer will give a nonzero mean vertical transfer of horizontal momentum: $\overline{uw} \neq 0$, where the overbar signifies a time average. The vertical transfer of momentum causes a net flow in the direction of wave propagation, which is called (Longuet-Higgins) "progressive wave streaming". (Deigaard et al., 1999)

Another process that may influence the current inside the boundary layer is the generation of 'wave shape streaming'. Differences in friction and turbulence appear between the on- and offshore phase of the wave for waves that have developed a non-sinusoidial form. Waves that have amplified crests give rise to a wave-averaged boundary layer current in the opposing direction of the wave propagation. (Kranenburg, 2013)

In a normal steady uniform flow the horizontal velocity distribution is logarithmic over the biggest part of the total water depth and z_0 is the level where the logarithmic distribution line will be/go trough zero. Once the flow becomes/is turbulent and has a rough bottom the level z_0 will be equal to $k_N/30$ (Roughness height, later in the boundary layer model).

But when there are waves present, the shape of the net current profile changes. Due to the increase of wave-induced mixing in the boundary layer, the net current velocity close to the bed is reduced. Which can be seen from:

$\tau_{xz} = -\rho\overline{uw} = \rho v_{tz}\frac{\partial \bar{u}}{\partial z}$ (3) , which is the Boussinesq hypothesis and shows that the turbulent shear stress is proportional to the turbulence-averaged velocity gradient. Increasing wave-induced mixing corresponds to an increased eddy viscocity (v_{tz}) and for a given mean bed shear stress, the velocity gradient inside the wave boundary layer must be reduced. Depending on the boundary condition there is no effect on the velocity profile further away from the bed if the pressure gradient is kept constant (and thus the same as if there are no waves). However, due to reduced near bed velocities the velocities over the total depth are smaller and result in smaller discharges than without waves. When instead of the pressure gradient the flow discharge would be kept constant, the reduced velocities close to the bed must be compensated by larger velocities further away from the bed. And thus the velocity gradient above the boundary layer will be larger than without waves (and an increased resistance requires a larger pressure gradient to keep the same discharge). (Dohmen-Janssen C. M., 1999)

2.2 Sediment transport

In this section the sediment transport related processes will be discussed. Processes near the bed are discussed first, followed by processes that occur higher in the water column.

2.2.1 Forces

The principle of sediment transport is the movement of sediment, caused by mobilizing forces on the sediment grains. If these mobilizing forces are larger than the stabilizing forces movement will occur. Figure 2 shows the forces on a sediment grain. Herein, the mobilizing forces are the lift (F_L) and the drag (F_D) (fluid force is the resulting vector), which are caused by the fluid movement over the sediment(s). The stabilizing force is the gravity (F_g).

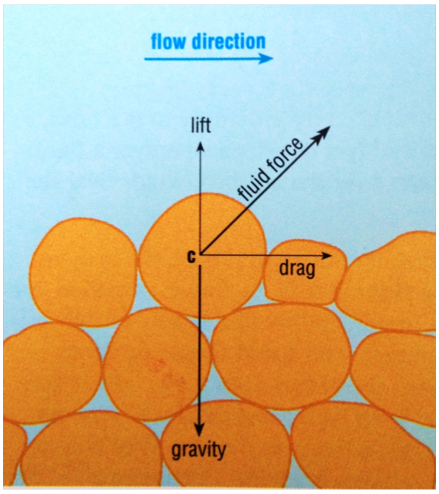

Figure 4: Forces on sediment grains (Park, 2008).

This stabilizing gravity force is the weight of the submerged particle and is:

$$F_g = \rho_w g(s-1)D^3 \; with \; s = \frac{\rho_s}{\rho_w} \qquad (4)$$

, wherein ρ_s and ρ_w are the densities of sediment and water respectively, g the gravity acceleration and D the sediment grain diameter. Note that the gravity force can also be a mobilizing force when considering sloping beds and ripples, however in this study only a flat bed is considered.

Both two mobilizing forces, lift and drag, are caused by fluid movement over the sediment(s) and therefore depend on the fluids density and velocity and are proportional to the surface area of the grain: F_D and $F_L \approx \tau D^2$ (where τ is a shear stress which includes the fluid density and velocity and lift and drag coefficients), see section 2.2.2 for shear stress.

2.2.2 Bed shear stress and friction

As mentioned before, orbital motions cause shear stresses, not only in between water layers, but also on the bed, called bed shear stress. The bed shear stress is therefore related to the orbital velocity, but also to the wave friction factor, which on itself is also depending on the orbital velocity. The maximum bed shear stress can be written as:

$$\tau_{b,max} = \frac{1}{2}\rho f_w U_m^2 \qquad (5).$$

Herein U_m is the amplitude of the horizontal orbital velocity, which can be written as:

$$U_m = \frac{\pi H}{T}\frac{1}{\sinh\frac{2\pi h}{L}} \qquad (6)$$

Wherein H is the wave height, T the wave period, h the water depth and L the wavelength.

In reality the water flow is often hydraulically turbulent over rough bed. Jonsson (1966) gives an implicit empirical equation for f_w(friction factor), which is approximated by Swart (1974) in:

$$f_w = exp\left(5.213\left(\frac{k_s}{A}\right)^{0.194} - 5.977\right) \qquad (7)$$

Wherein k_s is the roughness height and A the orbital excursion.

The ability to move a sediment particle can be determined by the ratio of the shear stress to the normal stress (mobilizing force vs. gravity force). This ratio is called the Shields parameter (Shields, 1936):

$$\theta(t) = \frac{\tau_b}{(\rho_s-\rho_w)gD} = \frac{\frac{1}{2}f_w\rho u^2(t)}{(\rho_s-\rho_w)gD} = \frac{\frac{1}{2}f_w u^2(t)}{(s-1)gD} with \; s = \frac{\rho_s}{\rho_w} \quad (8)$$

If the value of the Shields parameter stays below the critical value (θ_{cr}) the gravity is normative and the sediment particles do not move. When the forcing increases and the critical Shields value is > 0.03 to 0.06, the particles start to move. Above a value of 0.06 the particles are in motion. This continues to a value of 0.8 to 1.0, when arisen sand ripples will disappear (again) (Van der Wal, 1996).

2.2.3 Skewness and asymmetry

When a wave is pure symmetric the resulting flow will be a purely oscillatory flow (neglecting progressive wave streaming), which cannot result in a net on- or offshore sediment transport, because an equal amount of sediment is transported on- and offshore. However, a wave can also be skewed (velocity and/or accelerated).

Wave skewness is the gradual transition from a sinusoidal shape wave to a waveform with a peaking of the wave crest and flattening of the trough, which results in a more flat trough and a narrow peaked crests (Austin, Masselink, O'Hare, & Russell, 2009), see Figure 5 and section 2.1.1. With the change also the velocity skewness and the asymmetry (acceleration skewness) change.

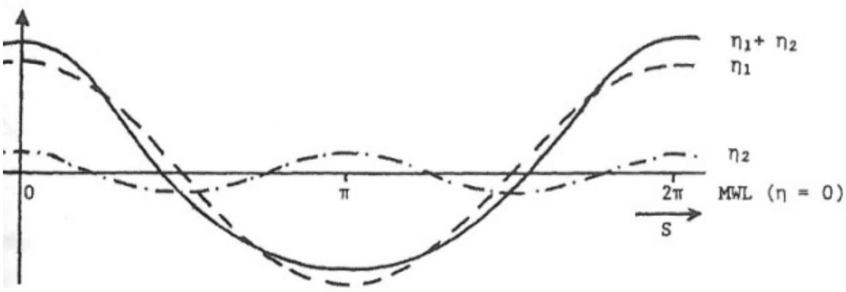

Figure 5: Wave skewness (Bosboom & Stive, 2011). Dashed line is reference; solid line is velocity-skewed wave.

Velocity skewness is the relative measure of larger orbital velocities under the wave crest compared to smaller orbital velocities under the wave trough; whereas asymmetry (acceleration skewness) is the relative measure of larger accelerations between trough and crest compared to smaller accelerations between crest and trough (Malarkey & Davies, 2012), see Figure 6.

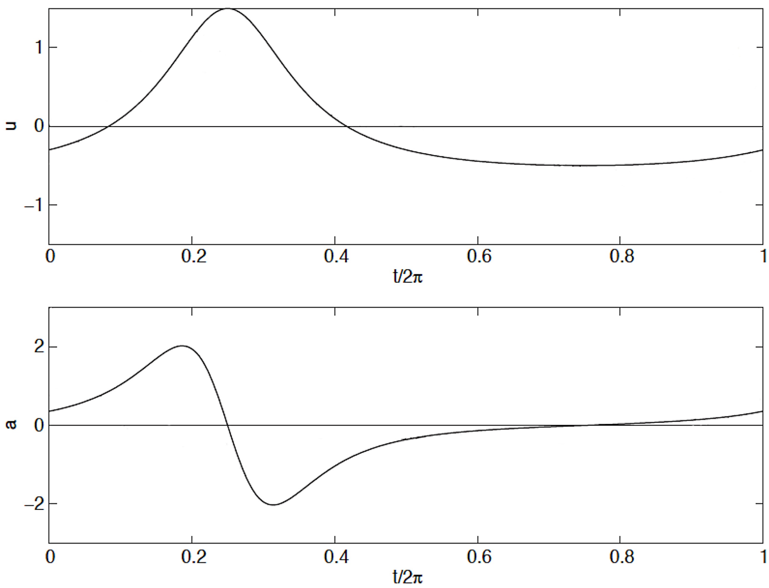

Figure 6: Velocity skewness (top) and acceleration skewness (bottom) (adopted from Malarkey & Davies, 2012).

Austin et al. (2009) mention that the skewness results in asymmetrical wave orbital velocities and therefore skewed fluid accelerations, with larger accelerations under the steep onshore face of the wave (leading the maximum onshore-directed velocity) than under the gently sloping rear face.

An important observation from tunnel experiments in the sheet-flow regime is that under (regular) velocity-skewed flow over coarse grains, the sediment transport is mainly onshore, but net transport decreases with decreasing grain sizes and can even become negative (O'Donoghue & Wright, 2004; Kranenburg et al., 2013).

For (regular) accelerated skewed waves in an oscillatory flow tunnel Silva et al. (2011) showed that a net sediment transport is produced in the direction of the highest acceleration and that in presence of an opposing current the net sediment is negative, against the direction of the highest acceleration, and reduces with an increase in flow acceleration.

Thus, both (regular) velocity and acceleration skewness (with opposing current) can either result in an on or offshore sediment transport (note that for irregular waves this process is even more complex than with regular waves and is further investigated, for irregular velocity skewed waves, in section 6).

2.2.4 Phase lag

With regular waves the crest of the wave gives an onshore movement of water and the trough an offshore movement of the water. With symmetric waves the sediment that is brought into suspension will normally settle down before the trough will bring it into suspension again and thus no net sediment transport occurs as mentioned earlier. However, with velocity skewed waves a phase lag effect might occur, sand entrained into the flow under the (short) positive (high velocity) wave half- cycle has not settled prior to flow reversal and is transported during the (longer) negative wave half- cycle (Grasso et al., 2011; Van der A et al., 2010). The lag between the sediment concentration and the flow is characterized by the ratio between the fall time of the sediment particle (which may be represented by the ratio between the sheet flow layer thickness and the settling velocity) and the wave period (Camenen & Larson, 2006).

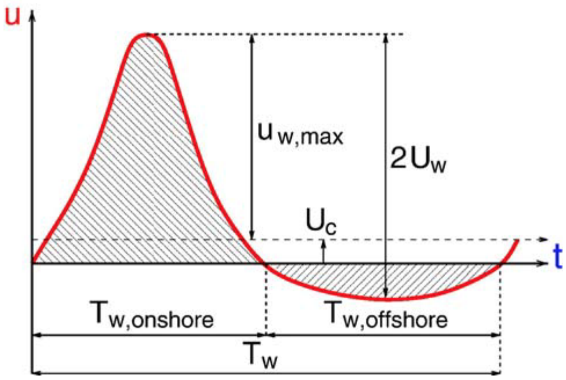

Figure 7: Velocity skewed wave sediment displacement (Camenen & Larson, 2006). Where for velocity skewed waves the $T_{w,onshore}$ is (always) smaller than the $T_{w,offshore}$.

Figure 7 shows that for a velocity skewed wave the crest will bring much more sediment into suspension from the bottom (and onshore directed) than the trough of the same wave (which will be offshore directed). In theory the net sediment transport will therefore be onshore. However, with phase lag effect occurring not all sediment has settled down yet prior to the flow reversal from on to offshore due to the possible low fall velocity, and therefore not only new bottom sediment will be displaced offshore by the trough but the sediment still in suspension as well. With this process occurring the (theoretical) graph of Figure 7 will thus look different in a way that more sediment is transported offshore. Although research by i.e. Dohmen-Janssen & Hanes (2002), O'Donoghue & Wright (2004), Hsu & Hanes (2004), Ruessink et al. (2009) and Schretlen (2012) has shown that the phase lag effect plays an important role in the net sediment transport it is also observed that the direction of the net sediment transport is highly dependent on the grain size. I.e. O'Donoghue and Wright (2004) observed that with an increasing percentage of fine sand in the bed the offshore sediment transport will become increasingly more dominant with the result that the net sediment transport decreases and ultimately can become offshore (negative).

To include this phase lag process into the transport formula, Dohmen-Janssen et al. (2002) characterized phase lag by the phase-lag parameter P_s as:

$$P_s = \frac{\delta_s \omega}{w_s} = 2\pi \frac{\Delta t_{settl}}{T} \tag{9}$$

where $\omega = 2\pi / T$, with T the wave period, w_s the sediment settling velocity, Δt_{settl} the time needed for particles for settling to the bed, and δ_s the sheet flow layer, defined as:

$$\delta_s = 13\, d_{50}\theta \qquad (10)$$

for $d_{50} \geq$ 0.21 mm, θ being the Shields number (dimensionless bed shear stress parameter). Following Ribberink et al. (2008) $P_s \geq 0,1 - 0,3$ indicates an unsteady behavior, for which phase- lag effects take place. The criterion $P_s \leq 0,1 - 0,3$ indicates that the settling time has to be an order of magnitude smaller than the wave period for a quasi- steady behavior to dominate.

2.3 Irregularity

The previous two sections mostly describe the known hydrodynamic and sediment transport processes diverted from regular wave experiments and model studies. For irregular waves, also known as real waves, the range of research is small. The scarce performed research has been done for either irregular skewed waves or for a wave group containing irregular waves.

2.3.1 Irregular skewed waves

Dibajnia and Watanabe (1998) conducted experiments on sand transport in sheet flow conditions under nonlinear asymmetric irregular oscillations with different frequency spectra. In their research they used an earlier, from experiments derived net sediment transport formula (Dibajnia and Watanabe, 1992) and observed that phase lag effect might occur with single velocity skewed waves. However, when the negative part of the single velocity skewed waves includes multiple maxima the effect of the phase lag reduces, resulting in less offshore directed net sediment transport. It was also found that for input (horizontal) velocities with a same energy spectrum a larger degree of nonlinearity gives a larger net sediment transport and no clear effect of spectral shape on the net sediment transport is observed. Finally, they concluded from their experiments that the number of large waves in a velocity time series is more important than their order of occurrence.

Grasso et al. (2011) used wave flume experiments with irregular waves to investigate the wave shape effect on sediment transport for cross-shore beach profile changes. Grasso et al. analyzed the net sediment transport rates on typical beach morphodynamics in regard to wave skewness and asymmetry, undertow, and ripple occurrence. It was found that for small skewness values, the sediment flux is onshore directed. In this situation the sediment is weakly mobilized and the crest velocities which exceed the trough velocities produce an onshore flux. The wave asymmetry additionally contributes to the transport in the same direction. For larger wave skewness, either the wave asymmetry is weak and the sediment is transported offshore (crest to trough phase lag effects), or the wave asymmetry is large enough (trough to crest phase lag effects) to reverse the trend and transports the sediment onshore.

Because of the low amount of research according irregular waves there is little evidence to indicate that for example research by Dibajnia and Watanabe (1998) does give satisfactory results. The approach is pragmatic given the absence of better knowledge, but there are a number of reasons why they should not be expected to work well in general: flow within the wave boundary layer under irregular waves differs substantially from that occurring under regular waves (Klopman, 1994) and sediment dynamics under waves can exhibit strong unsteady behaviour caused by intra-wave phase lag effects (Ruessink et al., 2009; Van der A et al., 2010). (O'Donoghue et al., 2011)

2.3.2 Wave group

Shi and Larsen (1984) recognized that the bound long waves under irregular wave groups can give an opposing contribution to the transport (Figure 8), because the bound long waves give a reverse flow under the high waves when the sediment concentrations are high, and a forward motion under the low waves with low sediment concentrations. (Deigaard et al., 1999)

Shi and Larsen (1984) also found and concluded that the reverse transport (Figure 8) rate is mainly controlled by the magnitude of the bottom orbital velocity. Other flow parameters, such as wave period and steady current velocity, exert only minor influence on the transport rate. The process is most effective in transporting silts and fine sands offshore but not clays. This sorting characteristic may be amplified when multicomponent size sediments are present in the seabed.

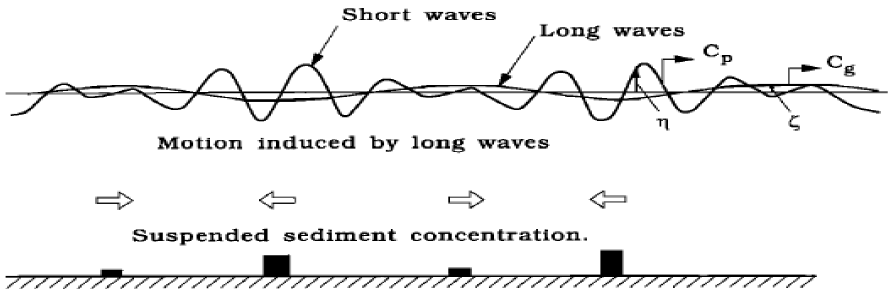

Figure 8: Reverse sediment transport under bound long waves, shown are surface elevations (adopted from Deigaard et al., 1999).

Sato (1992) did an experimental study for sediment transport under wave groups. He used coarse sediment for the experiments and found that wave groups give an increased transport in the direction of wave propagation. However, the coarse sediment was only in motion under the highest waves (Deigaard et al., 1999). For fine sediment conditions this was not researched yet.

2.4 Sediment transport in models

Dohmen-Janssen (1999) investigated how the orbital velocity, the grain size and the wave period influence the net sediment transport. This was done for two quasi-steady and two semi-unsteady “models” (these can also be seen as “formulas”) (QS: (1) Bailard, 1981 and (2) Ribberink, 1998. SU: (1) Dibajnia and Watanabe, 1992 and (2) a new developed semi-unsteady model). A quasi-steady model is a model based on the assumption that the instantaneous transport rate is directly related to some power of the instantaneous near-bed oscillatory velocity or bed-shear stress (Dohmen-Janssen, 1999). If the response time of sediment becomes comparable to the wave period or longer the sediment transport is not beheaving quasi-steady anymore (unsteady). In this case the sediment concentration and consequently the sediment transport rate might fall behind the instantaneous velocity (phase-lag effect). If the model does take this phase-lag effect into account, but does not describe the vertical distribution of the time dependent horizontal velocity and sediment concentration the model is called a semi-unsteady model.

For the quasi-steady models it was found that when the net sediment transport increases the orbital velocities should also increase. But both the wave period and grain size should decrease to increase the net sediment transport. For the semi-unsteady models it was found that if phase-lag effects are not important, Dibajnia and Watanabe (1992) model is independent of the wave period and a coarser sediment will result in increasing net sediment transport. For the new model, by Dohmen-Janssen (1999), non importance of phase-lag would result in Ribberink’s (1998) quasi-steady model. If the phase-lag effect is important ($p>$ 0.15-0.2), the new model reduces the maximum sediment transport with about 40%. Dibajnia and Watanabe (1992) model would even result in such a high reduction that the net sediment transport will be negative (in case of the largest ‘p’ values).

Previous discussed “models” are more or less based on experimental studies. Another type of “model” is the model based on numerical studies. Uittenbogaard et al. (2001) developed the one dimensional Point-Sand Model, an intra-wave net sediment transport model which aims to eventually include irregular waves and wave-induced streaming. This numerical model can be classified as a non-hydrostatic single phase RANS model. Where RANS stands for a (quasi-)single phase wave boundary layer model where (horizontal) flow velocities are solved from Reynolds averaged Navier-Stokes equations and sediment concentrations are solved from an advection-diffusion equation. The fluid velocity and sediment concentration are solved troughout the entire water colum, including the wave boundary layer. Bosboom & Klopman (2000) used the one dimensional Point-Sand model in numerical experiments and predicted increased onshore transport under propagating free surface waves compared to horizontally oscillating flow. The model however has been adopted and changed in time. The, in this Master thesis research, used boundary layer model of Kranenburg (2013) is an extension of the hydrodynamic model described by Kranenburg et al., (2012) with a sediment balance and feedback of sediment on the flow. The sediment formulations correspond to the model version used by Reussink et al.(2009), which was originally based on the Uittenbogaard et al. (2001) model, now extended with horizontal and vertical advective terms in the flow velocity, sediment concentration and turbulence equations, and some turbulence formulation and model forcing changes to get a better feedback of sediment on the flow trough stratification effects.

The advective transport of horizontal momentum, turbulence properties, and sediment marks the fundamental difference between modeling the horizontally uniform situation like in oscillating flow tunnels or the horizontally nonuniform situation beneath progressive surface waves in prototype situation, as in Ruessink et al. (2009), and wave flumes, as in Kranenburg (2013) boundary layer model. The progressive wave streaming is driven by the wave-averaged vertical advective transport of horizontal momentum into the wave boundary layer (wave Reynolds stress). (Kranenburg, 2013)

3. Model formulation

In this chapter the principles and the boundary conditions (sections 3.1 and 3.2 respectively) of Kranenburg's (2013) boundary layer model for sediment transport are explained.

3.1 Boundary Layer Model

Kranenburg's (2013) boundary layer model can be classified as a 1DV Reynolds averaged Navier-Stokes flatbed boundary layer model with *k-ε* turbulence closure and an extra addition. As an extension of the hydrodynamic model described by Kranenburg et al. (2012) a horizontal and vertical advection of momentum and some turbulence properties (i.e. to include turbulence for on and offshore wave propagation) have been added to get a better sediment balance and feedback of sediment on the flow. The Boundary layer model was extended to validate the hydrodynamics of a numerical Reynolds-averaged boundary layer model; and to apply the model to abtain insight in the balance between progressive wave streaming and wave shape streaming, and how this if affected by varying wave and bed conditions. Note that there are two different models available. One for the oscillatory flow *tunnel*, which has no wave propagation and u is the only component of orbital velocities (advection term turned off). The other is for a wave *flume*, which uses 1D wave propagation and has 2DV orbital motion components: u,w.

The fundamental unknowns solved by the boundary layer model are the horizontal flow velocity *u*, vertical flow velocity *w*, sediment concentration *c*, and its turbulent kinetic energy *k*, and its rate of dissipation *ε*. The main (driving) equations for the unknowns are given as described by Kranenburg, 2013.

To solve the flow velocities *u* and *w*:

$$\frac{\partial u}{\partial t} + u\frac{\partial u}{\partial x} + w\frac{\partial u}{\partial z} = \frac{1}{\rho_w}\frac{\partial p}{\partial x} + \frac{\partial}{\partial z}\left\{(\upsilon + \upsilon_t)\frac{\partial u}{\partial z}\right\} \qquad (11)$$

$$\frac{\partial u}{\partial x} + \frac{\partial w}{\partial z} = 0 \qquad (12)$$

,where p is the pressure, ρ_w is the fluid density, υ is the kinematic viscosity of water, υ_t is the turbulence viscosity, x is the horizontal coordinate (positive in onshore direction) and z is the vertical coordinate(positive in upward direction).

For the closure of υ_t a *k-ε* model (Rodi, 1984) is provided with a k, ε turbulence model and a constant (c_μ =0.09) related as:

$$\upsilon_t = c_\mu \frac{k^2}{\varepsilon} \qquad (13)$$

For the turbulence:

$$\frac{\partial k}{\partial t} + u\frac{\partial k}{\partial x} + w\frac{\partial k}{\partial z} = \frac{\partial}{\partial z}\left\{\left(\upsilon + \frac{\upsilon_t}{\sigma_k}\right)\frac{\partial k}{\partial z}\right\} + P_k - \varepsilon - B_k \quad (14)$$

$$\frac{\partial \varepsilon}{\partial t} + u\frac{\partial \varepsilon}{\partial x} + w\frac{\partial \varepsilon}{\partial z} = \frac{\partial}{\partial z}\left\{\left(\upsilon + \frac{\upsilon_t}{\sigma_\varepsilon}\right)\frac{\partial \varepsilon}{\partial z}\right\} + \frac{\varepsilon}{k}(c_{1\varepsilon}P_k - c_{2\varepsilon}\varepsilon - c_{3\varepsilon}B_k) \quad (15)$$

, where P_k is the turbulence production, k the turbulent kinetic energy, ε the energy dissipation rate, B_k the buoyancy flux and σ_k, σ_ε, $\sigma_{1\varepsilon}$, $\sigma_{2\varepsilon}$ are constants (1.0, 1.3, 1.44, 1.92 respectively). The P_k production term is defined as:

$$P_k = \upsilon_t\left(\frac{\partial u}{\partial z}\right)^2 \qquad (16)$$

For the sediment (volume) concentration c:

$$\frac{\partial c}{\partial t} + u\frac{\partial c}{\partial x} + w\frac{\partial c}{\partial z} = \frac{\partial w_s c}{\partial z} + \frac{\partial}{\partial z}\left\{\left(\upsilon + \frac{\upsilon_t}{\sigma_t}\right)\frac{\partial c}{\partial z}\right\} \qquad (17)$$

, where w_s is the fall velocity using the undisturbed settling velocity $w_{s,0}$ according to Van Rijn (1993).

Assuming uniformity of wave shape and height during propagating over the horizontal sediment bed, the model is reduced to a 1DV model by transformation of horizontal gradients of velocity, turbulence properties and sediment concentration into time-derivative with $\partial \ldots/\partial x = -1/c_p * \partial \ldots/\partial t$, with c_p being the wave propagation speed. This consideration of advective transport of horizontal momentum, turbulence properties and sediment shows the difference between the modeling of horizontal uniform situations like in oscillatory flow tunnels (boundary layer model tunnel version: advective terms are neglected) and the horizontally non-uniform situation beneath progressive surface waves in flumes (flume version of the boundary layer model).

The model is designed that it can be forced into two different ways. In the first forcing, named "match" model, the unknown *u(z)* is forced to match a predefined horizontal velocity signal at a certain leven z_{match} above the bed, desired at the location closest to 2.5* δs (the 2.5* δs is later also used as the domain size), with δs being the boundary layer thickness estimate of (Sleath, 1987):

$$\frac{\delta_s}{k_N} = 0.27\left(\frac{A}{k_N}\right)^{0.67} \quad (18)$$

,A the orbital excursion and k_N the Nikuradse roughness height (k_n=2*D_{50}) (for calculation see Appendix V). With the second manner of forcing, "free" model, the unsteady horizontal pressure gradient d*p*/d*x* is determined in advance from a given horizontal free stream velocity $\tilde{u}_\infty$. By doing this the net current streaming arising from the streaming mechanisms is not compensated by any mean pressure gradient and is allowed to develop freely. The first forcing allows to compare the model with measurements, that not only include boundary layer streaming mechanisms, but also possible return currents. Therefore this forcing might be used in this research to compare computed sediment transports with real measured sediment transports. The second forcing can be used if the balance between the boundary layer streaming mechanisms needs to be investigated and is later used to investigate the different processes within the intra-wave horizontal sediment flux occuring in irregular waves compared to regular waves.

From the model, the net sediment transport, q, is computed as:

$$q = \frac{1}{T}\int_0^T \int_{z_a}^d u(t,z)c(t,z)dzdt \quad (19)$$

, where T is the wave period, z_a the reference height (defined later) and d the top of the flow domain. For which the time period over which the sediment transport will be determined can be changed to for example 2 time periods.

3.2 Boundary conditions

For the boundary layer model to be able to solve Eqs. (11), (14) and (15), using the 1DV-approach, there are six boundary conditions needed. For the lower boundary the conditions are:

$$\left.\frac{\partial u}{\partial z}\right|_{z=0} = \frac{u_*}{9\kappa z_0}; \qquad k|_{z=0} = \frac{{u_*}^2}{\sqrt{c_\mu}}; \qquad \varepsilon|_{z=0} = \frac{{u_*}^3}{9\kappa z_0} \quad (20)$$

For the upper boundary the three conditions are:

$$v_t\left.\frac{\partial k}{\partial z}\right|_{z=top} = 0; \quad \left.\frac{\partial k}{\partial z}\right|_{z=top} = 0; \quad \left.\frac{\partial \varepsilon}{\partial z}\right|_{z=top} = 0 \qquad (21)$$

Herein u_* is the friction velocity, κ =0.41 is the Von Karman constant and z_0 the roughness height. The lower boundary conditions assume a hydraulic rough turbulent flow near the bed and are applied at a fixed bottom level. The z_0 is related to the median grain size D_{50} by application of the Nikuradse roughness height k_n=2*D_{50} and z_0 = k_n/30.

For the sediment (volume) concentration to be solved from the sediment balance in Eq. (10) a no flux boundary condition at the top of the boundary and a pick-up function at the reference height z_a=2*D_{50} is used. Which is:

$$w_s c_b + \left(\upsilon + \frac{\upsilon_t}{\sigma_t}\right)\frac{\partial c}{\partial z}\bigg|_{z=z_a} = 0 \quad (22)$$

, with for the reference concentration c_b the expression of Zyserman and Fredsoe (1994):

$$c_b(t) = \frac{0.331(\theta - \theta_c)^{1.75}}{1 + \frac{0.331}{C_m}(\theta - \theta_c)^{1.75}} \quad (23)$$

Which is a function of the Shields parameter θ and critical Shield parameter θ_c for initiation of motion (Van Rijn, 1993) and with constant C_m is 0.32 for oscillatory flow. In the layer beneath z_a $c(z) = c|_{z=z_a}$is applied.

4. Model Validation

Now it is clear what the principles and boundary conditions of the boundary layer model are, the validation process of the boundary layer model for irregular waves can be started, see section 4.2. However, to do so section 4.1 will first describe the used datasets for the validation.

4.1 Experiment data

In this paragraph the available experimental irregular wave data is discussed. It elaborates which different wave conditions and properties are used for the data analysis and the validation of the boundary layer model. Section 4.1.1 will discuss the background of the fine sediment datasets; section 4.1.2 will discuss the background of the medium sediment datasets.

4.1.1 Fine sediment experiments

In 2007 and 2008, Schretlen (2012) carried out sediment transport experiments for both regular and irregular waves in the Grosse Wellenkanal (GWK) of the Coastal Research Centre, Hannover, Germany. Regular and irregular surface waves, without breaking at the test section, were created and different measurements were carried out. The Large Wave Flume has a total length of 280m, a width of 5m and a depth of 7m. Within the flume at a distance of +111m from the wave paddle, which is at X=0m, the measurement equipment for the sheet flow was installed. At this location, the disturbed (by previous experimental runs) sand bed consisted of a fine grain size of 0.14mm and the sand bed was horizontal. The still water level during the experiments was 4.50m, corresponding with a 3.5m water depth. The experimental set-up is shown in Figure 9.

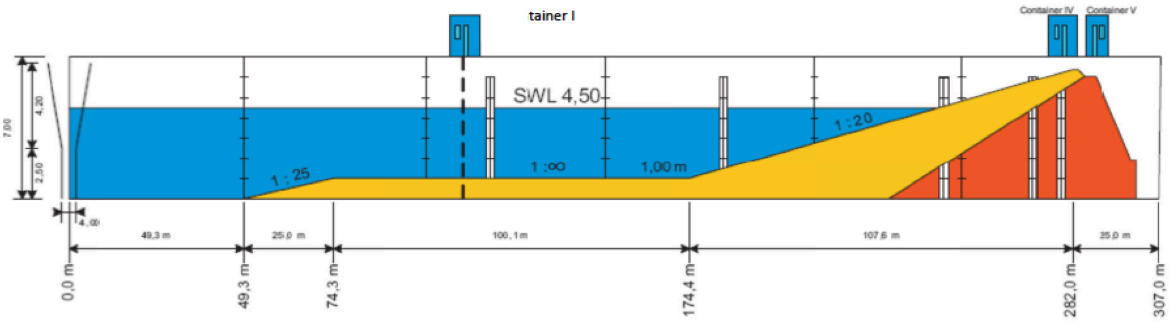

Figure 9: 2008 experiment schematization of the Large Wave Flume in Hannover, Germany. (Schretlen, 2012)

For the sheet flow measurements several measuring instruments were used, such as an acoustic velocity meter (for detailed velocity measurements; Ultrasound Doppler Velocity Profilers (UVP) and Acoustic Doppler Velocimeters (Vectrino)), electromagnetic flow meters (EMF) and conductivity bases CCM-probes (for sediment concentrations; CCM). To record the sand bed (change) along the flume echosounders were used on a movable measurements carriage (for measuring the net sediment transport). Measuring at two places ("A – C") forward and two places while moving backwards ("B – D"), after each run. From these and more measure instruments the following measurement data files are available:

- Labview (data-acquisition and instrument communication)
- UVP (velocity profile)
- Vectrino (velocity profile)
- CCM (sediment concentration)
- Echosounder (bed profile)

From these files only the UVP and Echosounders are used for validation of the Kranenburg (2013) Boundary Layer Model, which is discussed in section 3.2.

Beside the numerous regular wave experiments for fine and medium sediment, also experiments for three different irregular wave conditions with fine sand were carried out. These irregular wave condition experiments will be used here. Table 1 presents these three irregular wave condition input properties, the number of runs per condition and the grain size. Herein the H_s and T_p are the design significant wave height and wave peak period, respectively, at the wave paddle. The wave group period slightly differs and is ±100seconds for each run, in section 4.2.1 this is further elaborated.

Table 1: Irregular fine sand conditions, flume experiments Schretlen (2012).

Condition	H_s [m]	T_p [s]	Number of runs	D_{50} [mm]
gi436512	1,2	6,5	5	0,14
gi436515	1,5	6,5	5	0,14
gi437515	1,5	7,5	4	0,14

4.1.2 *Medium sediment experiments*

In 1999 cross-shore sediment transport experiments in the sheet flow regime with regular and irregular waves in the same Large Wave Flume in Hannover, Germany, were performed by Dohmen-Janssen (2002). The design however, slightly differs from the experiments in 2008. Instead of a continuous beach shaped bed profile with horizontal bed and slopes in 2008, a 45m long horizontal disturbed (by previous experimental runs) sand bed, with a medium grain size of 0.24mm, in the central part of the wave flume was used in 1999. The water depth slightly differed as well; a 3.75m water depth at the paddle was used, corresponding with a 3.0m depth at the sheet flow measurement location. For energy dissipation a coarse grained sloping beach (D_{50} = 0.3mm; 1:6) was only placed at the end of the wave flume and therefore did not affect measurements. The experimental set-up is shown in Figure 10.

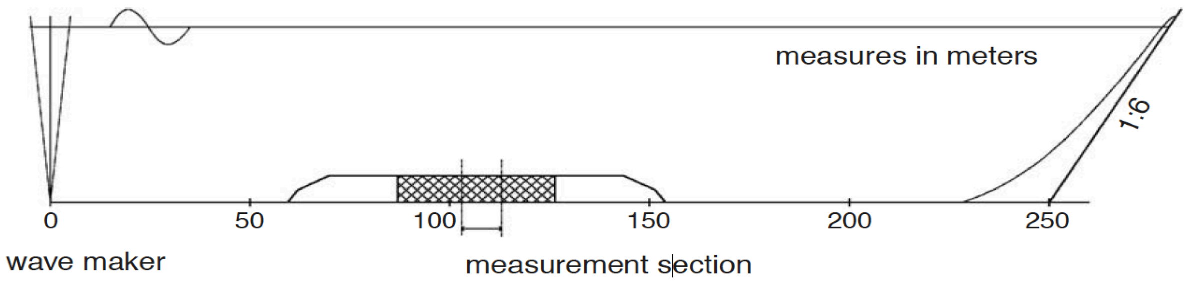

Figure 10: 1999 experiment schematization of the Large Wave Flume in Hannover, Germany. (Dohmen-Janssen, 2002)

Measurements were carried out in the middle of the sand bed (also at ±111m) as is shown in the figure. For the measurements during the experiments near-bed flow velocities were measured using Acoustic Doppler Velocimeters (ADV), time- varying suspended sediment concentration profiles with Acoustic Backscatter Sensors (ABS) and sediment concentration inside the sheet flow layer were measured using conductivity based CCM-probes (CCM). Although multiple measurement instruments were used only the following measurement data files are available, from which only the first one is used during validation:

- ADV (velocity)
- CCM (sediment concentration)

For a large part the experiments were based on regular (monochromatic) waves. However, two irregular wave conditions were tested as well. The two irregular wave conditions consisted of wave groups with irregular waves in it, which were repeated multiple times after each other (Dohmen-Janssen, 2000). The wave groups were generated by selecting one wave group from a narrow-banded Jonswap spectrum (γ=10) and repeating this wave group for a certain amount of times (±10times) in each experimental run (Dohmen-Janssen & Hanes, 2005). Table 2 presents the design significant wave height (H_s) and the peak wave period (T_p) at the paddle for both conditions. The number of runs, grain size and the wave group period are listed as well.

Table 2: Irregular medium sand conditions, flume experiments Dohmen-Janssen (2002).

Condition	H_s [m]	T_p [s]	Number of runs	T_{group} [s]	D_{50} [mm]
GP	0,9	9,1	10	90	0,24
GI	1	6,5	7	100	0,24

From the GWK99 experiments there are no raw bed profiles available anymore. However, Yu et al. (2010) does provide the mean net sediment transport rates for both the GP and GI conditions, since these were used for research on sediment transports under wave groups. During the experiments the net sediment was measured in two manners. The first net sediment transport measured rate is calculated on the basis of the survey of the entire sand bed (±45m section along the tank) and the second net sediment transport measured rate is calculated on the basis of the survey near the test area where the instruments are located (±5m test section). Since for the GWK08 conditions the echosounder profiles are used, and use the entire sand bed for calculation of the net sedíement transport, the net sediment transport of the first calculation is used here, see Appendix III.

4.2 Data processing and model set-up

Before the boundary layer model can be validated on reproducing the net sediment transport for irregular waves as it does in a proper way for regular waves (Kranenburg, 2013), a data processing is performed first. After checking if the model can handle time series (Appendix I) in the first section, section 4.2.1, ensemble averaging of the horizontal velocity signal is done to reduce the turbulence in the signal. In the second section, section 4.1.2, the net sediment transport is extracted from the echosounder data.

4.2.1 Ensemble averaging

From the fine sediment dataset (*from now on "GWK08"*) the UVP measurements for all conditions (3), and for each run (14 in total), are converted to input signals of the horizontal velocity u in the form of a time series (which is required by the boundary layer model as input). This was done for the ADV measurements (2 conditions, 17 runs in total) from the medium sand dataset (*from now on "GWK99"*) as well. For GWK08 UVP measurements were done on different heights z (mm) above and below the bed level, with -37mm ≤ z ≤ 79mm (note that the initial bed is at z=0, but does change during and after an experimental run). To produce the input signal for GWK08 the UVP-measured horizontal velocity signal at $z = z_{match}$ is used, with z_{match} being at 40mm above the initial still bed level, see section 3.1 and Appendix V for determination of z_{match} and the boundary layer thickness. For every run the initial input signal was taken manually to make sure the input signal at 40mm above the bed is used. The GWK99 ADV measurements were only done at z = 106mm above the bed.

On average every horizontal velocity input signal from GWK08 (except condition 1565 run3) consists of irregular waves in multiple wave groups (18-35 repetitions), packed in wave envelops, as can be seen in Figure 11. For the GWK99 runs only 4-10 repetitions of the wave groups were measured.

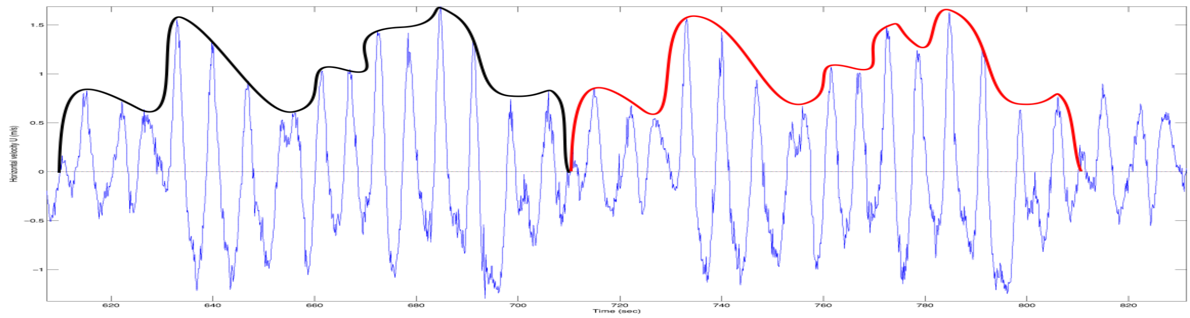

Figure 11: Blue line: Horizontal velocity timeserie (zoomed); Black and red line: 2 upper wave envelopes of 2 wave groups. (GWK08)

Figure 11 also shows a lot of turbulence and extreme peaks in the horizontal velocity. Since this turbulence and the extreme peaks might cause very rapid change of the pressure gradient in the model, and eventually result in abnormal net sediment transports, ensemble averaging is done to reduce both the turbulence and the extreme peaks in the horizontal velocities and to check whether this improves the eventual net sediment transport rates. However, ensemble averaging might also cause an underestimation of the final net sediment transport since it reduces the highest horizontal velocities, which might exactly be the velocities that cause an extra sediment transport boost and might cause more coarse sediment to actually move.

For the ensemble averaging itself the wave groups (or wave envelopes), within each time series, were placed over each other and an average wave group/ time series with irregular waves was produced. See Table 3 for the amount of single wave groups that were used for each run to create the ensemble averaged.

Hence, most of the first and last waves/wave groups were removed since these started or ended in the middle of a wave group. The starting time and repetition time of the wave group were initially chosen by estimating the start of the wave group using upward zero-crossing and whenever the same upward excursion would occur again (indicating the start of a new wave group). The final starting time and repetition time of the wave group were then found by finding the lowest standard deviation of the ensembled wave groups. Which was done by calculation of the standard deviation for ten time steps before and after the estimated starting time. Figure 12 presents the ensemble averaging of the wave groups and the ensemble average horizontal velocity for a wave group, which includes irregular waves.

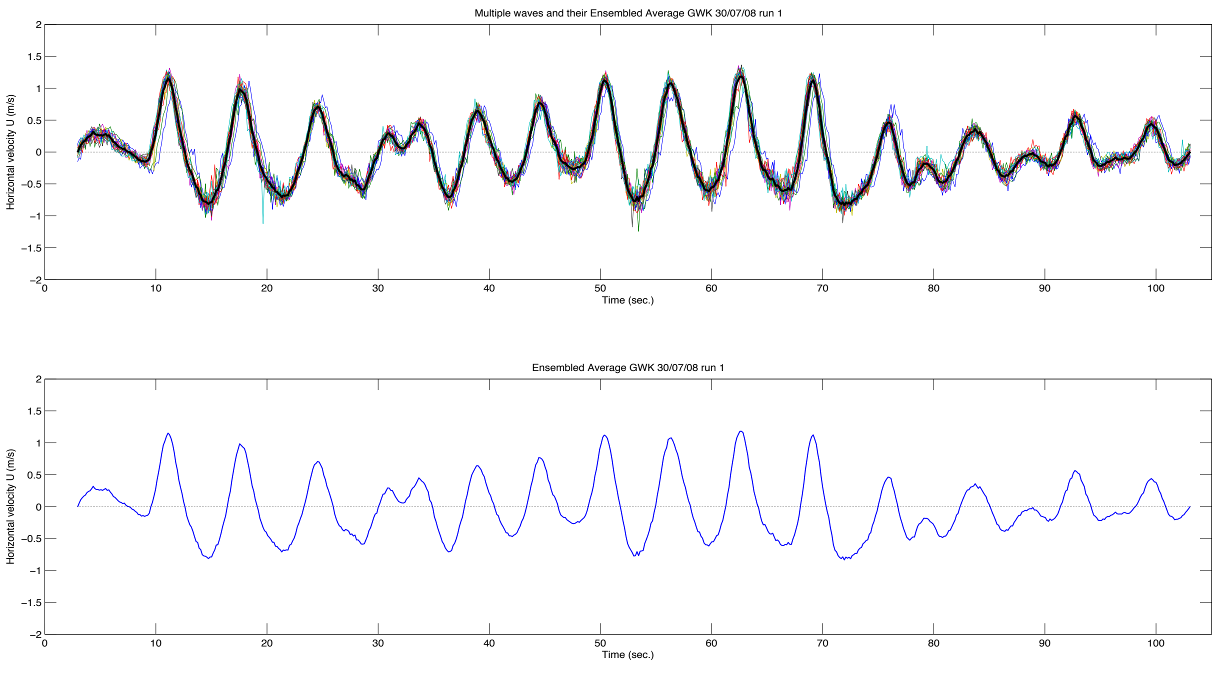

Figure 12: Top: Multiple wave groups ensembled and averaged. Bottom: Ensemble average of horizontal velocity of one run (GWK08 condition 1265 run 1).

In both graphs of Figure 12 it can be noticed that the positive values of the horizontal velocity have higher maximums than the absolute negatives (minimums), and these positives have a steeper slope. This is because in intermediate depths (L/20 <h<1/2L) and in shallow waters (h<L/20) skewness of the waves results in asymmetric orbital motions with smaller seaward velocities than the velocities onshore. *Note that for some of the runs of the experiments, the measuring equipment changed the on- and offshore direction. This was manually corrected.*

To be able to compare the net sediment transport of the ensemble averaged time series the initial horizontal velocities of the irregular wave runs were also converted to input signals in the form of time series. Hence, because for the ensemble average time series the first and/or last waves/wave groups were removed this was also done for the new original input signals (*New original runs*).

To be able to run the condition runs in the boundary layer model properly (giving the net sediment transport time to adapt), the ensemble-averaged time series is repeated a certain amount of times. This amount of times is defined as the total time series length of the "New original run" divided by the repetition time (Table 4) of the specific run. The removed first and/or last waves/wave groups are therefore now excluded.

Table 3: Ensemble average and original timeseries overview.

Dataset	Condition	Initial runs	New original runs	Ensemble averaged runs
GWK08	1265	5	5	5
	1565	5	4	3
	1575	4	4	4
GWK99	GP (0991)	10	10	0
	GI (1065)	7	6	0

Table 4: Number of used single wave groups and repetition time for ensemble averaging of GWK08.

Condition	1265					1565			1575			
Run	1	2	3	4	5	1	4	5	1	2	3	4
Number of wave groups	18	34	33	32	34	34	31	31	32	35	34	34
Repetition time (s)	100.11	100.10	100.10	100.10	100.10	100.11	100.05	100.75	100.10	100.26	100.10	100.10

As Table 3 shows, *not* for all runs and conditions ensemble average is possible. For two runs of GWK08 condition 1565 ensemble averaging is not possible. From one run (run 2) the repetition time of the wave group changes during the experiments and therefore no ensemble averaged could be made. Only the original timeserie is used. The other run (run 3) does not even consist of wave groups and cannot be ensembled to get an average. Since this run is the only one that does not consist of wave groups with irregular waves it is chosen to not use the new original time series either.

For the condition runs of GWK99 it turns out that every run experiences the same problem as run 2 from GWK08 condition 1565, a changing repetition time of the wave group, and therefore *no ensemble averages can be produced for this dataset.* From condition GWK99 GI for one run an original timeserie cannot be produced either, which is due to equipment failure at some points during the measurements.

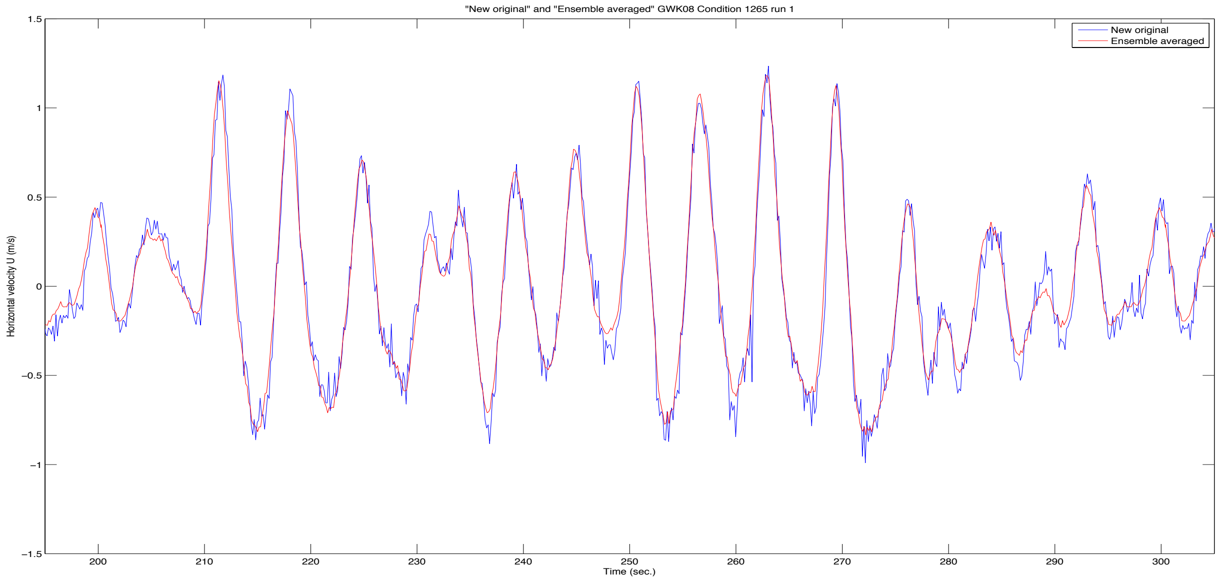

Figure 13: New original and ensemble averaged timeserie comparison (GWK08 condition 1265 run 1).

As an example, Figure 13 shows that the ensemble average timeserie indeed does cut off the high peaks as said earlier. But it also shows that especially at the maxima and minima the turbulence is reduced with the help of ensemble averaging, which might be better for the change of failure of the boundary layer model since the pressure gradient will not change abruptly.

4.2.2 Boundary layer model input settings

With all the time series of the five conditions produced only a few input settings, from initial regular input settings, of the boundary layer model need to be changed before actual running the model. The only settings that changed are the time interval over which the net sediment transport is calculated, the grain size (D_{50}), the domain (which is kept at 2.5 times the estimated boundary layer thickness (δs)), the water depth, the roughness height (z_0) and the forcing method of the model. Since this is the validation process of net sediment transport of experimental irregular waves and the signal have a possibility of included return currents the forcing method is set at "match". See Table 5 for flow and bed characteristics and the boundary layer model input settings, also see Appendix V for the boundary layer thickness calculation.

Table 5: Flow and bed characteristics, and boundary layer model input settings for validation.

Condition	Wave peak period T_p [s]	Grain size D_{50} [mm]	Roughness height k_s [m]	Max hor. velocity u_{max} [m/s]	Max. orbital excursion A [m]	Boundary layer thickness δs [m]	Roughness height z_o [m]	Domain [m]	Water-depth h [m]	Used force method
GWK99: GP	9.1	0.24	4.80E-04	1.84	2.67	0.04	1.60E-05	0.10	3.5	Flume-match
GWK99: GI	6	0.24	4.80E-04	1.65	1.58	0.03	1.60E-05	0.07	3.5	Flume-match
GWK08: 1265	6.5	0.14	2.80E-04	1.47	1.52	0.02	9.33E-06	0.06	3.5	Flume-match
GWK08: 1565	6.5	0.14	2.80E-04	1.87	1.93	0.03	9.33E-06	0.07	3.5	Flume-match
GWK08: 1575	7.5	0.14	2.80E-04	1.91	2.28	0.03	9.33E-06	0.08	3.5	Flume-match

4.3 Validation results

With the data processing done, the net sediment transport rates for the new original runs, ensemble averaged runs and the measured runs can now be calculated using the boundary layer model, see section 4.3.1. The results can then be compared with one another. This is done in two ways. First, section 4.3.2, the ensemble averaged runs are compared with the original runs to check whether the ensemble averaging did had a positive result on the net sediment transport rate. Second, section 4.3.3, the condition average net sediment transport rate of the new original runs are compared with the condition average rate of the measured runs.

4.3.1 Net sediment transport

All timeseries are imposed in the (flume version of the) boundary layer model with their corresponding properties (i.e. z_{match}, D_{50}, roughness height, etc.). All these runs result in a single computed net sediment transport rate. For each wave condition the mean and standard deviation are determined for comparison with those of the experimentally measured net sediment transport rates.

For GWK08 these experimentally measured net sediment transport rates are determined from the echosounder data, which are taken after each run. To determine the net transport rates the conservation of mass, also known as the mass balance, is used. All mass that enters an arbitrary system must either be accumulated or leave the system. Using the following equation:

$$\langle q_s(x_i)\rangle = \frac{-\Delta x\ (\Delta z)}{\Delta t}(1-\varepsilon) - \langle q_s(x_{i-1})\rangle \qquad (24)$$

, with q_s the net sediment transport rate and ε being the porosity of the sand bed, the net sediment transport rate at all measure locations can be determined. The value of the porosity may vary but is assumed as a constant of 0.4 since it was not measured during the measurements (Schretlen, 2012). The bed level difference, Δz, which is used, is the change of the bed level height during the run. Since the echosounder measured four profiles a mean is taken from the four as the net sediment transport rate for each run. *Note that for run 1 of condition 1265 there is no echosounder profile available since there was no measurement of the bed done before the irregular wave experiments started. This run is therefore not used for validation.*

For GWK99 there are no bed level profiles available. However, Yu et al. (2010) provides the mean net sediment transports rates for each of the GWK99 conditions. For both datasets the mean net sediment transports and standard deviations (GWK08 only) of their conditions are listed in Table 6. The net sediment transport rates for all echosounder profiles of all condition runs are listed in Table 15, Appendix II.

Table 6: Condition average net sediment transport rates and standard deviations from the Boundary layer model original and ensemble average timeseries, and measured profiles, for both GWK08 and GWK99. *"BLM" is the abbreviation for "boundary layer model"*.

Condition	BLM: New original <qs > [10^-6 m²/s]	Standard Deviation New original [10^-6 m²/s]	BLM: Ens. averaged <qs> [10^-6 m²/s]	Standard Deviation Ens. Avg. [10^-6 m²/s]	Measured <qs> [10^-6 m²/s]	Standard Deviation Measured [10^-6 m²/s]
GWK99: GP	21.5	4.8	-	-	30.2	-
GWK99: GI	12.7	3.4	-	-	12.6	-
GWK08: 1265	9.1	5.3	8.8	4.7	10.4	2.5
GWK08: 1565	17.0	4.6	11.6	2.5	16.4	1.9
GWK08: 1575	24.1	6.2	22.2	4.5	19.5	1.5

4.3.2 New original versus ensemble average runs

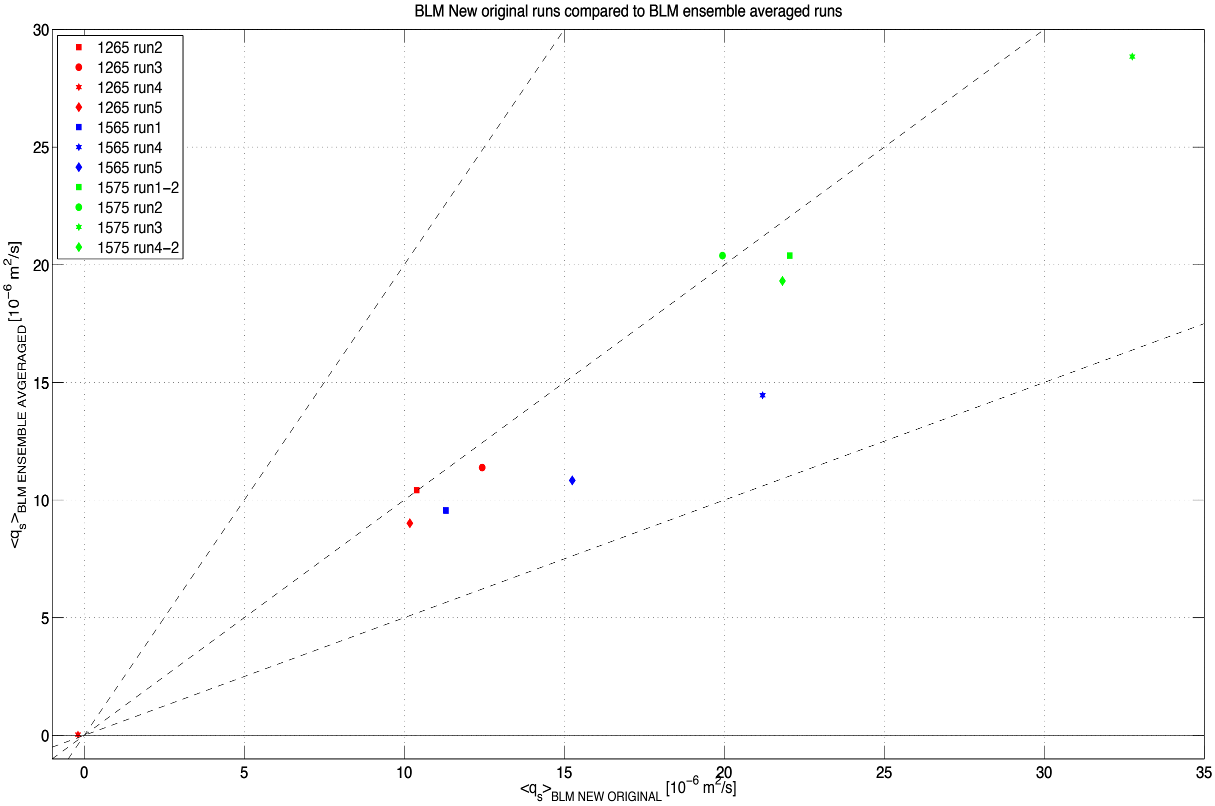

Figure 14: Net sediment transport rates boundary layer model new original runs vs. ensemble averaged runs, for GWK08. Dashed grey lines are the factor 0.5, 1, and 2 comparison lines (from bottom to top).

Before comparing the measured net sediment transport rates with the rates from the boundary layer model the rates of the ensemble averaged timeseries runs and the new original timeseries runs are being compared first in Figure 14.

From the net sediment transport of the new original timeseries, the ensemble average timeseries can reproduce 74%, 75% and 93%, for GWK08 conditions 1265, 1565 and 1575 respectively. On average this is 80% and is an underestimation. From this slightly low reproduction it can be said that from the ±20% shortcoming of the average net sediment transport a majority is caused by cutting of the extreme peaks in the horizontal velocities and the residual is caused by reducing the turbulence in this horizontal velocity signal. This therefore supports the expected result mentioned earlier.

With this result *and* including the fact that not for all conditions (GWK99) and not for a several condition runs (of GWK08) an ensemble average could be produced *the new original timeseries of the horizontal velocity will be held as the input for the boundary layer model.*

Two comparison figures (Figure 38 and Figure 39) of both original timeseries and ensemble averaged timeseries versus the measured net sediment transport rates are added in Appendix IV. Also showing that the net sediment transport rates produced by the original timeseries runs fit better to those of the measured runs, done by the echosounder.

4.3.3 *Condition average new original versus measured*

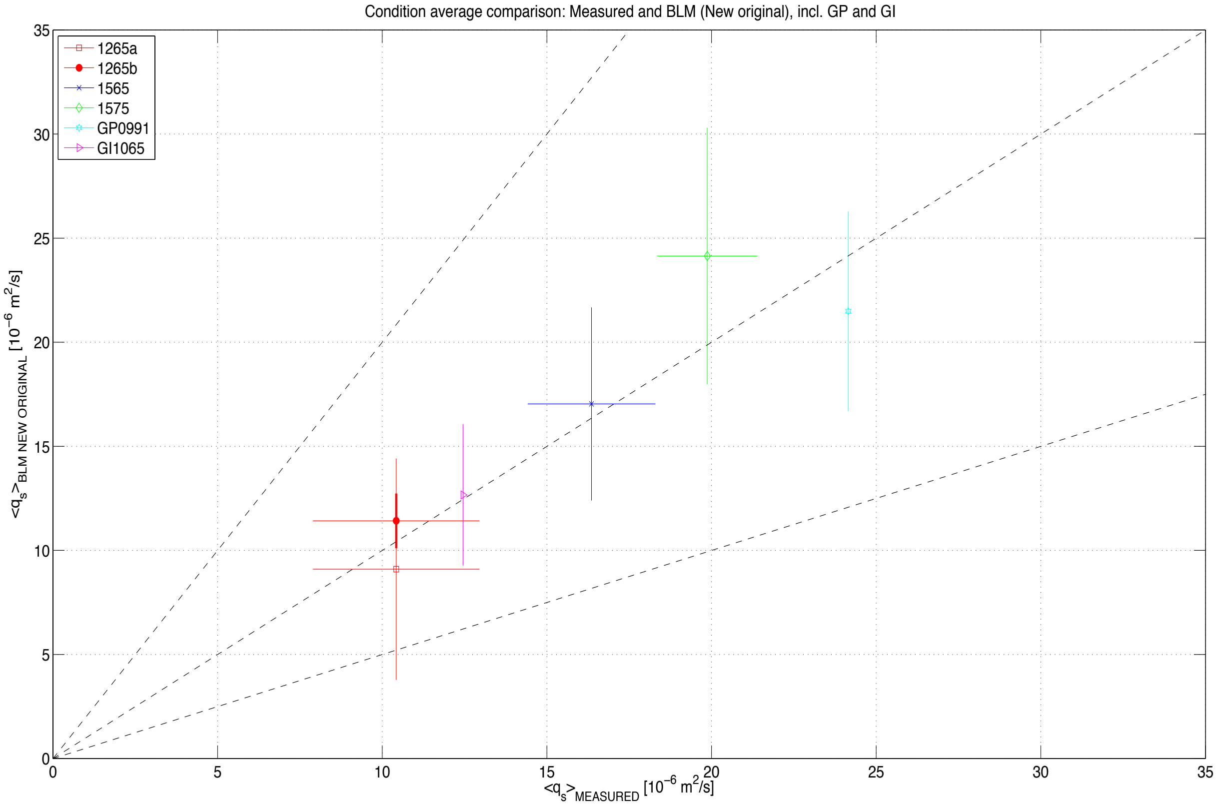

Figure 15: Condition average net sediment transport comparison of measured and new original time series from the boundary layer model, including fine sediment condition GWK08 (1265a, 1565 and 1575) and medium sediment condition GWK99 (GP0991 and GI1065). Dashed grey lines are the factor 0.5, 1, and 2 comparison lines (from bottom to top). 1265b is included changes.

In Figure 15 all condition averaged net sediment transport rates of the original timeserie are compared to the measured rates. Herein the standard deviations are included. Note that for both medium sand conditions there are no standard deviations shown since the measured condition average net sediment transport rates were gathered from research of Yu et al. (2010), no individual run measurements for the net sediment transport are available.

Although the figure with separate runs (Figure 14) showed that for one run the direction of sediment transport is computed the wrong way by the boundary layer model, on average the model computes that for all conditions the direction, onshore (positive sediment transport values), is computed the right way.

For both fine (D_{50}≤0.14mm) and medium (D_{50}≥0.24mm) sediment the model computes all averages between factor 0.87 and 1.24 (0.87, 1.04, 1.24 for GWK08 conditions 1265, 1565 and 1575 and 0.89, 1.02 for GWK99 GP and GI respectively. Two of the three fine sediment conditions (1265 and 1565) almost have factor 1.0. One of the two medium sediment conditions (GI) has factor 1.0.

4.4 Conclusion

For both datasets (fine sediment GWK08 and medium sediment GWK99) the factor range of "the computed net sediment transport divided by the measured net sediment transport is between 0.87-1.24 and 0.89-1.02 (GWK08 and GWK99 respectively). When taking both datasets together the average reproduction factor of the net sediment transport by the boundary layer model compared to the measured net sediment transport is 1.01. The net sediment transport results of both datasets separate, and when taken together, are considered a good quantitative reproduction for net sediment transport (Davies et al., 2002; Kranenburg, 2013). Therefore, it can also be concluded that the boundary layer model of

Kranenburg (2013) is validated for net sediment transports using irregular waves as a time series input signal.

As an addition and example to get the overall equity (GWK08 and GWK99) closer to each other, some changes of the GWK08 1265 condition (fine sediment) can be done. By removing a run with an extreme net sediment transport rate, the average factor value of 0.87 (computed/measured) can be improved to 1.1 (see 1265b in Figure 15). This means that the 87% reproduction of the net sediment transport by the boundary layer model can be improved to 110% reproduction, which is a small overestimate but does mean a small decrease in the standard deviation of the total reproduction average (of all GWK08 and GWK99 conditions) from 0.15 to 0.12 10^{-6} m^2/s.

5. Comparison between simulated irregular and representative regular waves

With the validation of the boundary layer model for net sediment transports of irregular waves done, the model can now be used to examine the differences in net sediment transport between irregular and regular waves.

From the grain size effect studies; Dibajnia and Watanabe, 1992; Dohmen-Janssen et al., 2002; O'Donoghue and Wright, 2004; Van der A et al., 2009, and from the irregularity studies; Shi and Larsen, 1984; Sato, 1992; Dibajnia and Watanabe, 1998, it is concluded that the relative importance of suspended load over sheet-flow transport will increase for fine sediment. Therefore the focus of the comparison of the irregular and regular waves will be on fine sediments only.

The comparison simulations will also be carried out for the wave flume and a oscillatory flow tunnel versions of the boundary layer model. With the oscillatory flow tunnel there is the posibility to simulate near-bed flow with prototype flow velocities and oscillation periods. The vertical component of the orbital velocity is absent, related wave-induced currents are not reproduced and difficulties and uncertainties related to scaling of turbulence and sediment related process are disabled, which gives the ability to relate observations to transport processes directly. The wave flume simulations however do include these restrictions and allow for a more complete representation of the processes in the field.

To start, from different irregular waves the wave characteristics are gathered in section 5.1. In section 5.2 two-modification methods for a representative regular wave of the irregular wave are given. After the representative regular waves are produced the irregular and both representative regular waves are then used, in section 5.3, to produce net sediment transports with the boundary layer model, for both flume and oscillatory flow tunnel, see section 5.4.

5.1 Wave characteristics of the time series

From the model validation, section 4, twelve ensemble-averaged timeseries (GWK08 conditions: 1265, 1565, 1575), or horizontal velocity signals, are available. From these, one signal, condition 1265 run 4, is removed because the boundary layer model did not provide a net sediment transport result from the signal in earlier research. The SINBAD project department in Aberdeen, Scotland also provided an irregular velocity skewed wave group (IRRvSK). Finally, Deltares (AUKE-PC) provided a signal of a Stokes 2nd order horizontal velocity of an irregular wave as well, which had the set input characteristics: water depth (h) = 3.5m, wave period (T_s) =6.5s, wave height (H_s) =1.4m and a Jonswap spectrum with γ=3.3. This makes a total of thirteen time series that can be used to reproduce net sediment transport by a representative regular wave of an irregular wave.

However, before modifying the irregular wave to a representative regular wave, the following wave characteristics of the time series are extracted first and discussed: $T_{p\,(1)}$, $T_{s\,(2)}$, $T_{mean\,(3)}$, $U_{0\,(4)}$, $U_{rms\,(5)}$, $U_{max,on,red\,(6)}$, $U_{max,off,red\,(7)}$, $U_{1/3,on,red\,(8)}$, $U_{1/3,off,red\,(9)}$, $\langle u(t)^2\rangle_{(10)}$, $\langle u(t)^3\rangle_{(11)}$, $R_{(12)}$, $Sk_{u\,(13)}$, $\beta_{(14)}$ and $Sk_{a\,(15)}$ (see Table 19, Appendix VI).

5.1.1 Wave characteristic definitions

For the first wave characteristic, the wave peak period (T_p), a Fourier analysis was done for the frequency domain analysis. Note that before analyzing, the mean value of the time series is removed by detrending, $u_{red}=u(t)-U_0$. This is often applied to remove a feature thought to distort or obscure the relationships of interest (Meko, 2013).

For the wave characteristics 2 and 3 and 6 up to 9 a time-domain analysis was performed using an upward zero-crossing method. Herein the irregular wave time series is split up in single waves. Every time the velocity profile passed the zero value (upward) the timeserie will be split as being the start of a new single wave. When the profile goes *upward* trough the zero value again this means it is the end of the (split up) single wave. It then has already gone trough the zero value downward as well. Note that the time series is the reduced horizontal velocity signal ($u_{red}=u(t)-U_0$).

From all the single waves, an average and the mean of the highest one-third wave period values of the waves are taken for the T_{mean} and the T_s, respectively. The $u_{max,red}$ *-on* and *off*shore are the highest positive ("onshore") and the highest negative ("offshore") values of the horizontal velocity amplitudes from all the single waves, and thus the entire time series. The $u_{1/3,red}$ *-on* and offshore are the means of the highest one-third positive ('onshore') and negative ('offshore') horizontal velocity amplitudes, also from all the single waves and thus the entire time series. The U_0, which is already used for the Fourier analyses, is extracted from detrending, however it can also be calculated by taking the mean of the total horizontal velocity signal. The u_{rms} (velocity root mean square) is calculated over the total horizontal velocity signal as:

$$u_{rms} = \sqrt{\frac{1}{N}\sum_{i=1}^{N}(u_i^2)} \qquad (25)$$

with N being the horizontal velocity at every time step of the total signal. The $\langle u^2 \rangle$ and $\langle u^3 \rangle$ are the averages of the second-order and third-order of the total horizontal velocity moment.

To define the velocity skewness of the irregular horizontal velocity signal the equation from Van der Werf et al. (2006) is used:

$$R = \frac{u_{1/3,on,red}}{u_{1/3,on,red} + |u_{1/3,off,red}|} \qquad (26)$$

For symmetric (no velocity skewness) waves R equals 0.5, whereas when the mean of the highest one-third velocity at the crest is larger than at the trough, R>0.5. When R<0.5, the mean of the highest one-third velocity of the velocity at the trough is larger than that of the crest, however this is less common in nearshore propagating waves (Abreu et al., 2010).

An alternative parameter often used for the velocity skewness is Sk_u, which is defined as:

$$Sk_u = \frac{\langle u^3 \rangle}{\langle u^2 \rangle^{3/2}} \qquad (27)$$

where a value of zero corresponds to no velocity skewness.

Svendsen et al. (1978) has shown that for several measurements that breaking and surf zone waves present a sawtooth-shaped surface profile, with large values of velocity skewness and differences between crest-to-trough and trough-to-crest half periods (Torres-Freyermuth et al., 2007). This last kind of vertical asymmetry can be formulated in terms of an acceleration skewness coefficient, β, defined as (Abreu et al., 2010):

$$\beta = \frac{a_{max}}{a_{max} + |a_{min}|} \qquad (28)$$

Wherein a_{max} and a_{min} are the maximum and minimum horizontal acceleration. Acceleration wise symmetric waves present β=0.5, indicating to waves whose maximum and minimum acceleration magnitudes are equal. β>0.5 and β<0.5 indicate a larger acceleration at the crest than that at the trough and an absolute value of the acceleration at the trough than that at the crest, respectively.

An alternative parameter, which can be used for the acceleration skewness, is Sk_a, whose definition is analogous to Eq. (27):

$$\beta_{irr} = \frac{\langle a^3 \rangle}{\langle a^2 \rangle^{\frac{3}{2}}} \qquad (29)$$

where a value of zero corresponds to no acceleration skewness.

5.2 Wave modification

With the wave characteristics in section 5.1 clear, modification of an irregular wave to a representative regular wave can be done. The representation of the irregular wave in a regular wave is based on four principles: (1) the representative wave should have the same velocity skewness, (2) the peak wave period should remain the same and (3) the regular wave amplitudes of the representative wave should have the same energy as the irregular wave spectrum. Since the representative regular wave is based on keeping the velocity skewness the same, a high value for the acceleration skewness might cause significant difference in the net sediment transport, therefore the chosen time series have a β that is close to 0.5. In this research all thirteen timeseries are used.

The fourth principle (4) is that for the creation of the representative regular wave, Stokes second order solution for the horizontal velocity is used, wherein remaining the peak wave period of principle (2) is already included:

$$u(t) = \hat{u}_1 \cos\left(\frac{2\pi}{T_p} t\right) + \hat{u}_2 \cos\left(\frac{2\pi}{T_p/2} t\right) \qquad (30)$$

With the total wave energy being proportional to the amplitude squared ($E \propto u^2$), Eq. (30) and $u_{rms} = \sqrt{\langle u(t)^2 \rangle}$ (31), following that $\langle u(t)^2 \rangle = u_{rms}{}^2$ (32), it follows that the u_{rms} is held the same as well for the modification.

To derive both $\hat{u}_1$ and $\hat{u}_2$ and to produce a single representative regular wave for an irregular wave, based on Eq. (30), two different methods are used.

5.2.1 Method one: Full signal influence approach

The first method is based on the use of the entire time series in Eq. (27), for which follows that $\langle u(t)^3 \rangle = Sk_u * \langle u(t)^2 \rangle^{1.5}$ (33), and the use of an "approximation method" to derive $\hat{u}_2$.

With both the Sk_u parameter and the u_{rms} known from section 5.1 and the use of Eq. (32), following from Eq. (31), $\langle u(t)^3 \rangle$ can be calculated with Eq. (33) or can be derived by taking the time-average of the third order of the entire horizontal velocity signal (the timeseries). To be able to use the "approximation method" (explained later on) an equal equation for $\langle u(t)^3 \rangle$, including $\hat{u}_2$, is needed. This equation, Eq. (37), follows from substitution of Eq. (35) in Eq. (36):

$$\langle u(t)^2 \rangle = \frac{\int_0^{T_p} u(t)^2 dt}{T_p} = \frac{1}{2}\hat{u}_1^2 + \frac{1}{2}\hat{u}_2^2 = u_{rms}{}^2 \qquad (34)$$ (See Part VII.A Appendix VII for derivation)

which gives: $\hat{u}_1^2 = 2\langle u(t)^2 \rangle - \hat{u}_2^2$ (35)

$$\langle u(t)^3 \rangle = \frac{3}{4}\hat{u}_1^2 \hat{u}_2 \qquad (36)$$ (See Part VII.B Appendix VII for derivation)

$$\langle u(t)^3 \rangle = \frac{3}{2}\langle u(t)^2 \rangle \hat{u}_2 - \frac{3}{4}\hat{u}_2^3 \qquad (37)$$

The "approximation method" implies that the initial value of $\hat{u}_2$ within Eq. (37) is set at zero. This value is then increased with steps of 1^{-4} until the difference of the $\langle u(t)^3 \rangle$ from Eq. (37) and the $\langle u(t)^3 \rangle$ from Eq. (33) reaches a predefined accuracy, which is set at one thousandth of Eq. (33).

Once the accuracy is reached and the best $\hat{u}_2$ is found, $\hat{u}_1$ can be derived from Eq. (35) (see Table 19, Appendix VI for the values of $\langle u(t)^2 \rangle$, $\hat{u}_2$ and $\hat{u}_1$):

$$\hat{u}_1 = \sqrt{2\langle u(t)^2 \rangle - \hat{u}_2^2} \qquad (38)$$

With both regular wave amplitude components derived a validation check is done for both the velocity skewness parameters and the u_{rms}. The newly derived regular wave amplitude components are used to check whether the velocity skewness and the u_{rms} of the new to be made representative regular wave are the same as the one from its irregular wave. For the skewness parameters this is done with Eq. (26) and the "normal" velocity skewness parameter:

$$R = \frac{(u_{max})}{(u_{max}) - (u_{min})} = \frac{(\hat{u}_1 + \hat{u}_2)}{(\hat{u}_1 + \hat{u}_2) - (-\hat{u}_1 + \hat{u}_2)} = \frac{(\hat{u}_1 + \hat{u}_2)}{2\hat{u}_1} \quad (39)$$

For the velocity skewness parameter R the value is limited at 0.625. When R> 0.625 an unphysical secondary maximum appears in the wave trough (when using second-order Stokes) and higher harmonics are required to compensate for it (Malarkey, 2008). If this occurs the validity range of second order Stokes equation (Eq. (30)) is exceeded, these are made red in Table 19, Appendix VI.

For the u_{rms} this is done with:

$$u_{rms} = \sqrt{\frac{1}{2}\hat{u}_1^2 + \frac{1}{2}\hat{u}_2^2} \quad (40)$$

which follows from Eq. (32) and Eq. (34).

5.2.2 *Method two: Partial signal influence approach*

The second method is based on the use of Eq. (26), Eq. (34) and Eq. (39) to derive both $\hat{u}_1$ and $\hat{u}_2$. Herein only a part of the horizontal velocity signal is used to define the velocity skewness, namely the highest one-third of the peaks (positive/onshore). The average of the highest one-third of the peaks is used as the $u_{1/3,on,red}$ input in Eq. (26). The $u_{1/3,off,red}$ is the averaged value of the offshore (negative) directed peaks which follows directly after the used onshore (positive) directed peaks for $u_{1/3,on,red}$. To retain the same total energy of the irregular wave in the representative regular wave the $\langle u(t)^2 \rangle$ and u_{rms}(related with Eq. (32)) of the entire irregular wave signal is used.

To derive $\hat{u}_2$ Eq. (34) and Eq. (35) are used and result in:

$$\hat{u}_2 = \sqrt{2\langle u(t)^2 \rangle - \hat{u}_1^2} \quad (41)$$

To derive $\hat{u}_1$ another $\hat{u}_2$ is needed for substitution with Eq. (41). Therefore, from Eq. (39) $\hat{u}_2$ is derived as well as:

$$\hat{u}_2 = (2R - 1)\hat{u}_1 \quad (42)$$

After substitution of both $\hat{u}_2$'s (see Part VII.C, Appendix VII for substitution), $\hat{u}_1$ follows as:

$$\hat{u}_1 = \sqrt{\frac{2u_{rms}^2}{(2R-1)^2+1}} \quad (43)$$

However, although Eq. (42) has been derived from the "normal" equation for velocity skewness (Eq. (39)) the used "R" in both Eq. (42) and Eq. (43) is the "R" explained above, Eq. (26) from Van der Werf et al. (2006).

For this method a validation check for both velocity skewness parameters and the u_{rms} is done as well. This is done the same way as described for method one, in section 5.2.1.

5.3 Wave simulation set-up

With both methods resulting in the input for Stokes second order solution for the horizontal velocity, the representative regular wave signals are made (see Figure 16 for an example). The total amount of simulations for both "Flume" and "Oscillatory Flow Tunnel" simulations is now thirty-nine, and can be carried out in the relevant versions of the boundary layer model. Depending on the wave characteristics for every wave condition, the settings of the boundary layer model need to be changed, see Table 7. Most of the settings are kept the same as the initial regular input setting from Kranenburg (2013). The only settings that changed are the time interval over which the net sediment transport is calculated, the grain size (D_{50}) (kept the same for all conditions), the domain (which is kept at 2.5 times the estimated boundary layer thickness (δs)), the water depth (kept the same for all conditions), the roughness height (z_0) and the forcing method of the model.

It is chosen to use the "free" forcing method of the boundary layer model, which means that the net current arising from the streaming mechanisms is not compensated by any mean pressure gradient and the mean velocity is allowed to develop freely. For this the assumption is made that the input, the horizontal velocity signal, is the signal above the boundary layer, free stream velocity. A requirement for the forcing is that the averaged horizontal velocity U_0 is removed from the oscillating free stream velocity, therefore the $u_{red} = u(t) - U_0$ is used.

Table 7 (Part I): Flow and bed characteristics, and boundary layer model input settings of the irregular and regular wave signals. (Part II shows those of the regular wave signals)

Condition	Wave peak period T_p [s]	Grain size D_{50} [mm]	Roughness height k_s [m]	Max hor. velocity u_{max} [m/s]	Max. orbital excursion A [m]	Boundary layer thickness δs [m]	Roughness height z_o [m]	Domain [m]	Water-depth h [m]	Used force method
Irregular wave signal										
1265 (GWK08)	6.5	0.14	2.80E-04	1.27	1.31	0.02	9.33E-06	0.05	3.5	Flume-free/ Tunnel-free
1565 (GWK08)	6.5	0.14	2.80E-04	1.61	1.67	0.03	9.33E-06	0.06	3.5	Flume-free/ Tunnel-free
1575 (GWK08)	7.5	0.14	2.80E-04	1.62	1.93	0.03	9.33E-06	0.07	3.5	Flume-free/ Tunnel-free
IRRvSK (SINBAD)	6.0	0.14	2.80E-04	1.61	1.54	0.02	9.33E-06	0.06	3.5	Flume-free/ Tunnel-free
AUKE-PC (DELTARES)	6.5	0.14	2.80E-04	2.73	2.82	0.04	9.33E-06	0.09	3.5	Flume-free/ Tunnel-free

Table 7 (Part II)

Condition	Wave peak period T_p [s]	Grain size D_{50} [mm]	Roughness height k_s [m]	Max hor. velocity u_{max} [m/s]	Max. orbital excursion A [m]	Boundary layer thickness δs [m]	Roughness height z_o [m]	Domain [m]	Water-depth h [m]	Used force method
Regular wave signal										
1265 (GWK08)	6.5	0.14	2.80E-04	0.84	0.86	0.02	9.33E-06	0.04	3.5	Flume-free/ Tunnel-free
1565 (GWK08)	6.5	0.14	2.80E-04	1.03	1.07	0.02	9.33E-06	0.05	3.5	Flume-free/ Tunnel-free
1575 (GWK08)	7.5	0.14	2.80E-04	1.09	1.30	0.02	9.33E-06	0.05	3.5	Flume-free/ Tunnel-free
IRRvSK (SINBAD)	6.0	0.14	2.80E-04	1.09	1.04	0.02	9.33E-06	0.05	3.5	Flume-free/ Tunnel-free
AUKE-PC (DELTARES)	6.5	0.14	2.80E-04	1.01	1.05	0.02	9.33E-06	0.05	3.5	Flume-free/ Tunnel-free

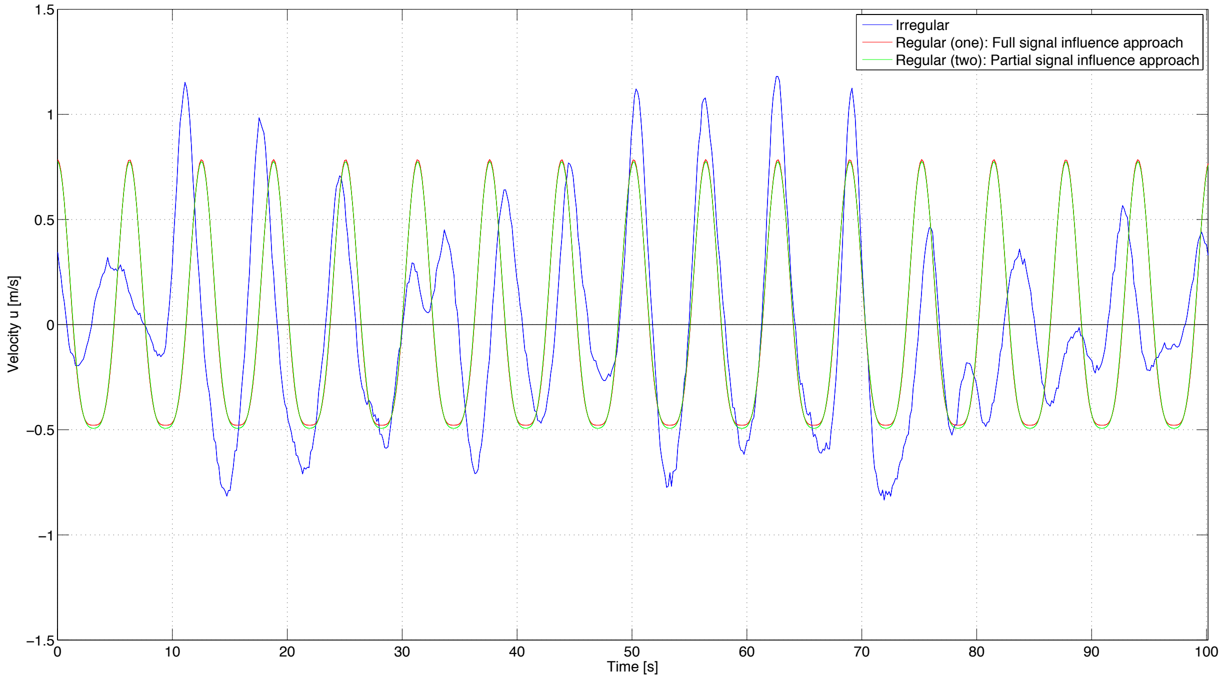

Figure 16: Irregular waves signal and the two representative regular wave signals. Example is condition 1265 (GWK08) simulation 1.

5.4 Wave simulation results

With the input settings for the boundary layer model inserted, the model has simulated the net sediment transport rates for all irregular and all regular (two methods) wave signals. The net sediment transport rates of the flume simulations, simulated by the flume version of the boundary layer model, are listed in section 5.4.1. The flume results are discussed in section 5.4.2. The net sediment transport rates of the tunnel simulations, simulated by the tunnel version of the boundary layer model, are listed in section 5.4.3. The tunnel results are discussed in section 5.4.4.

5.4.1 Flume simulations: net sediment transport

Table 8 provides the net sediment transport rates and the third-order moment of the (reduced) horizontal velocity ($<u_{red}^3>$) for the irregular wave signals and their representative regular wave signals derived in section 5.2. The reason why $<u_{red}^3>$ is used instead of $<u^3>$ is because the latter is sensitive for U_0 variations and U_0 is depending on the height of the velocity measurements (Kranenburg, 2013).

Table 8: Flume simulations; net sediment transport rates and $<u_{red}^3>$ for the irregular wave signals and their representative regular wave signal for method one (full signal influence approach) and method two (partial signal influence approach)..

Condition	Run	Wave peak period T_p	Irregular $<q_s>$ [10^{-6} m^2/s]	Irregular $<u_{red}^3>$ [m^3/s^3]	Regular method one $<q_s>$ [10^{-6} m^2/s]	Regular method one $<u_{red}^3>$ [m^3/s^3]	Regular method two $<q_s>$ [10^{-6} m^2/s]	Regular method two $<u_{red}^3>$ [m^3/s^3]
1265 (GWK08)	1	6.5	10.9	0.046	11.4	0.046	11.0	0.043
	2		11.6	0.047	15.4	0.047	15.0	0.044
	3		11.5	0.051	15.0	0.051	14.6	0.049
	4		9.5	0.044	8.6	0.044	7.6	0.036
Condition average			*10.9*	*0.047*	*12.6*	*0.047*	*12.0*	*0.043*
1565 (GWK08)	1	6.5	20.0	0.098	35.5	0.098	35.5	0.098
	2		25.7	0.083	30.9	0.083	32.3	0.096
	3		22.7	0.071	25.2	0.071	26.7	0.084
Condition average			*22.8*	*0.084*	*30.5*	*0.084*	*31.5*	*0.092*
1575 (GWK08)	1	7.5	32.0	0.090	39.9	0.090	43.1	0.123
	2		34.0	0.068	37.2	0.068	39.6	0.090
	3		40.0	0.092	42.7	0.092	41.5	0.079
	4		28.4	0.067	32.3	0.067	29.0	0.043
Condition average			*33.6*	*0.079*	*38.0*	*0.079*	*38.3*	*0.084*
IRRvSK (SINBAD)		6	32.6	0.124	34.4	0.124	33.4	0.103
AUKE-PC (DELTARES)		6.5	31.4	0.114	31.3	0.114	26.9	0.073

5.4.2 Flume simulations: results

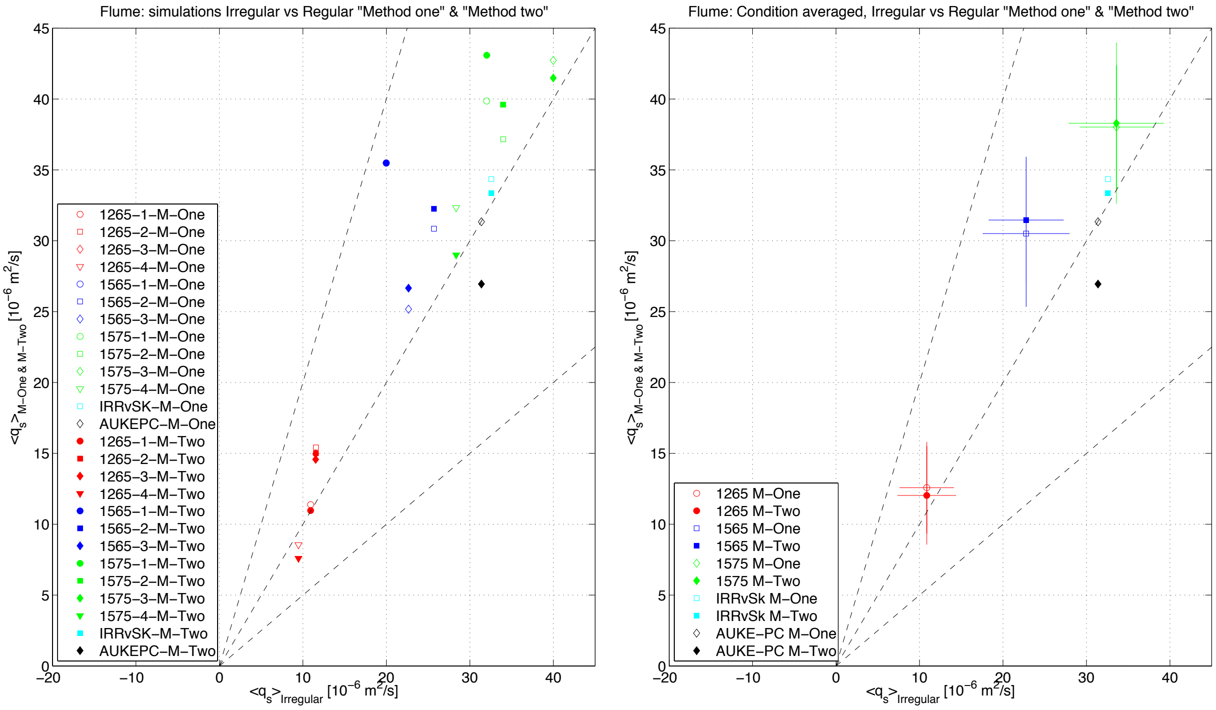

Figure 17: *Left:* Flume simulations; net sediment transport results of both "full signal influence approach" (M-One) and "partial signal influence approach" (M-Two) method versus the net sediment transport of their related irregular wave. *Right:* Flume condition averaged; net sediment transports results of both "full signal influence approach" (M-One) and "partial signal influence approach" (M-Two) method versus the net sediment transport of their related irregular wave. Dashed grey lines are the factor 0.5, 1, and 2 comparison lines (from bottom to top).

In Figure 17 (left) for every simulation (thirteen in total) the net sediment transport results of both "full signal influence approach" –and "partial signal influence approach" methods (regular waves) are compared versus the net sediment transport of their related irregular wave. Figure 17 (right) shows the condition averaged net sediment transports results of the two representative methods versus their related irregular wave. For the GWK08 conditions 1265, 1565 and 1575, respectively four, three and four simulation results are combined.

The validation of the boundary layer model for irregular waves (in a flume) in section 4 showed that the boundary layer model simulates a positive, onshore directed, net sediment transport for irregular waves, which corresponded with the experimental net sediment transport results of the echosounder profiles. Here, Figure 13, the boundary layer also shows a positive, onshore directed, net sediment transport for both the irregular and the corresponding representative regular waves. For regular waves, fine sediment conditions, Kranenburg (2013) also showed that the net sediment transport is directed in the onshore direction.

Figure 17 and Table 8 further show that for almost all simulations both representative regular wave methods give a higher net sediment transport than their related irregular wave. Only for the AUKE-PC (Deltares) simulation the "full signal influence approach" method gives an almost equal net sediment transport (slightly lower) and the "partial signal influence approach" method gives a lower net sediment transport compared to the net sediment transport of the irregular wave. For both the (condition averaged) 1265 (GWK08) and IRRvSK (SINBAD) conditions, the representative regular waves give a net sediment transport slightly higher than their related irregular wave, factor 1.03 and 1.12 (both representative regular wave methods combined) respectively. For both the condition averages net sediment transport results of the 1565 (GKW08) and 1575 (GWK08) condition it can be noticed that the overestimation of the representative regular wave methods is slightly more than the previous named conditions, factor 1.14 and 1.38 (both representative regular wave methods combined) respectively.

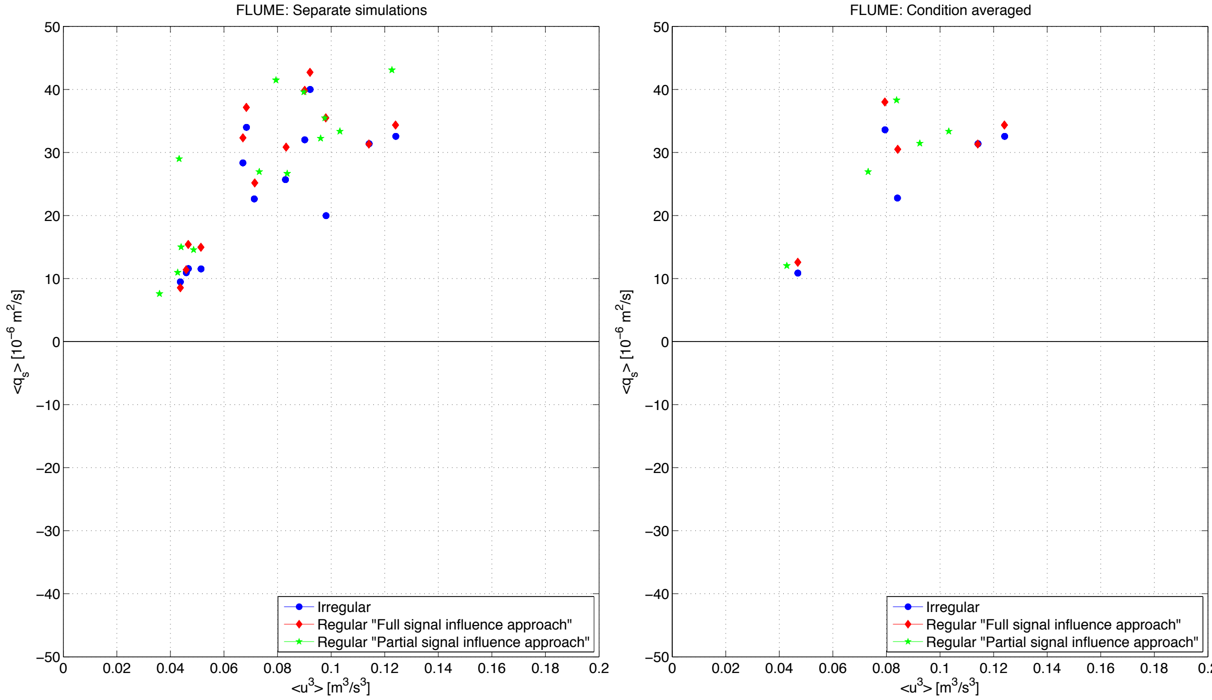

Figure 18: *Left:* Flume simulations; net sediment transport results of the irregular wave simulations and the representative regular waves of both "full signal influence approach" –and "partial signal influence approach" methods versus their $<u_{red}^3>$. *Right:* Flume condition averaged; net sediment transport results of the irregular wave simulation and the representative regular waves of both "full signal influence approach" –and "partial signal influence approach" methods versus their $<u_{red}^3>$. Dashed grey lines are the factor 0.5, 1, and 2 comparison lines (from bottom to top).

Kranenburg (2013) showed that for regular waves simulations of Schretlen (2012) and Dohmen Janssen and Hanes (2002) the net sediment transport for fine sediments in a flume are generally increasing while the third-order moment of the horizontal velocity ($<u_{red}^3>$) is increasing as well. From Figure 18 it can also be observed that for both the representative regular waves this is also valid. For the irregular waves in these flume simulations it can be observed that the net sediment transport also results in a positive, generally (with respect to outliers), increase while the $<u_{red}^3>$ is increasing.

5.4.3 Oscillatory flow tunnel simulations: net sediment transport

Table 9 provides the net sediment transport rates and the third-order moment of the (reduced) horizontal velocity ($<u_{red}^3>$) for the irregular wave signals and their representative regular wave signals derived in section 5.2.

Table 9: Oscillatory flow tunnel simulations; net sediment transport rates and $<u_{red}^3>$ for irregular wave signal and their representative regular wave signal for method one (full signal influence approach) and method two (partial signal influence approach).

Condition	Run	Wave peak period T_p	Irregular $<q_s>$ $[10^{-6}\ m^2/s]$	Irregular $<u_{red}^3>$ $[m^3/s^3]$	Regular method one $<q_s>$ $[10^{-6}\ m^2/s]$	Regular method one $<u_{red}^3>$ $[m^3/s^3]$	Regular method two $<q_s>$ $[10^{-6}\ m^2/s]$	Regular method two $<u_{red}^3>$ $[m^3/s^3]$
1265 (GWK08)	1	6.5	2.5	0.046	7.1	0.046	6.7	0.043
	2		0.8	0.047	8.7	0.047	8.2	0.044
	3		0.3	0.051	8.9	0.051	8.4	0.049
	4		4.5	0.044	6.2	0.044	5.2	0.036
Condition average			*2.0*	*0.047*	*7.7*	*0.047*	*7.1*	*0.043*
1565 (GWK08)	1	6.5	-16.5	0.098	11.9	0.098	11.8	0.098
	2		-11.0	0.083	12.8	0.083	14.5	0.096
	3		-4.1	0.071	12.4	0.071	14.1	0.084
Condition average			*-10.6*	*0.084*	*12.3*	*0.084*	*13.5*	*0.092*
1575 (GWK08)	1	7.5	-1.7	0.090	12.2	0.090	16.2	0.123
	2		2.0	0.068	9.8	0.068	12.7	0.090
	3		-1.3	0.092	11.1	0.092	9.6	0.079
	4		2.4	0.067	11.2	0.067	7.3	0.043
Condition average			*0.4*	*0.079*	*11.1*	*0.079*	*11.5*	*0.084*
IRRvSK (SINBAD)		6	-16.9	0.124	7.1	0.124	5.9	0.103
AUKE-PC (DELTARES)		6.5	-12.9	0.114	18.6	0.114	13.7	0.073

5.4.4 Oscillatory flow tunnel simulations: results

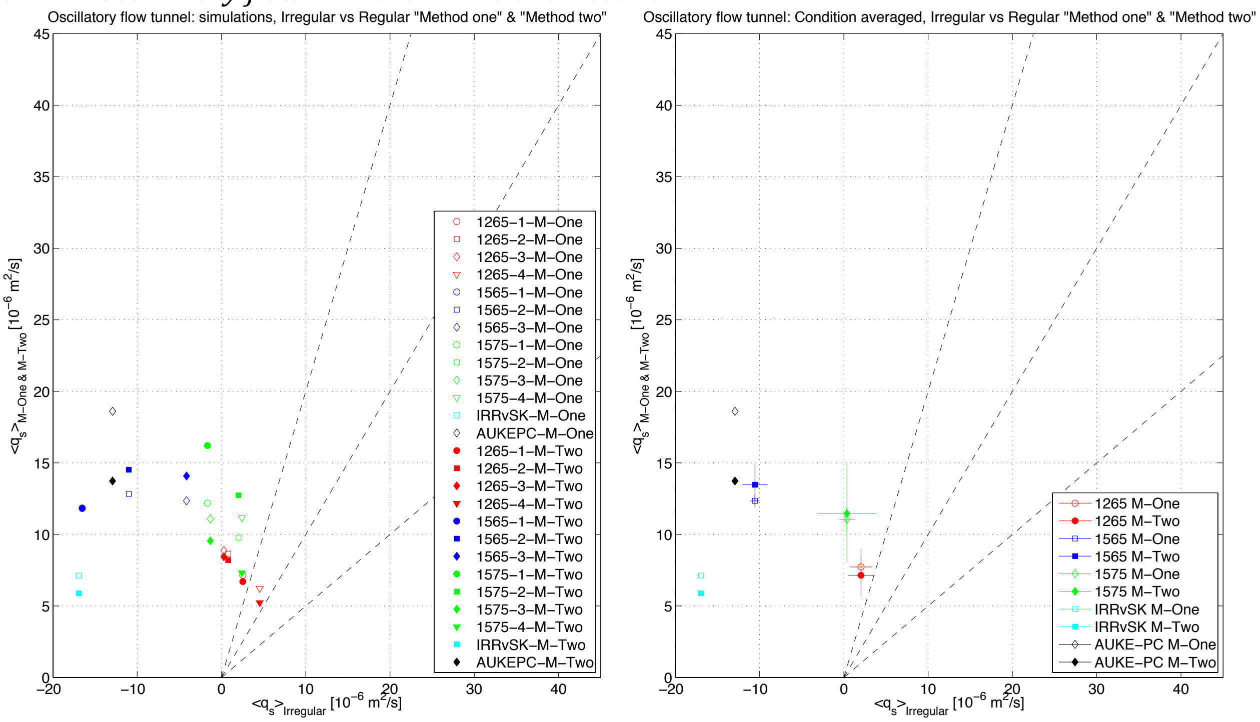

Figure 19: ***Left:*** **Oscillatory flow tunnel simulations; net sediment transport results of both "full signal influence approach" –and "partial signal influence approach" method versus the net sediment transport of their related irregular wave.** ***Right:*** **Tunnel condition averaged; net sediment transports results of both "full signal influence approach" –and "partial signal influence approach" method versus the net sediment transport of their related irregular wave. Dashed grey lines are the factor 0.5, 1, and 2 comparison lines (from bottom to top).**

In Figure 19 (left) for every simulation (thirteen in total) the net sediment transport results of both "full signal influence approach" –and "partial signal influence approach" methods (regular waves) are set up versus the net sediment transport of their related irregular wave. Figure 19(right) shows the condition averaged net sediment transports results of the two representative methods versus their related irregular wave. For the GWK08 conditions 1265, 1565 and 1575, respectively four, three and four simulation results are combined.

For the representative regular waves all the net sediment transports are positive, onshore directed. For the 1265 (GWK08), IRRVSK (SINBAD) and the AUKE-PC (Deltares) conditions the regular waves of the "partial signal influence approach" method show a net sediment transport which is slightly lower than the regular waves of the "full signal influence approach" method. For the irregular waves the direction of the net sediment transport differs for almost all conditions. Except for the (condition averaged) 1265 (GWK08) and 1575 (GWK08) conditions the net sediment transports are all negative, indicating an offshore net sediment transport. For the 1575 (GWK08) condition the net sediment transport is almost negligible, however the single simulation results on the left side of Figure 19 show that within the condition simulations there is both an on- and offshore directed net sediment transport. For the 1265 (GWK08) condition all results are onshore directed.

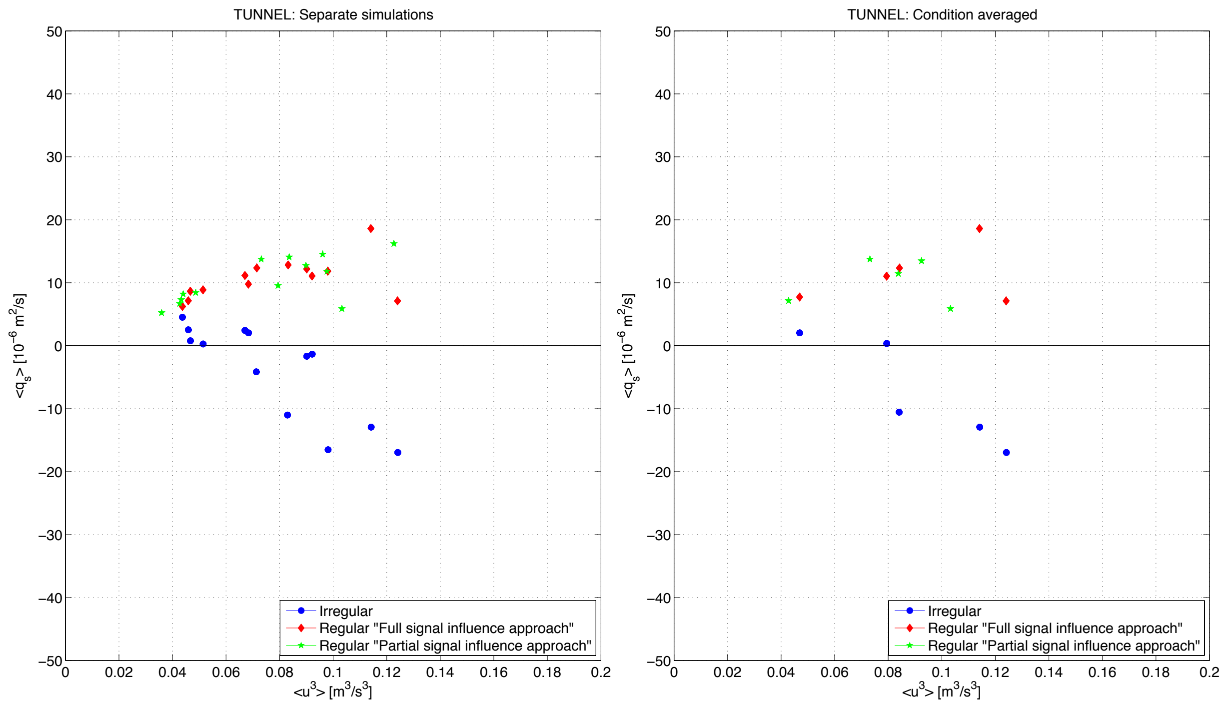

Figure 20: ***Left:*** **Oscillatory flow tunnel simulations; net sediment transport results of the irregular wave simulations and the representative regular waves of both "full signal influence approach" –and "partial signal influence approach" methods versus their $<u_{red}^3>$.** ***Right:*** **Tunnel condition averaged; net sediment transport results of the irregular wave simulations and the representative regular waves of both "full signal influence approach" –and "partial signal influence approach" methods versus their $<u_{red}^3>$. Dashed grey lines are the factor 0.5, 1, and 2 comparison lines (from bottom to top).**

Beside the net sediment transport results of Kranenburg (2013) for the flume simulation (fine sediment), tunnel simulations were also performed for regular waves. For the regular waves it was observed that the net sediment transport will increase with an increasing $<u_{red}^3>$, followed by a transition from onshore to offshore transport when the $<u_{red}^3>$ becomes ~0.15m^3/s^3 or higher. In Figure 20 the net sediment transport results of both the regular waves are tending to deflect, however, the range of the $<u_{red}^3>$ from the used simulations is only reaching a maximum of 0.124m^3/s^3. Therefore it can be assumed that the transition from onshore to offshore transport will occur when the $<u_{red}^3>$ of the regular waves is higher. For the irregular waves however the results have similarity with Kranenburg (2013) regular wave results (fine sediment) in an oscillatory flow tunnel. Figure 20 shows that with an increasing $<u_{red}^3>$ the net sediment transport of the irregular waves at first starts to increase. *Note that it* *is assumed here that for a* $\langle u_{red}^3 \rangle$ *smaller than the most left blue circle in the condition averaged graph, the net sediment transport is lower (or is higher and becomes lower with an even smaller* $\langle u_{red}^3 \rangle$*, based on the fact that the net sediment transport of the second blue circle in the condition averaged graph is lower than its previous)*. It then reaches a maximum and is decreasing again with a continuing increasing $\langle u_{red}^3 \rangle$. The net sediment transport will then encounter a transition from onshore to offshore-directed transport. The difference with the regular wave simulations of Kranenburg (2013) however is that the transition of these irregular waves tends to occur with a smaller $\langle u_{red}^3 \rangle$, ~0.08 m^3/s^3 compared to ~0.15m^3/s^3.

5.5 Conclusion

Based on both the net sediment transport results and their comparison versus their $\langle u_{red}^3 \rangle$ it can be concluded that for the *flume simulations* the boundary layer model produces the net sediment transports for both the representative regular waves in a good way compared to their irregular related waves. They are all directed in the same, onshore, direction and are all close to the factor 1.0 comparison line.

The net sediment transport results in the *oscillatory flow tunnel* showed that the transport direction of the regular waves is the opposite of the irregular wave transport, offshore compared to onshore. From the comparison of the net sediment transport with the related $\langle u_{red}^3 \rangle$ it can be concluded that for both irregular and regular wave simulations follow a same curve as described by Kranenburg (2013) for regular waves. However, for irregular waves the simulations show that the transition from onshore to offshore-directed net sediment transport is occurring faster compared to observations done for regular waves simulations. The presumption is that phase lag processes in the irregular wave signals might play a more important role than for regular waves and might be the reason why there is a faster occurring transition. The difference(s) and the/its origin(s) is/are therefore elaborated in section 6.

When comparing both used representative regular wave methods, the key difference between the two is that the velocity skewness is defined in a slightly different way, but the total wave energy is the same in both methods. Both the net sediment transport results and the comparison with their $\langle u_{red}^3 \rangle$ showed that this does not provide any significant differences between the two results. The net sediment transport results of the second method, "partial signal influence approach", for both flume and oscillatory flow tunnel simulations, show a larger deviation compared to the results of the irregular wave for both flume and oscillatory flow tunnel simulations. Therefore it can be concluded that the "full signal influence approach" method is a better representative regular wave for the irregular wave, so far.

6. Irregular and regular-wave process differences and relations, in and between oscillatory flow tunnel and flume simulations.

The phase lag influence presumption resulting from the irregular and regular wave oscillatory flow tunnel observations, done in section 5, is supported by research of Ribberink et al., (2008), who stated that large phase lag in concentrations play an important role in the intra-wave horizontal sediment flux. However, allthough the results in the research do come from oscillatory flow tunnel experiments, the experiments involved assymetric flow (i.e. velocity-skewed flow with zero acceleration skewness, β=0) for *regular waves* only.

In this section the phase lag effect for a irregular wave condition compared to its representative regular wave condition is further examined. However, since the second method, the "partial signal influence approach", in section 5 did not prove to be bring significant differences compared to the first method, the "full signal influence approach", a new third method is introduced first in section 6.1. The goal of this third method is to achieve a better representative regular wave for the irregular wave signal in the *oscillatory flow tunnel,* since the first method can already be seen as a good representative regular wave for the irregular wave signal in *flume simulations*.

After the introduction of the new method, the first method, introduced in section 5, and the new third method will be used to examine the differences and relations in processes, including phase lag effect, between irregular and the representative regular waves in a closer perspective (section 6.2 and 6.3) for oscillatory flow tunnel simulations. The differences and relations between the flume simulations and the oscillatory flow tunnel simulations will be examined in section 6.4.

6.1 Method three: high wave, signal influence approach

This third method, for representing an irregular wave signal in a single regular wave, is a modification of the "full signal influence approach" method. Instead of defining the velocity skewness and wave energy separately, only the wave energy of one-third of the highest velocity wave peaks (onshore: $u_{1/3,on,red}$ and offshore: $u_{1/3,off,red}$, *note that the reduced (red) velocity signal is used*), instead of using the same total energy as in the total irregular wave signal, which was included in the u_{rms}, is used to define the two velocity components, $\hat{u}_1$ and $\hat{u}_2$, and to define the velocity skewness with Eq. (26).

The $u_{1/3,on,red}$ and $u_{1/3,off,red}$ both include the two velocity components, $\hat{u}_1$ and $\hat{u}_2$, as used in Stokes second-order solution for the horizontal velocity, as follows:

$$u_{1/3,on,red} = \hat{u}_1 + \hat{u}_2 \tag{44}$$

$$|u_{1/3,off,red}| = \hat{u}_1 + \hat{u}_2 \tag{45}$$

Substitution of both Eq. (44) and Eq. (45) (see Part VII.D, Appendix VII,) results in:

$$\hat{u}_1 = \frac{1}{2}|u_{1/3,off,red}| + \frac{1}{2}u_{1/3,on,red} \tag{46}$$

$$\hat{u}_2 = \frac{1}{2}u_{1/3,on,red} - \frac{1}{2}|u_{1/3,off,red}| \tag{47}$$

Using the same changes in the wave simulation set-up as described in section 5.3 and the boundary layer input settings in Table 10, the new representative regular wave can be made and simulated for both flume and oscillatory flow tunnel simulations in the boundary layer model. *Note that for these simulations a time step of 0.5seconds is used for the boundary layer model to calculate the net sediment transport, instead of the repetition time that was used in section 5.* An example of the AUKE-PC irregular and the two, method one and method three, regular waves is plotted in Figure 21. The net sediment transport results of the three wave signals, including the new method, are also listed in Table 11 for both flume and oscillatory flow tunnel simulations.

Table 10: Flow and bed characteristics, and boundary layer model input settings of the regular wave signal by the "high wave signal influence approach" method, (method three).

Condition	Wave peak period T_p [s]	Grain size D_{50} [mm]	Roughness height k_s [m]	Max hor. velocity u_{max} [m/s]	Max. orbital excursion A [m]	Boundary layer thickness δs [m]	Roughness height z_o [m]	Domain [m]	Water-depth h [m]	Used force method
AUKE-PC (DELTARES) Method 3	6.5	0.14	2.80E-04	1.32	1.37	0.02	9.33E-06	0.06	3.5	Flume-free/ Tunnel-free

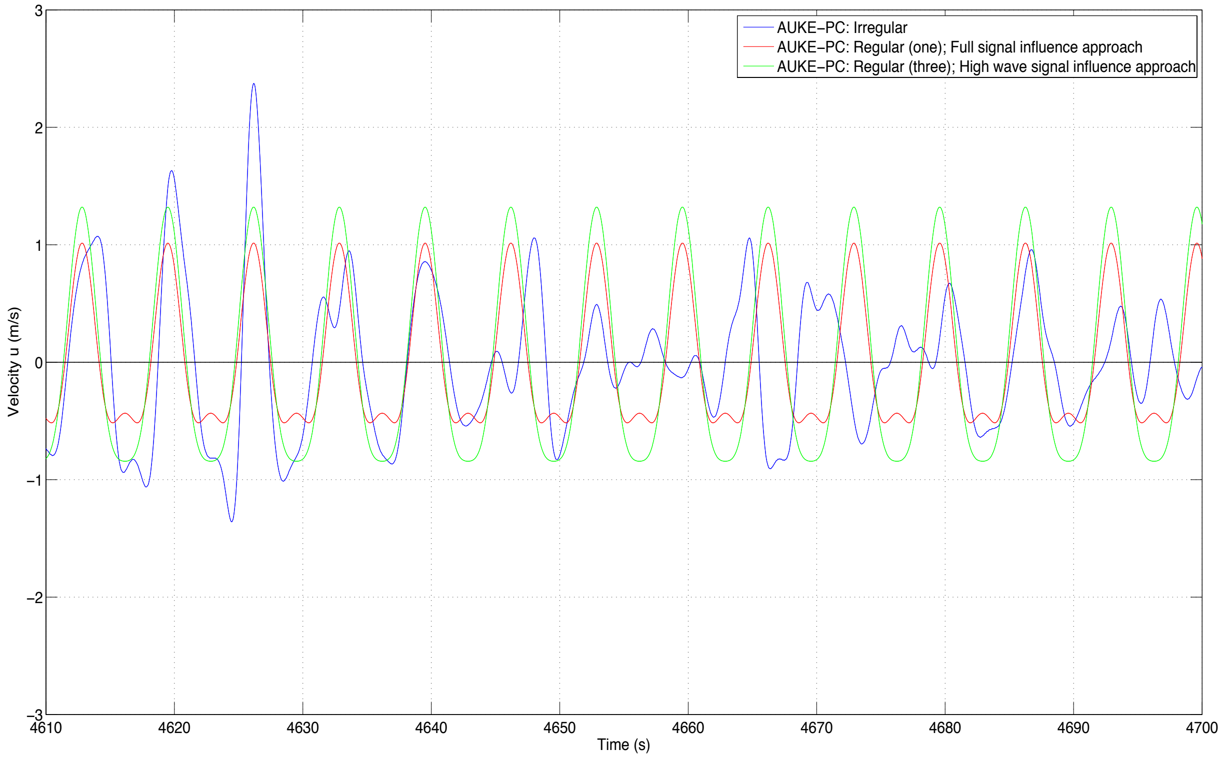

Figure 21: AUKE-PC irregular and methods one and three representative regular waves signals. Timescale zoomed to 4600-4700s out of 4600-5000s.

Table 11: Oscillatory flow tunnel and flume simulation net sediment transport rates for method one and method three.

Simulation	Irregular $<q_s>$ $[10^{-6}\ m^2/s]$	Regular method one $<q_s>$ $[10^{-6}\ m^2/s]$	Regular method three $<q_s>$ $[10^{-6}\ m^2/s]$
Oscillatory flow tunnel	-15.5	16.5	-19.3
Flume	29.2	28.9	56.9

6.2 Intra-wave differences between irregular and regular-waves in oscillatory flow tunnel simulations

As Eq. (19) in section 3.1 shows, the boundary layer model calculates the net sediment transport by taking a time averaged of a double integration over a height above the bed and over a time period, from the horizontal velocity in the entire boundary layer multiplied by the concentration in the entire boundary layer.

6.2.1 Intra-wave horizontal sediment fluxes

When one examines the sediment transport equation closer it is found that the sediment transport is coming from intra-wave horizontal sediment fluxes (Φ), and is a combination of (phase-averaged) horizontal particle velocities and concentrations (Ribberink et al., 2008):

$$\varphi(z,t) = u(z,t)C(z,t) \qquad (48)$$

Both the horizontal velocity (u(z,t)) and concentration (C(z,t)) can be decomposed in time-averaged and oscillatory component as:

$$u(z,t) = \langle u(z) \rangle + \tilde{u}(z,t) \qquad (49)$$

$$C(z,t) = \langle C(z) \rangle + \tilde{C}(z,t) \qquad (50)$$

Combining Eq. (49) and Eq. (50) in Eq. (48) and time averaging the flux results in a net averaged sediment flux distribution (*Φ*(z,t)) and its current-related and wave-related components:

$$\varphi(z,t) = \varphi_{current\ related} + \varphi_{wave\ related} = \langle u(z) \rangle * \langle C(z) \rangle + \langle \tilde{u}\ (z,t) * \tilde{C}(z,t) \rangle \qquad (51)$$

6.2.2 *Total sediment flux*

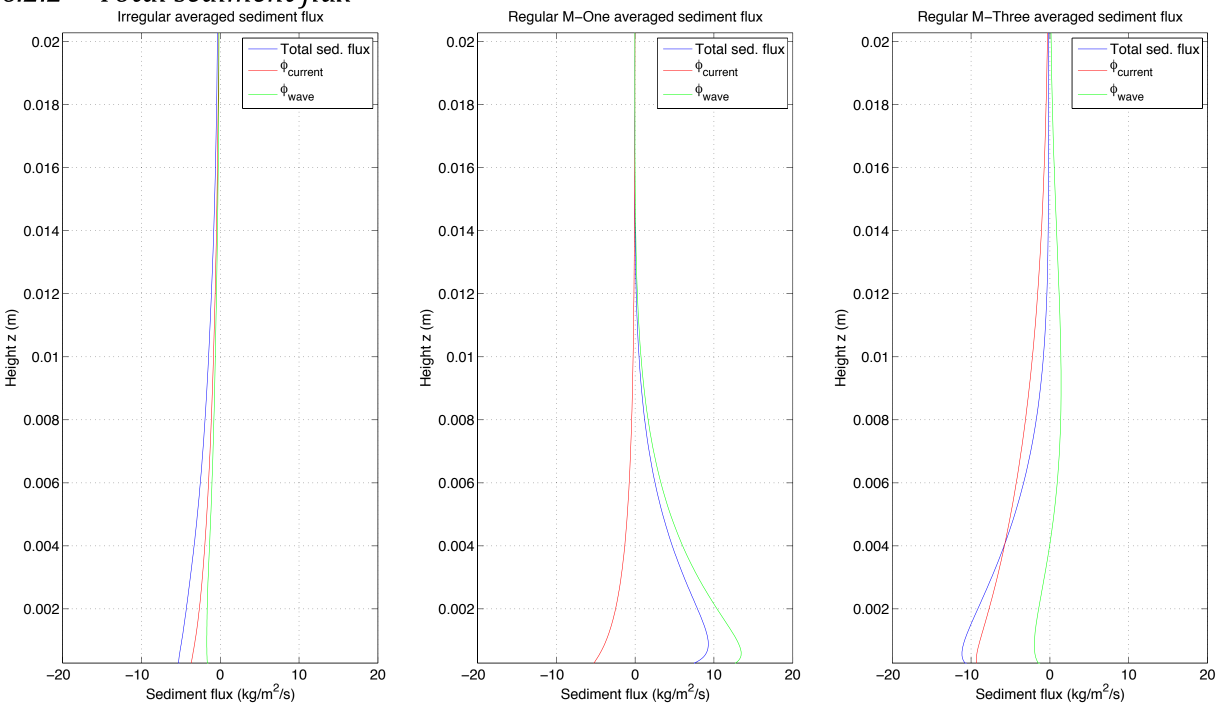

Figure 22: Oscillatory flow tunnel: Total net sediment flux and its current and wave-related components for the irregular wave signal (AUKE-PC condition) left; and its two representative regular wave signals in the middle and on the right (M-One referring to the "full signal influence approach" method and M-Three referring to the "high wave, signal influence approach" method).

Figure 22 shows the *total* sediment flux and its wave and current-related components for the irregular and both representative regular waves by methods one and three. The total sediment flux is calculated as Eq. (51) describes for which the first term, the current-related component, is determined as $\varphi_{current} = \langle u(z) \rangle * \langle C(z) \rangle \quad (52)$, Figure 23 shows this current related component for the *vertical profile* of the irregular and both representative regular waves. The wave-related component is the subtraction of the current-related component of the total sediment flux.

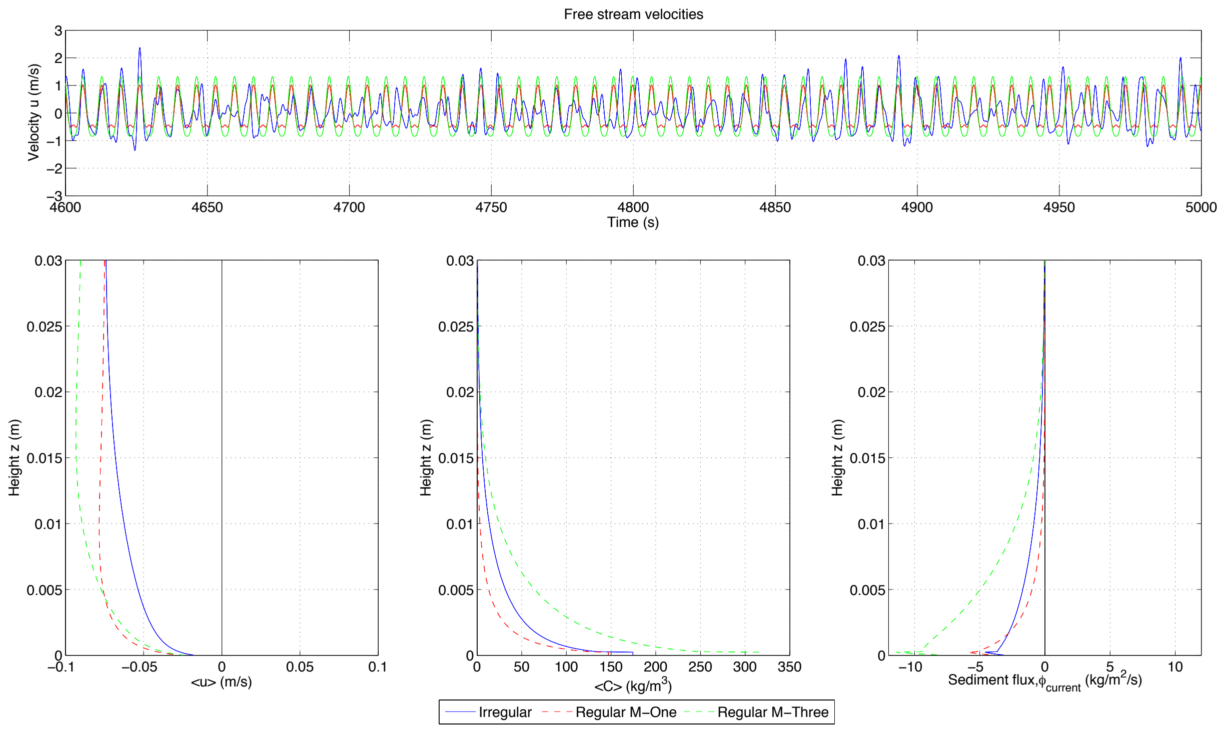

Figure 23: Current-related fluxes. *Top*: Free stream velocities for the last 400 seconds of the irregular wave signal (AUKE-PC condition) and the two representative regular wave signals, used for the <u>, <C> and sediment flux$_{current}$. *Left*: vertical profile of the horizontal period averaged velocity signals. *Middle*: Vertical profile of the period averaged sediment concentrations. *Right*: Vertical profile of the period averaged sediment flux$_{current}$. (M-One referring to the "full signal influence approach" method and M-Three referring to the "high wave, signal influence approach" method)

The top graph of Figure 23 shows the free stream velocity profile for the three wave signals. The left graph shows the horizontal period averaged velocities for the lowest part of the boundary layer, where the signal is becoming less negative (towards zero) while closing towards the seabed, and shows a small overshoot for the method one regular wave. The middle graph shows the period averaged sediment concentrations where in all simulations the sediment concentration is increasing while closing towards the seabed. What can be seen is that for a real small layer, from just above the seabed at z= $2.8{*}10^{-4}$ m towards the seabed, the sediment concentration drops vertically and stays around 175kg/m^3 for the remaining $2.8{*}10^{-4}$ m towards the seabed. This is the result of the sediment concentration boundary condition at the bottom of the boundary layer set in the boundary layer model. Herein the sediment concentration balance of Eq. (17) is solved using a no-flux condition at the top of the boundary and a pick-up function is used at the reference height $z=z_a=2{*}D_{50}$. The sediment concentration in the remaining layer (between z=0 and the reference height z_a) is kept constant, $c(z) = c|_{z=z_a}$ is applied. This does not influence the total simulated transport for fine sediment as was found by Hassan and Ribberink (2010) in research with a suspension model with bed load formula to model the flux beneath $z=2{*}D_{50}$. Finally, the right graph shows the current related sediment flux, a multiplication of the previous two graphs as described in Eq. (52).

For the regular wave of method three it can be observed that all, absolute, rates in the three lower graphs of Figure 23 are bigger than those of the irregular wave and regular wave method one, which corresponds with the higher amount of energy included in method three.

Note that the small deviation in the current related sediment flux close to the seabed is caused by the transition of the simulations by the boundary layer model and the boundary condition. Therefore the vertical height profile in Figure 22 *is given from the reference height ($z=z_a=2{*}D_{50}$) until halfway the estimated boundary layer thickness, see Appendix V.*

With Figure 23 showing that the current-related sediment fluxes are all directed in the same direction and follow the same curve (and magnitudes of irregular and method one are approximately the same), and Figure 22 showing that the total sediment flux is directed different for the regular wave of method one compared to the irregular, it can be concluded that the difference in the net sediment transport direction between irregular and regular waves in the oscillatory flow tunnel simulations is related to the wave-related component in the intra-wave horizontal sediment flux. However, Figure 22 also shows that based on the total sediment flux and the net sediment transports in Table 11, the new introduced representative regular wave, method three, represents the irregular wave better in case of the oscillatory flow tunnel simulations. For the flume simulations the net sediment transports in Table 11 proves that this does not apply.

6.3 Wave-related component influence(s)

Now it is clear for the oscillatory flow tunnel simulations in which sediment flux component the sediment transport direction difference between irregular and regular waves the origin is found, the presumption from section 5, that phase lag effect might play a (more) important role for irregular waves than for regular waves, is further examined for *oscillatory flow tunnel simulations*. This is done by comparing the sediment concentrations profiles of the irregular and representative regular wave signals and relating the differences and relations to the influence(s) of the wave signal (free stream velocity, bed shear stress, velocity skewness).

For the irregular and the representative regular wave signals (method one and three) the sediment concentrations and the bed shear stresses are plotted in Figures 24, 25 and 26 (irregular, regular method one and regular method three respectively) for the time range between seconds 4610 and 4640 of the AUKE-PC wave signals. Here the variety between high and low horizontal velocity waves is better visible than in other parts of the AUKE-PC irregular wave signal. The sediment concentrations are also given for three different heights, 1mm-3mm-5mm, above the seabed for the irregular wave signal and the two representative regular wave signals (method one and method three), in Figures 27, 28 and 29 respectively.

Note that the vertical scale differs due to the fact that the sediment concentration in Figure 24 is shown for two-third of the irregular wave estimated boundary layer thickness and in Figure 25 and 26 for two-third of the regular wave estimated boundary layer thickness. The bed shear stress vertical scale for the irregular wave also differs from the regular wave signal.

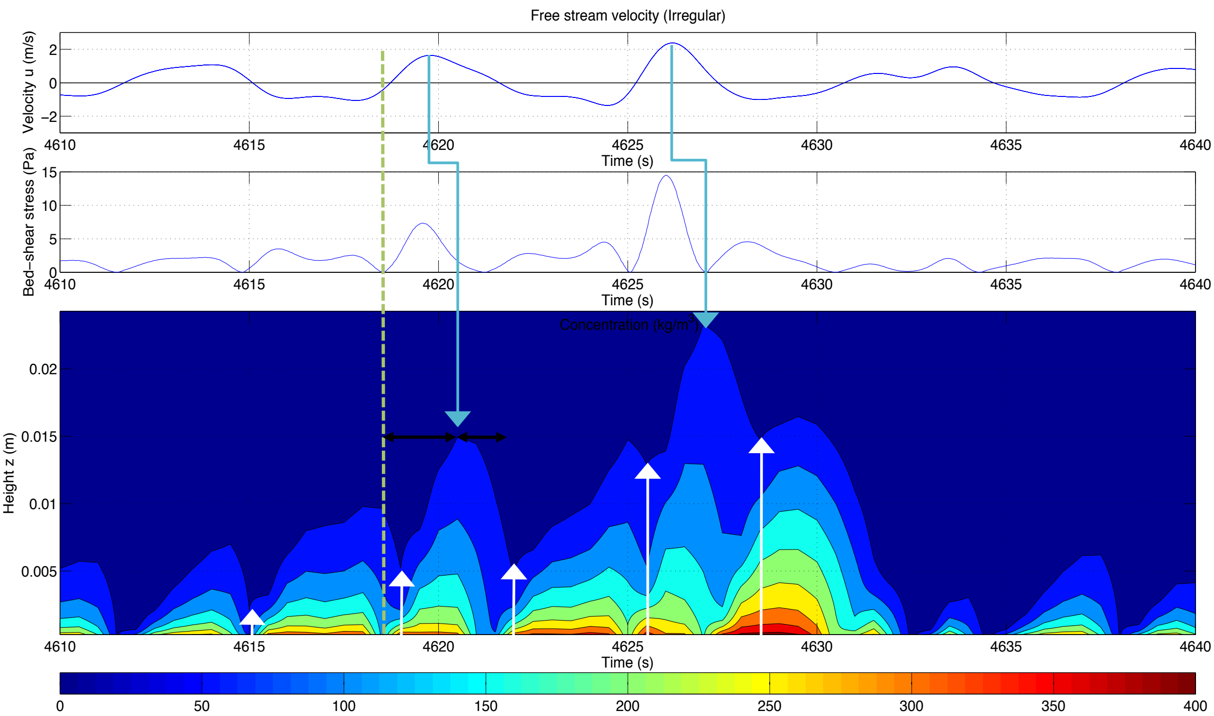

Figure 24: Oscillatory flow tunnel, irregular wave (AUKE-PC condition): *Top*: Free stream velocity for the time range between seconds 4610 and 4640. *Middle:* Bed shear stress. *Bottom*: Sediment concentration profile for the vertical height (z) range between the reference height (z_0) and two-third of the irregular wave estimated boundary layer thickness.

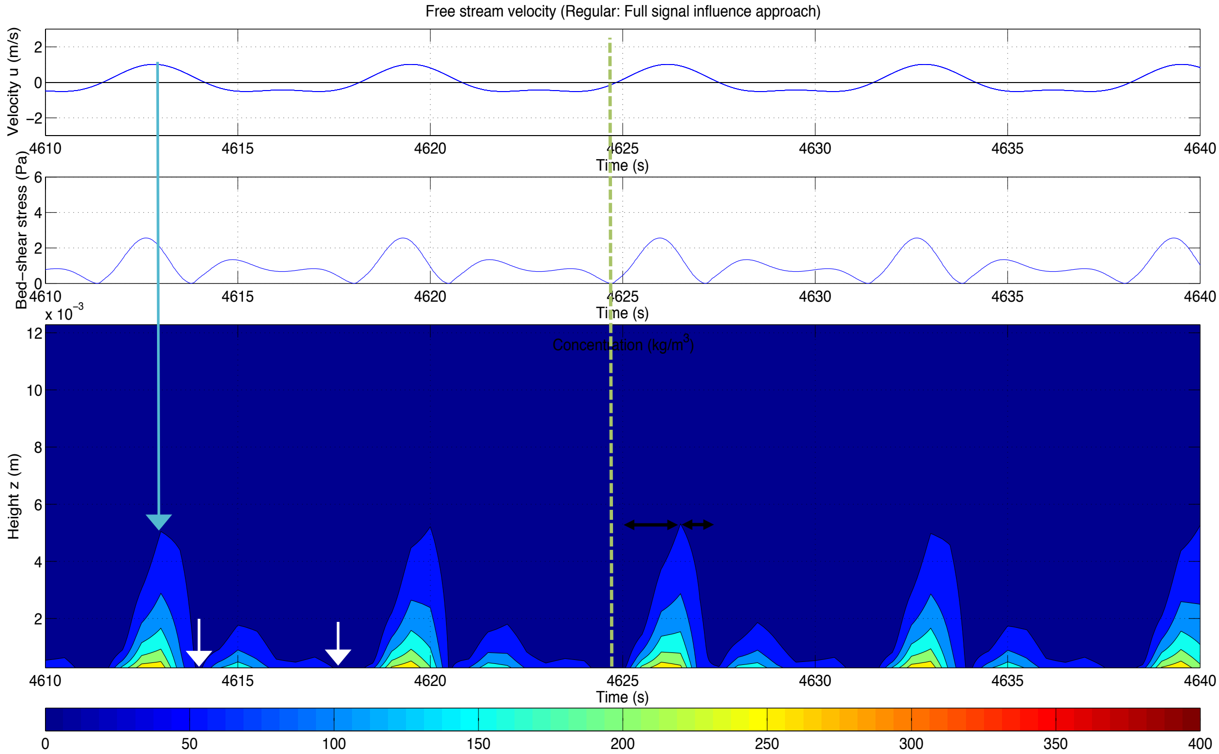

Figure 25: Oscillatory flow tunnel, regular wave signal (method one; "full signal influence approach") (AUKE-PC condition): ***Top*****: Free stream velocity for the time range between seconds 4610 and 4640.** ***Middle:*** **Bed shear stress.** ***Bottom*****: Sediment concentration profile for the vertical height (z) range between the reference height (z_0) and two-third of the regular wave estimated boundary layer thickness.**

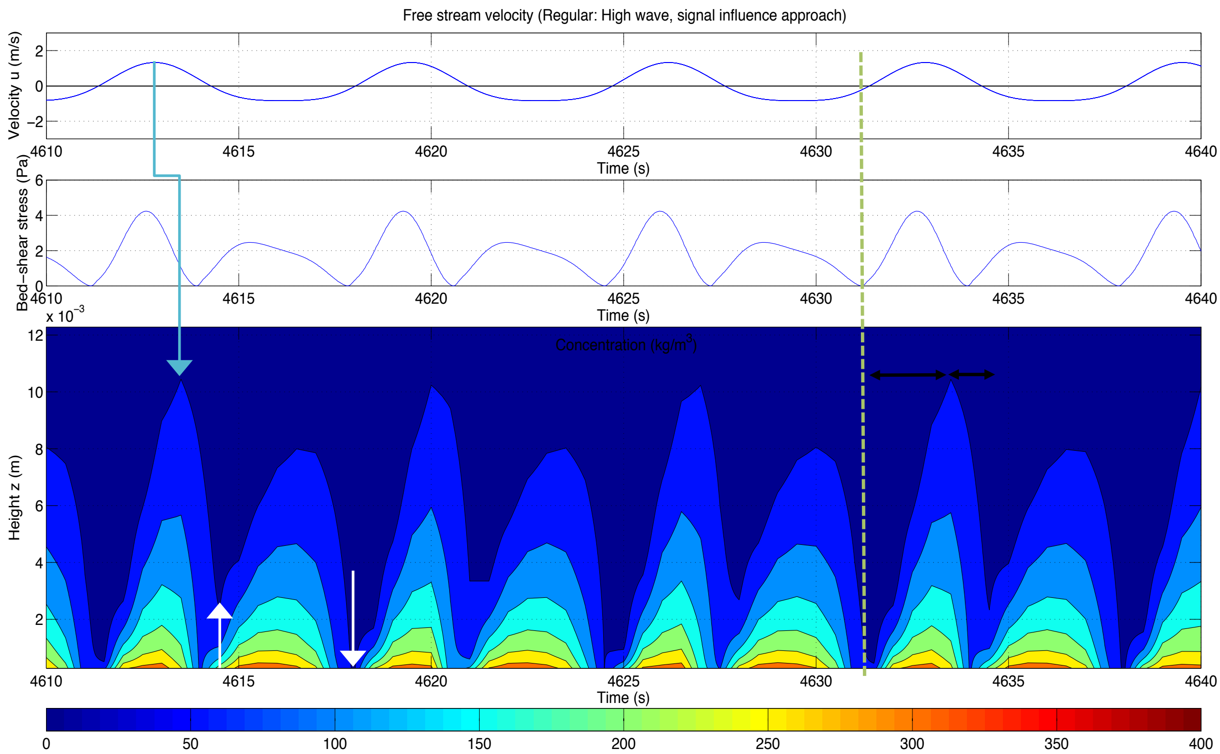

Figure 26: Oscillatory flow tunnel, regular wave signal (method three; "high wave, signal influence approach") (AUKE-PC condition): ***Top*****: Free stream velocity for the time range between seconds 4610 and 4640.** ***Middle:*** **Bed shear stress.** ***Bottom*****: Sediment concentration profile for the vertical height (z) range between the reference height (z_0) and two-third of the regular wave estimated boundary layer thickness.**

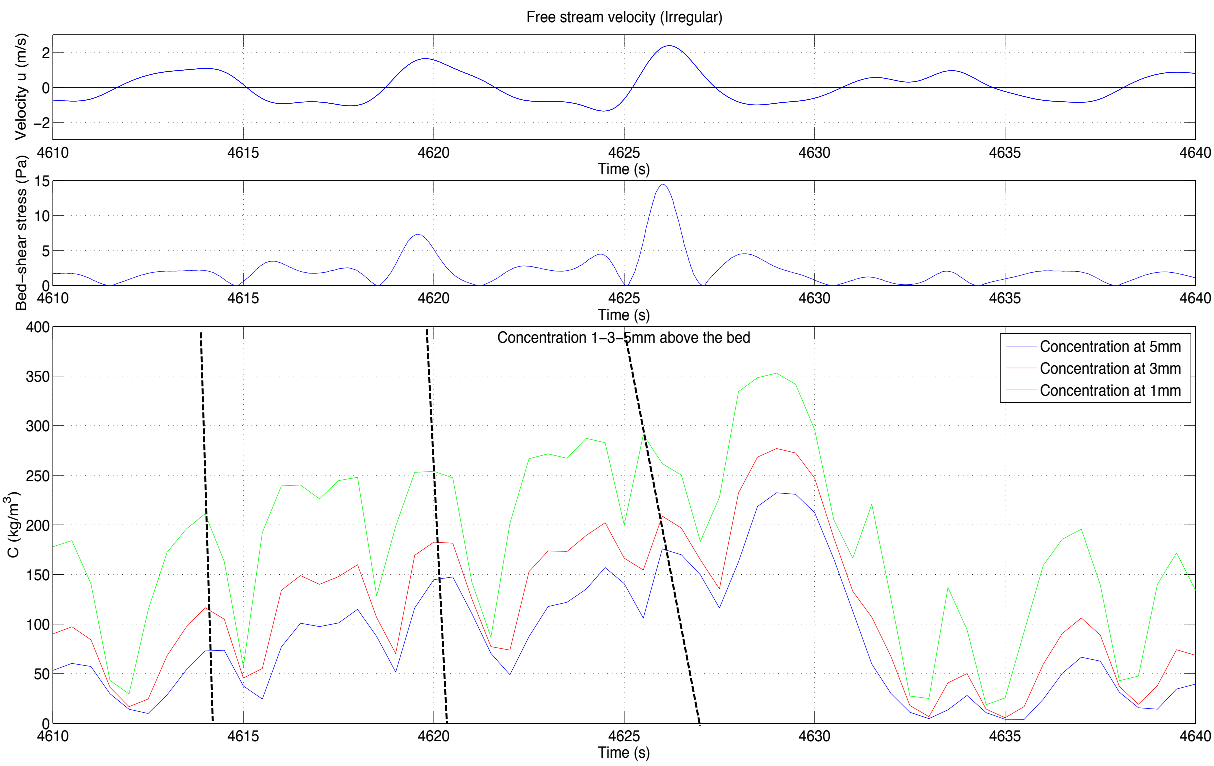

Figure 27: Oscillatory flow tunnel, irregular wave (AUKE-PC condition): *Top*: Free stream velocity for the time range between seconds 4610 and 4640. *Middle:* Bed shear stress. *Bottom*: Sediment concentration for 1mm, 3mm and 5mm above the seabed; green line, red line and blue line respectively.

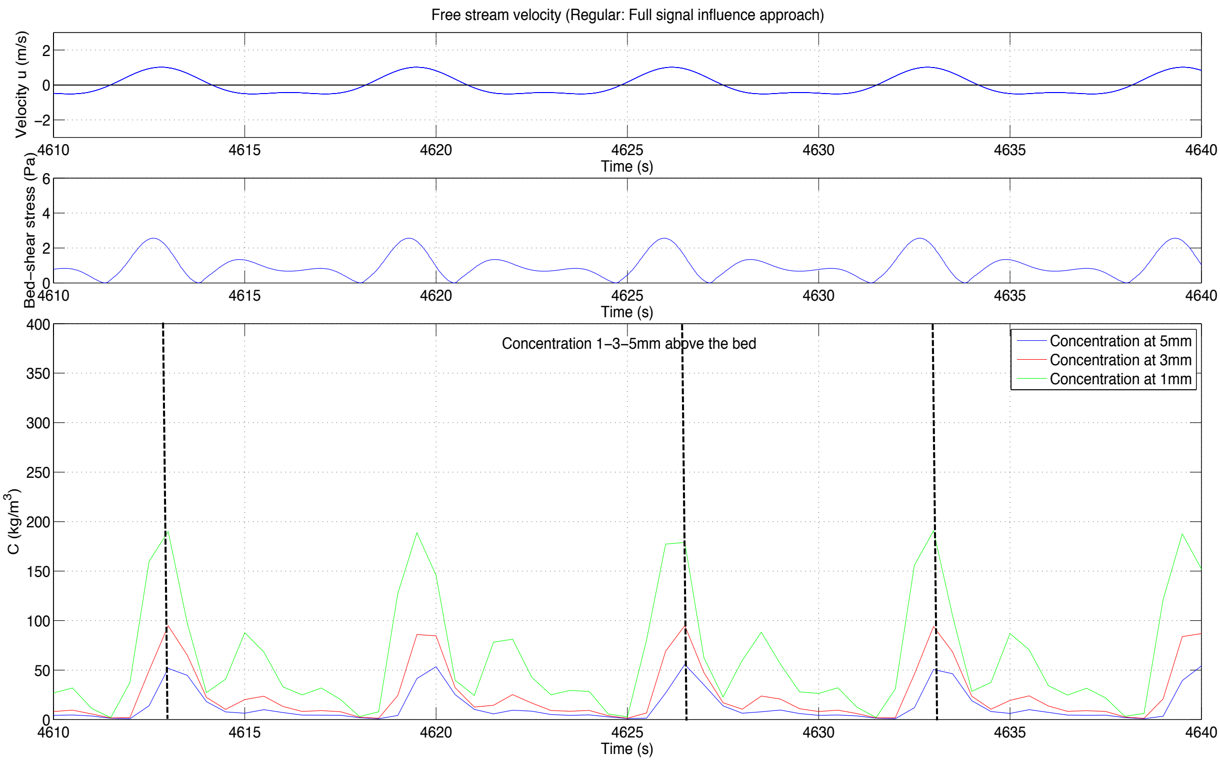

Figure 28: Oscillatory flow tunnel, regular wave signal (method one; "full signal influence approach") (AUKE-PC condition) for the time range between seconds 4610 and 4640. *Middle:* Bed shear stress. *Bottom*: Sediment concentration for 1mm, 3mm and 5mm above the seabed; green line, red line and blue line respectively.

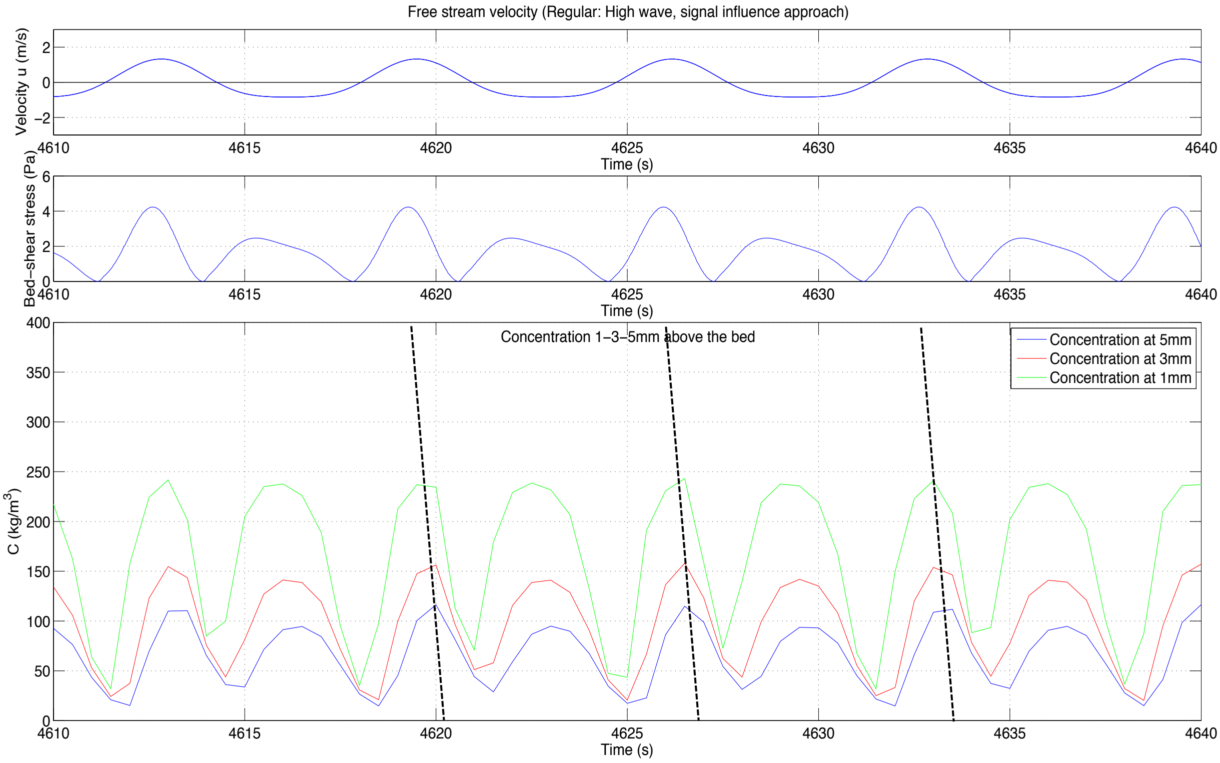

Figure 29: Oscillatory flow tunnel, regular wave signal (method three; "high wave, signal influence approach") (AUKE-PC condition) for the time range between seconds 4610 and 4640. *Middle:* Bed shear stress. *Bottom*: Sediment concentration for 1mm, 3mm and 5mm above the seabed; green line, red line and blue line respectively.

6.3.1 Sediment suspension-and settling time

In Figures 24, 25, 26 and Figure 30 the *green dashed line* shows that for all wave signals the pick up of the sediment at the bottom is related to the bed shear stress at the bottom. It also shows that the bed shear stress is slightly ahead in phase compared to the free stream velocity (the bed shear stress is already increasing again while the free stream velocity is still decreasing), see the *green arrows* in Figure 30. The *blue lines* in the figures also show that for the irregular and regular (method three) wave signals there is a lag between the maximum free stream velocity and the maximum sediment concentration and an even bigger lag between the maximum bed shear stress and the maximum sediment concentration. However, for the regular wave of method one it does not seem to show this lag. The *black dashed lines* in Figures 27, 28 and 29 also show this lag and can be explained by the fact that between the pick up of sediment and the maximum sediment concentration, the stress needs to spread out its influence to the layers above, which needs time and is depending on the magnitude of the free stream velocity (more time needed for larger free stream velocity). This can be seen very well at the irregular wave signal, where different onshore directed flow magnitudes of single waves show different time ranges, indicated by the skewness of the *black dashed lines* in Figure 27, compared to the same repeating time in Figure 28 and 29, indicated by the less skewed *black dashed lines.*

The *black arrows* in Figure 24, 25 and 26 show that for all wave signals the time for a single wave (onshore directed flow) to reach the maximum sediment concentration is larger than the time needed for the sediment to settle down to the seabed again. This time to settle the sediment down is depending on the fall velocity (w_s) of the sediment grains, which is related to the grain size (D_{50}) and the time it takes for the maximum free stream velocity to reach zero velocity and change direction, onshore to offshore or offshore to onshore.

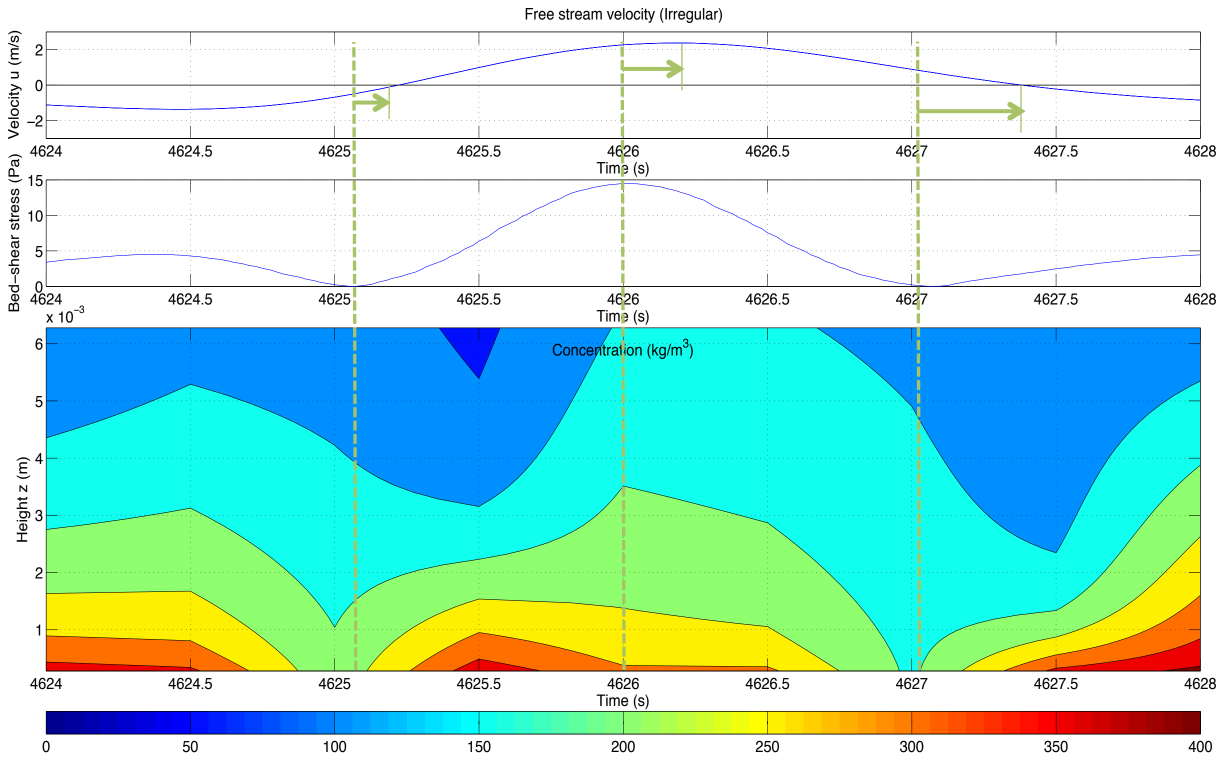

Figure 30: Zoomed result plot between second 4624 and 4628, oscillatory flow tunnel, irregular wave (AUKE-PC condition): *Top:* Free stream velocity. *Middle:* Bed shear stress. *Bottom:* Sediment concentration profile. Green arrows indicate examples of the phase lead of bed shear stress compared to the free stream velocity.

6.3.2 Phase lag and sediment pumping

In Figure 24, 25 and 26 the white arrows show that not for all wave signals there is enough time for the sediment to settle down all the way to the seabed again. For the regular wave, method one (Figure 25), it can be seen that after the onshore directed flow (positive free stream velocity) the sediment concentration is ~25kg/m^3 at 1mm above the seabed (Figure 28) and after the offshore-directed flow (negative free stream velocity) the sediment concentration is zero. A real small phase lag occurs between the transition from onshore to offshore, however the amount of sediment from the onshore directed flow that is taken with the following offshore transport is negligible since the magnitude of the onshore directed sediment is larger than that of offshore (higher sediment concentration due to higher free stream velocity). It also confirms that the net sediment transport is onshore, positive, directed.

For the regular wave, method three (Figure 26), after the onshore-directed flow (positive) a much larger remaining sediment concentration is present, ~85kg/m^3 at 11mm above the seabed (Figure 29). After the offshore-directed flow (negative) there is a remaining sediment concentration as well, ~40kg/m^3 at 1mm above the seabed. Both remaining sediment concentrations indicate that a phase lag occurs. Although Figure 26 shows a higher sediment concentration due to the onshore-directed flow, the offshore-directed flow has a longer period due to velocity skewness (wider sediment concentration profile) and therefore takes more sediment offshore than the onshore-directed flow takes onshore. This confirms the negative net sediment transport result of method three.

For the irregular wave signal (Figure 24), after all the on-and offshore directed flows of the single waves, between second 4612 and second 4632, a remaining sediment is present, see the *white arrows*. However, as for the regular waves the amount of remaining sediment concentration is the same after each onshore and after each offshore-directed flow, for the irregular wave the remaining sediment concentration increases after each single wave, an accumulation occurs. Vincent and Hanes (2002) named this phenomenon in the boundary layer "pumping" of sediment and finds its occurrence during a sequence of high waves. With the sequence of high waves, the phase lag effects and the pumping effect, the net sediment transport is directed offshore since the period of negative (offshore) flow is larger with velocity-skewed waves than the period of positive (onshore) flow.

6.3.3 Conclusion

Although shown that the pumping effect plays an important role with a sequence of high waves, the pumping effect will not be noticeable when there is a sequence of low waves in the irregular wave signal and will thus not be present during the entire wave signal. It therefore cannot be fully concluded that both the phase lag and pumping effects determine that the net sediment transport is always offshore directed, also see Table 9 in section 5.4.3. The "high wave, signal influence approach" method however, did show that with higher regular velocity skewed waves (more wave energy than in the original irregular wave signal) the phase lag effect does occur and that due to the velocity skewness (flattened offshore flow) of the wave the sediment is transported offshore. Although it *seems* that the constant returning phase lag in the regular wave signal, of method three, compensates the alternation of 'the presence of both phase lag and pumping effect (high wave sequence)' and 'neither of the two (low wave sequence)', it can be concluded that the regular wave signal of this third method shows more similarity with the irregular wave signal and is a better representation for oscillatory flow tunnel simulations than the first method, the "full signal influence approach".

The presence of phase lag and the pumping effect however, might suggest that the sequence of (higher) waves in a wave group contributes to determination of the final net direction of the sediment transport. In section 7 this suggestion is examined closer.

6.4 Oscillatory flow tunnel and flume simulation relation

In section 5.4 and in Table 11 it was found and shown that for *flume simulations* there is hardly any difference between the net sediment transport of the irregular wave (*including phase lag*) and the representative regular wave of method one (*without phase lag*); they are both onshore directed and only differ $0.3*10^{-6}$ m^2/s, which is negligible.

It was also found that for oscillatory flow tunnel simulations method one resulted in a onshore net sediment transport while irregular waves mainly resulted in an offshore net sediment transport for the same oscillatory flow tunnel simulations. Research (section 6.1-6.3) with a new representative regular wave method and on intra-wave horizontal fluxes showed that the difference between the irregular wave (*including phase lag*) and the regular wave (method one, *without phase lag*) in *oscillatory flow tunnel simulations* is related to the wave-related component of the intra-wave horizontal sediment flux. For this wave-related component itself it was found that the phase lag effect plays an important role on the net sediment transport direction in oscillatory flow tunnel simulations, which was confirmed by the third method. However, as Table 11 shows, method three does not result in a satisfying net sediment transport result for the flume simulation since it is almost twice the amount of the irregular wave signal.

Although the phase lag effect is present in the irregular wave signal in the oscillatory flow tunnel simulations, it should therefore also be present in the flume simulations. Figure 31 and 32 show that for these flume simulations the wave-related sediment flux changes from offshore to onshore. The current-related sediment flux however, also changed from offshore to onshore. What else can be observed is that for the regular wave of method three the wave-related sediment flux (and the total sediment flux) also changed from offshore to onshore and the current-related sediment flux becomes less offshore (almost zero).

Research of Kranenburg (2013) showed that for regular waves the horizontal sediment advection ($u\partial c/\partial x$) and the vertical momentum advection ($w\partial u/\partial z$) processes have a clear influence on the net sediment transport rates trough onshore contribution to the net sediment flux over the entire vertical. With it, it was also shown that the contribution of the horizontal sediment advection to the net sediment flux was largely related to the wave-related component and the contribution of the vertical momentum advection to the current-related component (see "M-one and M-three regular $\varphi_{current}$" in Figure 32). From the research it was also concluded that the vertical sediment advection ($w\partial c/\partial z$) and the horizontal momentum advection ($u\partial u/\partial x$) processes do lead to onshore fluxes, in higher parts of the boundary layer, and offshore fluxes in the lower parts of the boundary layer, however only contributed in only small effects on the net sediment transport.

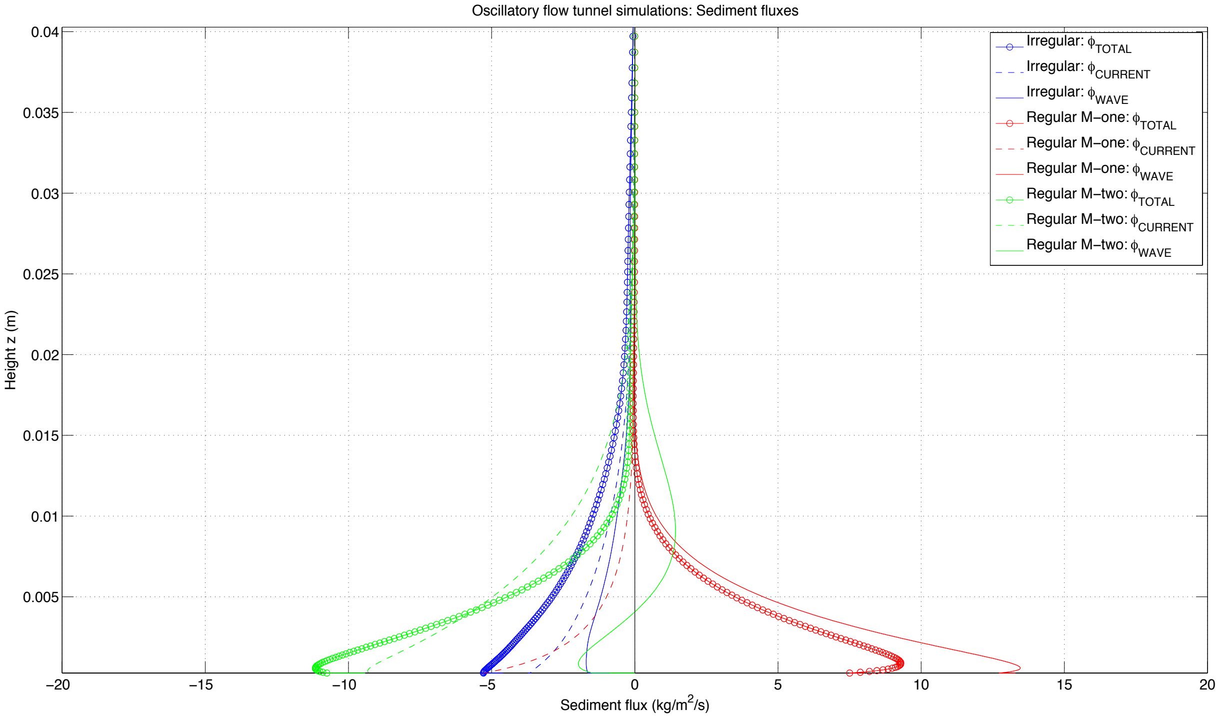

Figure 31: Oscillatory flow tunnel simulations: Averaged total net sediment flux (circled line), -current-related sediment flux (dashed line) and -wave-related sediment flux (solid line) for the irregular wave signal (blue), regular wave signal method one (red) and regular wave signal method three (green) (AUKE-PC condition).

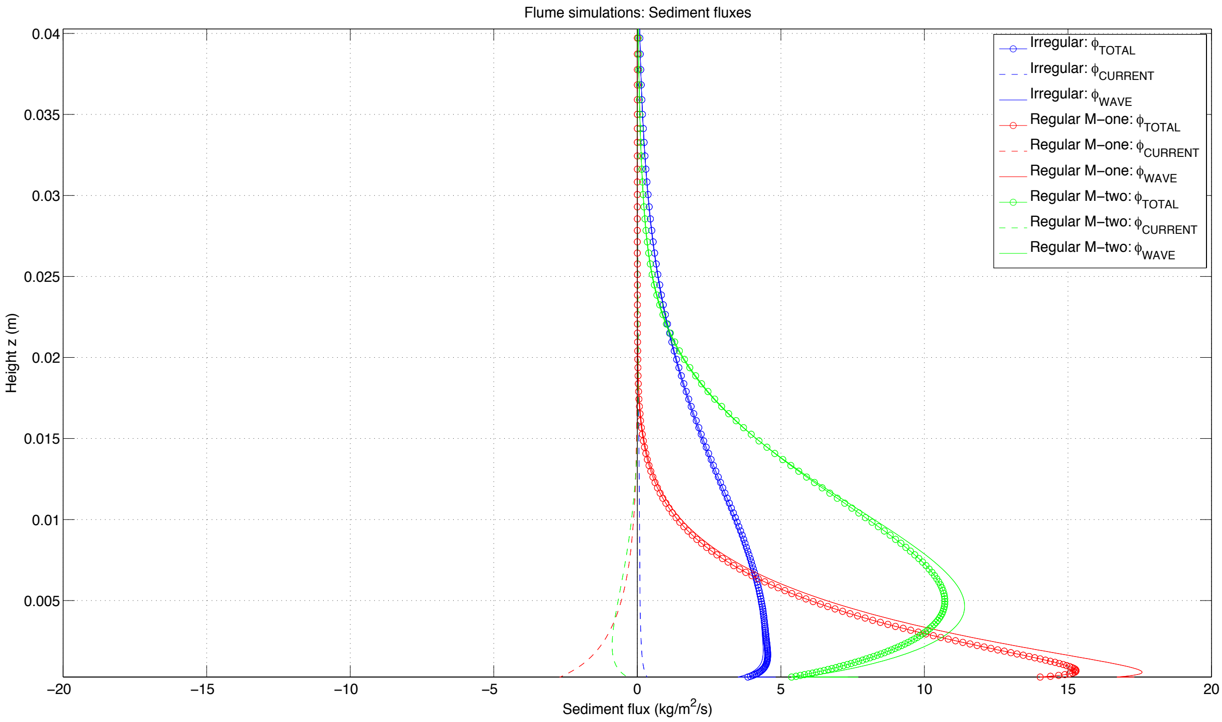

Figure 32: Flume simulations: Averaged total net sediment flux (circled line), -current-related sediment flux (dashed line) and -wave-related sediment flux (solid line) for the irregular wave signal (blue), regular wave signal method one (red) and regular wave signal method three (green) (AUKE-PC condition).

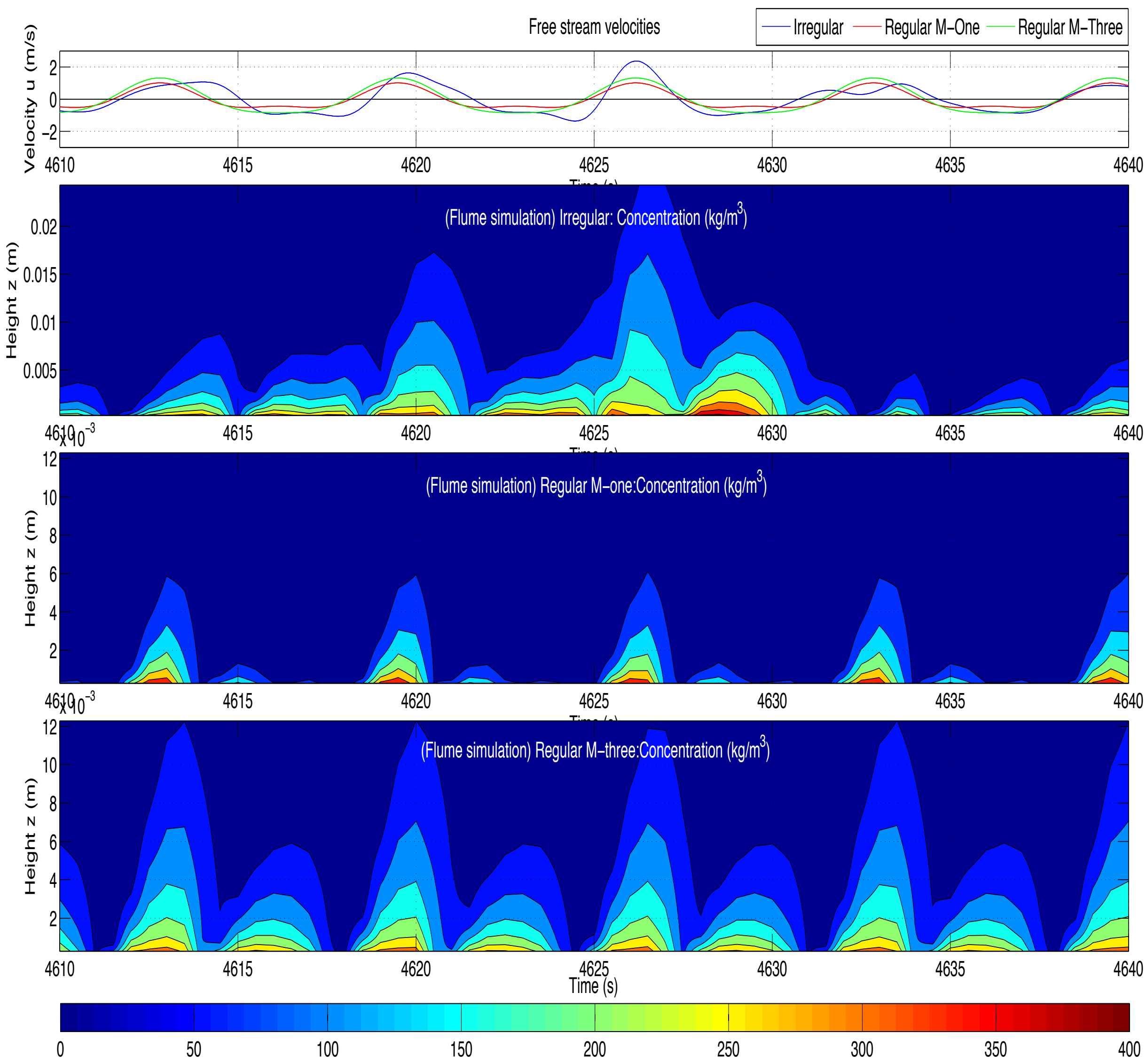

Figure 33: Flume simulations: Sediment concentration profiles of the irregular (second panel) and both regular waves (method one (M-one); third panel and method three (M-three); fourth panel), and their free stream velocities (first panel) for comparison with Figure 24, 25 and 26.

6.4.1 Conclusion

From Figure 32 (current-related components) it can be seen that the vertical momentum advection is becoming *less* important with an increasing wave energy (method three) or when the wave signal is irregular. But the vertical sediment advection and the horizontal momentum advection do get *more* important with a regular wave with more wave energy (and phase lag) and with an irregular wave (also with phase lag) and can be seen in the following; for both the irregular wave and the regular wave of method three an overshoot is appearing (for the regular wave of method three this is already present but the absolute value is getting larger) and the sediment flux in higher boundary layers becomes more important.

Kranenburg (2013) stated that the vertical orbital motion contributes to onshore transport trough *vertical sediment advection* and introduces a difference between the on- and offshore phase of the wave: at the reversal of the flow from on- to offshore, the orbital motion will be downward, while it will be upward during off- to onshore flow reversal. This becomes relevant for the sediment concentration when grains are stirred up to levels where the vertical velocity $\tilde{w}$ is in the order of the grain settling velocity w_s, and results in the fact that the concentration at these levels will decrease faster after the onshore flow and slower after the offshore flow. The faster decrease of the sediment concentration after onshore flow can be seen when comparing Figure 33 (sediment concentration profiles of the flume simulations) with Figure 24, 25 and 26 (sediment concentration profiles of the oscillatory flow tunnel simulations; especially the irregular wave and regular wave of method three) and in fact decreases the amount of phase lag and also the contribution to the pumping effect occurring for irregular waves (amount of sediment concentration due to offshore flow), resulting in more onshore-directed sediment transport.

For the representative regular wave of method three it can be concluded that for oscillatory flow tunnel simulations higher wave energy and the resulting phase lag effect is of importance, but for flume simulations the higher wave energy seems to allow to much sediment in the higher parts of the boundary layer *or* the offshore flow has been flattened out to much resulting in less offshore transport.

7. Influences of wave group skewness in an oscillatory flow tunnel

As the suggestion in section 6.3.3 notes, the phase lag and pumping effect occurring in a certain sequence of high waves (in a wave group) may contribute to the net direction of the sediment transport for oscillatory flow tunnel simulations with fine sediment. Research on wave group influence with irregular waves showed that for coarse sediment an increased transport of sediment in the propagation direction occurs (Sato, 1992; section 2.3.2). However, for fine and medium sediment conditions and for different wave groups (skewed wave groups) research is scarce. Therefore, in this section the influence of wave group skewness with fine (D_{50}=0.16mm) and medium (D_{50}=0.26mm) sediment conditions is examined for oscillatory flow tunnel simulations. In section 7.1 the boundary layer model input conditions (different group wave signals) and their simulation set-up are elaborated. The net sediment transport rates are shown in section 7.2 and will be discussed in section 7.3.

7.1 Boundary layer model input conditions and simulation set-up

The SINBAD project department in Aberdeen, Scotland provided four wave group signals. One regular wave group with velocity skewed waves and three different irregular skewed wave groups; an irregular single wave velocity skewed group (also referred as "normal" irregular wave group), an irregular single wave velocity skewed waxing group and an irregular single wave velocity skewed waning group. The regular wave group is held as the representative wave group (by the SINBAD department in Aberdeen, Scotland) for the "normal" irregular wave group and is used as a comparison signal for the different wave groups. The "normal" irregular wave group will be held as a reference signal for the two waxing and waning wave groups. Both the waxing and waning wave group are modifications of the irregular velocity skewed wave group. The *waxing* wave group consists of a steeper/faster growth of the high waves and the *waning* wave group consists of a more gradual growth of the high waves (Figure 34). Table 12 provides characteristics of the different wave conditions (as provided by SINBAD, Aberdeen).

Table 12: Wave conditions and wave characteristics skewed wave groups and regular wave group.

Wave	Type/ method	u_{rms}	T	r	phi	M	N	R	Sk
Irregular Vel. SK	**SINBAD**	0.632	6	0.36	-1.57	1.55	10	0.603	0.492
Irregular Vel. SK WAXING	**SINBAD**	0.629	6	0.374	-1.57	1.55	10	0.603	0.492
Irregular Vel. SK WANING	**SINBAD**	0.635	6	0.355	-1.57	1.55	10	0.603	0.473
Regular Vel. SK	**SINBAD**	0.632	6	0.431	-1.57		10	0.613	0.493

Herein the u_{rms} is the velocity root mean square, T is the wave period, r is the index of skewness or nonlinearity from Abreu et al. (2010), phi the phase from Abreu et al. (2010), N is the number of single waves within the wave group, M is the amplitude parameter of the modulating signal, which in this case is sine wave amplitude that modulates the signal. Additionally the R, velocity skewness parameter for regular waves; Eq. (26), and the Sk, velocity skewness parameter used for irregular waves; Eq. (27), are added.

The regular velocity skewed wave group input signal and the different irregular velocity skewed wave group input signals; waxing, waning and the normal velocity skewed wave group, are shown in Figure 34.

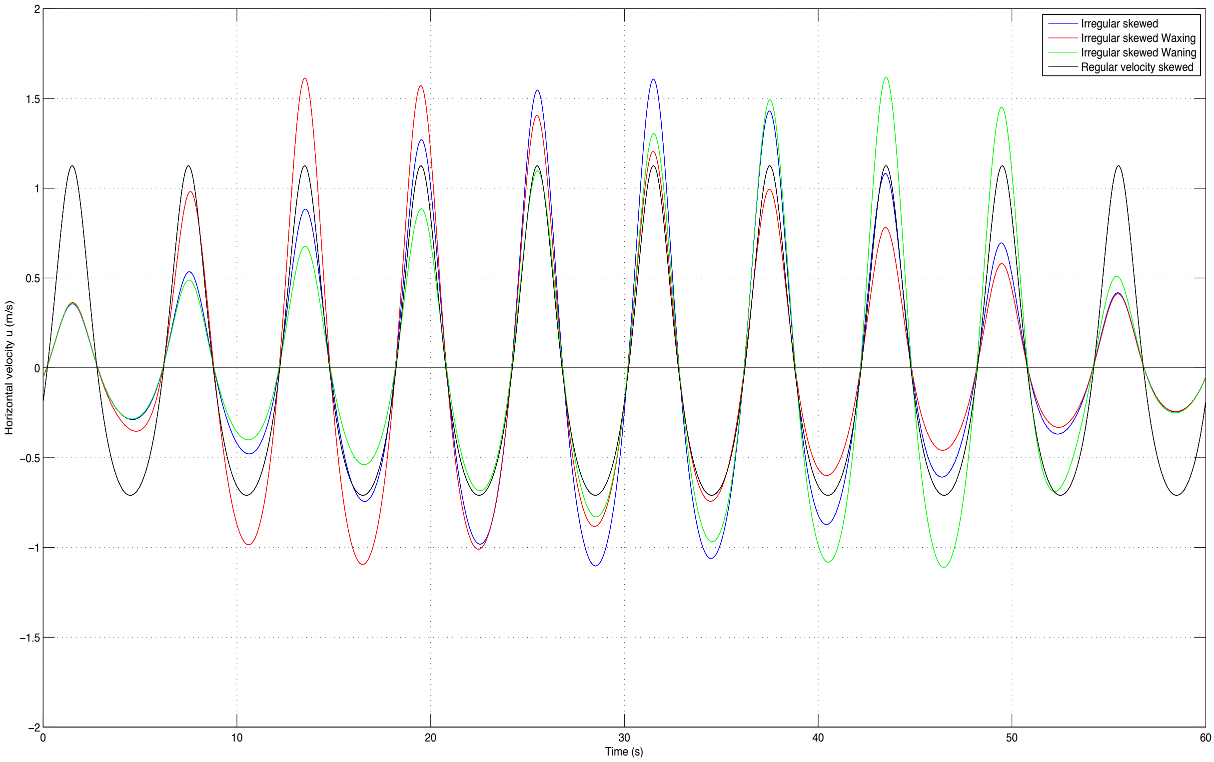

Figure 34: Regular velocity skewed wave group, irregular skewed wave group, irregular skewed waxing wave group and irregular skewed waning wave group.

To give the net sediment transport, simulated by the boundary layer model, more time to adapt and reach a consistent output, the group wave signals are repeated ten times each. The boundary layer model now has 600seconds of timeseries, including 10 wave groups for each condition. The boundary layer model will determine the net sediment transport over the final two wave groups. Most of the input settings of the boundary layer model are kept the same as for previous simulations. The only settings that changed are the time interval, the grain size (D_{50}), the estimated boundary layer thickness (δ_s), domain, roughness height (z_0) and the used forcing method of the model is "free", see Table 13.

Table 13: Flow and bed characteristics, and boundary layer model input settings, skewed wave groups.

Condition	Wave (group) period T_p / T_{gr} [s]	Grain size D_{50} [mm]	Roughness height k_s [m]	Max hor. velocity u_{max} [m/s]	Max. orbital excursion A [m]	Boundary layer thickness δs [m]	Roughness height z_o [m]	Domain [m]	Water-depth h [m]
Fine	6 / 60	0.16	3.20E-04	1.54	1.61	0.03	1.07E-05	0.06	Tunnel-free
Medium	6 / 60	0.26	5.20E-04	1.54	1.61	0.03	1.73E-05	0.07	Tunnel-free

7.2 Net sediment transport

The net sediment transport results of the four wave group conditions, each for fine and medium sediment, are shown in Table 14.

Table 14: Net sediment transport results for the skewed wave groups. Fine and medium sediment conditions in oscillatory flow tunnel simulations.

Oscillatory flow tunnel: *<q_s>* [*10⁻⁶ m²/s*]			
	D_{50}:	0.16mm	0.26mm
Wave group	Sediment condition:	Fine	Medium
Irregular, single wave velocity skewed, ("normal") wave group		-8.4	14.4
Irregular, single wave velocity skewed, *waxing* wave group		-8.0	14.5
Irregular, single wave velocity skewed, *waning* wave group		-6.4	15.0
Regular, single wave velocity skewed, wave group		13.1	15.6

7.3 Wave group skewness process observations

In this section, the differences between the sediment conditions are discussed first, followed by the discussion, and an (expected) explanation, of the net sediment transport results for each skewed wave group.

7.3.1 Sediment condition

When comparing the net sediment transport rates of the fine and medium sediment condition of the four wave groups, it can be seen that for the fine sediment condition the same contradiction for the net sediment transport direction occurs between irregular and regular waves as was seen and discussed in section 5 and 6. For the medium sediment condition however the oscillatory flow tunnel simulations show a similar net sediment transport direction, both onshore-directed, and a similar magnitude (between 14.4-15.5 $*10^{-6}$ m^2/s), for the regular and different irregular skewed wave groups. This difference between the two sediment conditions can be explained by less sediment pickup, higher sediment fall velocity (w_s), which results in less phase lag and less offshore sediment transport for medium sediment conditions.

When considering the influences of wave group skewness, the differences "between" the net sediment transport results of the boundary layer model simulations for the different skewed wave groups are taken into account. For the fine sediment condition the net sediment transport of the waxing wave group is slightly less offshore directed than the "normal" irregular wave group variant and the waning variant is even less offshore directed (in principle this is more onshore directed). For the medium sediment condition the same observations can be done; the net sediment transport of the waxing variant is slightly higher, and more onshore, than the "normal" irregular wave group and for the waning wave group the net sediment transport is even more onshore directed.

7.3.2 Irregular, single wave velocity skewed, wave group

From the irregular, single wave velocity skewed, wave group it might be expected that sediment is brought into suspension gradually and onshore directed (with respect to the Shield parameter and based on the fact that the wave groups starts with a positive horizontal velocity), however faster than waxing and slower than waning. With the following offshore-directed wave period (second part of the single wave period) sediment already/still in suspension (phase-lag effect) is moved into the offshore direction faster, since for this sediment no new critical Shield parameter should be reached first to subsequently be moved and brought into further suspension. The following, new single, wave has higher absolute horizontal velocities and the same process repeats, now with more impact (suggestion to the pumping effect). This continuous to the maximum absolute horizontal velocities, followed by a less impact having movement of the sediments when the absolute horizontal velocities decrease again, however still net offshore-directed. From section 2.1.4 it is known that the increasing of the absolute horizontal velocities also induces a wave shape streaming, which is directed in the opposing direction (offshore) of the wave propagation. The influence on fine sediment will therefore be more noticeable than with medium sediment, since fine sediment are brought into suspension easier (section 7.3.1). However, section 6 already provides an elaboration of the responsible processes.

7.3.3 Irregular, single wave velocity skewed, waxing wave group

For the waxing wave group, sediment is brought into suspension rapidly, again followed by an offshore-directed oscillation. The gradually decreasing absolute horizontal velocities in this waning variant can be compared to the second half of the normal variant only de gradually decrease is slower. The (sudden) high amount of sediment brought into suspension in the beginning, and thus no gradually build up of the amount of sediment in suspension, is moved in both on and –offshore direction, but the amount of the new suspended sediment by the following waves is slowly decreasing. The total transported sediment might therefore be less than at both the normal and waxing variant.

7.3.4 Irregular, single wave velocity skewed, waning wave group

For the waning wave group, the gradual build up of the absolute horizontal velocities to the maximum absolute horizontal velocities is slower. Here it can be assumed that the same process as with the "normal" wave group, until the maximum absolute horizontal velocities, will occur, only slower. The sudden decrease of the absolute horizontal velocities at the end of the wave group might be causing a difference compared to the "normal" irregular wave group. The low absolute horizontal velocities will not result in a lot of new suspended sediment and the sediment already in suspension will also not be brought far on-or offshore since the absolute horizontal velocity is decreased (significant). Therefore it can be expected that less sediment is transported and the net sediment transport of the waxing variant is slightly less offshore or less onshore (depending on the grain size) direct than the normal variant.

7.3.5 Regular, single wave velocity skewed, wave group

Although the regular wave group is mainly used as check it did show that for the medium sediment condition it can be seen as a good representative regular wave group for the irregular wave group. However, for the fine sediment condition it is not applicable, but from section 5 it is known that more wave energy will contribute in more/a phase lag effect and more offshore-directed net sediment transport in oscillatory flow tunnel simulations. The $\langle u(t)^3 \rangle$ of the regular wave group, which is ~0.12m^3/s^3, also confirms that it is still beneath the 0.15m^3/s^3 limit for which regular waves will experience a transition from onshore net sediment transport to offshore (Kranenburg, 2013) and thus the onshore direction is as can expected.

Note that this also indicates that for finding the good representative regular wave for an irregular wave the representative regular wave should have a $\langle u(t)^3 \rangle > 0.15 m^3/s^3$.

7.3.6 Conclusion

As observed from the net sediment transport results in Table 14 the direction of the sediment transport for fine sediment is offshore directed and the medium sediment transports are onshore directed. For the amount of transported sediment for the waxing wave group the model shows, for both sediment conditions, that less sediment is transported compared to the "normal" wave group. Finally, for the waning wave group the model shows that with fine sediment there is less sediment transported compared to the "normal" and waxing wave group. However, with medium sediment there is more sediment transported onshore, which is due to phase lag effects in fine sediment conditions.

Although these small differences are noticeable in the net sediment transport results of the different skewed wave groups, it should be noted that the magnitude of all the net sediment transport rates is of an order 10^{-6} m^2/s and the differences between the skewed wave groups are of order 10^{-7} m^2/s, which is basically zero. Therefore it can be concluded that there is *no influence of wave group skewness* on (the direction of) the net sediment transport, when considering different modified, "normal", waxing and waning wave group, with single irregular velocity skewed waves in it, for both fine sediment and medium sediment conditions.

From this it can also be concluded that a sequence variation of several high waves (irregular) within a wave group does not result in a significant influence on the final net sediment transport.

Do note that a single wave period of 6 seconds and an u_{rms} *range between 0.629 and 0.635 m/s are used only. When (additional) experimental research would be done with a wider range of both the wave peak period and the* u_{rms}, *and when different water depths are used, one might expect a wider range in magnitudes of net sediment transport results. This might also result in more in-depth information and more reliability of the conclusions made.*

In addition, the SINBAD department in Aberdeen, Scotland requested to simulate the wave averaged horizontal velocity (U_0*) for coarse sediment conditions for eight different wave group signals, including the four used (skewed) wave groups used in this section. Appendix VIII shows these simulations, however, no significant new observations were done compared to existing research on wave group influences.*

8. Discussion

Model validation and spectral analyses

The in this research conducted model validation of the boundary layer model of Kranenburg (2013) is primarily done on the net sediment transport for irregular waves for the wave-flume only, not for the oscillatory flow tunnel. The used horizontal velocity input signal here, is a timeseries from (flume) experiments, reduced by deducting the wave group averaged streaming (U_0) of it. However, to get more detail on differences (i.e. in turbulence) occurring between the model simulations and measured data, model validation could also be done on the concentration profile. However, this does mean that during experiments the concentration should be measured in the entire vertical. Validation of the horizontal velocity is not needed here, because the measured horizontal velocity is used as an input signal in the boundary layer model.

It is needed when one uses a different sets up of the research, namely when spectral input is used as model input rather than a timeseries including the horizontal velocity. An advantage of this approach would not only be that it is easier to apply more variety in for example, u_{rms}, T_p, velocity skewness and acceleration skewness (if investigated), but it also gives a better ability to control the input wave characteristics. A wider range of the wave characteristics (e.g. max horizontal velocity, u_{rms}, T_p, $<u(t)^3>$) can be easier and faster used to investigate their influences on the net sediment transport, horizontal velocity or the sediment concentration.

The used irregular waves include multiple different short waves, all having their own wave period, including a specific wave energy that contributes to the amount of sediment transported. When considering multiple single waves together, as in a wave group, a bound long wave can arise, due to interaction between all single waves. Deigaard et al. (1999) showed that this bound long wave could give a negative contribution to the sediment transport, because the backward motion in the long waves is coupled with the high waves and high sediment concentrations (see Figure 8).

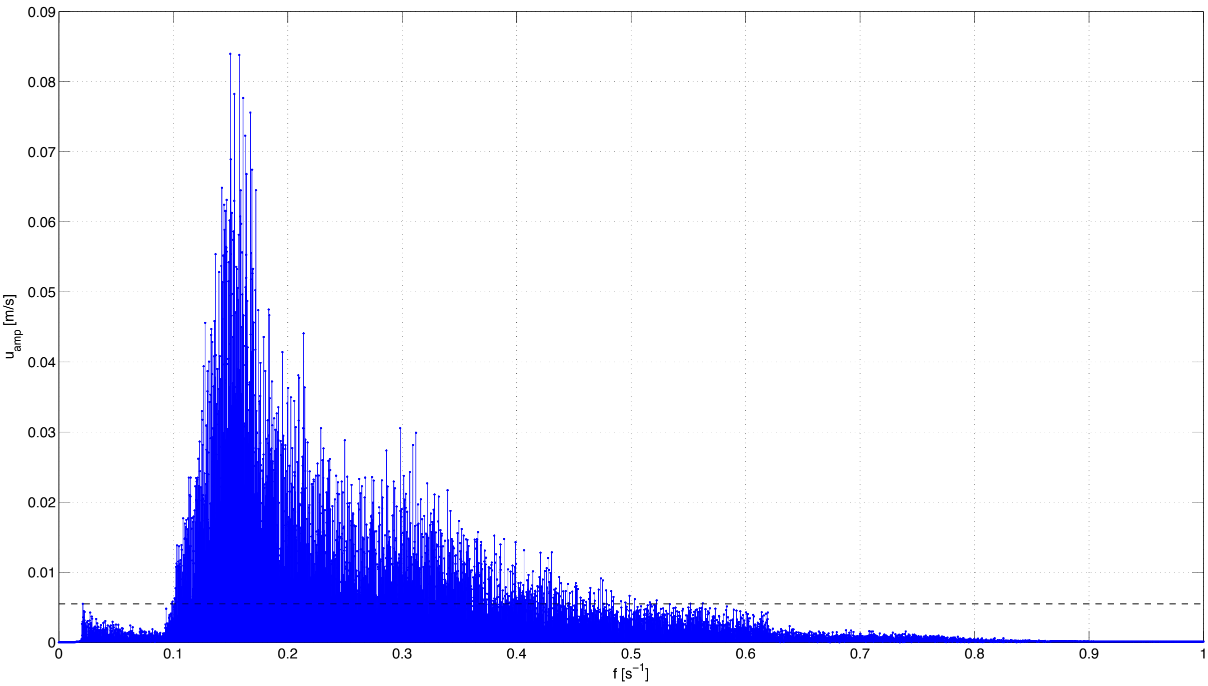

Figure 35: Spectral analyses irregular wave, AUKE-PC condition.

When considering a spectral analyses for the iregular AUKE-PC condition, as was used in section 6, it is shown (Figure 35) that for a 0.021s^{-1} frequency a small wave energy peak occurs, indicating a small wave energy occurrence at a wave period of 47.6seconds (bound long wave). The dashed black line shows that between the 0.1s^{-1} and 0.6s^{-1} frequencies, indicating single wave periods between 1.7 and 10 seconds, the amount of energy, for this entire range, is a lot higher than that for the bound long wave (high frequency). Deigaard et al. (1999) found that the net sediment transport depends on the grain size and the transport intensity: For very fine sand the mean water motion and the forward drift of the sediment dominate, giving a positive net transport. For coarser sand the coupling between backward motion and high sediment concentration dominates, giving a negative contribution. Combining the non-significant influence of the bound ling wave energy and the fine sediment condition of the irregular AUKE-PC condition, it can be concluded that this bound long wave has no (significant) influence on the net sediment transport direction. For medium sediment conditions there was no research done yet, and therefore, it cannot be said if the bound long wave does indeed contributes to a positive, onshore, net sediment transport. Future research might be needed to substantiate the statement of Diegaard et al. (1999) for the irregular wave condition, such as the AUKE-PC condition.

Sediment conditions

During research on the difference between irregular and regular waves, only fine sediment conditions are investigated (except for the model validation and section 7). The differences between fine and coarser sediment is therefore not considered. Also the water depth is considered fixed and the range of the wave heights and wave periods in the implemented wave conditions (horizontal velocities as input) is not extensive. Although for irregular waves it did show (oscillatory flow tunnel experiments, section 5.4.4) that there is a transition from onshore to offshore directed transport (with respect to the $\langle u(t)^3 \rangle$) and this appearance seems to occur faster than for regular waves, there are not a lot of irregular waves with a small or large value of $\langle u(t)^3 \rangle$ (subsequently related to different wave period and wave heights) implemented (small range). As a result only a few onshore results are produced and with the representative regular waves the transition occurring for regular waves could not be made visible yet.

Representative waves

In this research, two methods to approach a representation of an irregular wave in a regular wave are used with multiple experimental wave data (the irregular waves). However, the third method is only used to explain the observed differences between irregular and regular waves in the oscillatory flow tunnel simulations and the differences between the oscillatory flow tunnel and flume simulation for irregular waves, in terms of hydrodynamic and sediment transport related processes. The higher wave energy involvement in the representative regular wave might not always bring satisfactory results in case of oscillatory flow tunnel simulations, as it does for the AUKE-PC condition. Although the result did overestimated the irregular wave results a lot, it did include phase lag effects better and resulted in the same net sediment transport direction. More irregular waves conditions, with different wave characteristics, should be investigated, as was actually done for methods one and two already. It can be expected that for flume simulations the net sediment transport will then increase with larger wave periods (T_p) and decrease for lower wave periods. When using the same irregular waves, as used in section 5, it is expected that this method results in regular waves with higher $\langle u(t)^3 \rangle$ rates and the observed “curve”, as seen in Figure 20, would be wider and showing a transition from onshore to offshore directed net sediment transport (as shown by Kranenburg, 2103). However, since the method is now using one-third of the highest waves included in the irregular wave signal, and it is showing an overestimation of the net sediment transport for flume simulations, it might be better to implement less wave energy by only including one-tenth of the highest waves of the irregular wave signal.

Input signal

For the use of the boundary layer, a horizontal velocity signal is needed as input. The model does not convert a water level elevation timeseries to a horizontal velocity input for a certain water depth. This restriction was well reflected when more additional research for the SINBAD project was done for flume simulations. The, by the SINBAD project department in Aberdeen, Scotland, provided input data consisted of water level excursions for several flume wave conditions and its was requested to produce the net sediment transport results, with the boundary layer model. Two first steps are provided in Appendix IX, where a derivative of the water level elevation is used to get the velocity signal, and where the velocity signal from Malarkey & Davies (2012) saw tooth function (provided by the SINBAD project department Aberdeen, Scotland) is taken, to be both used as a horizontal velocity signal in the boundary layer model. As Appendix IX shows, the results cannot be considered correct, since the two used methods used vertical and horizontal velocities (respectively) of the waves *at the surface*, as horizontal velocities near the seabed, resulting in a large overestimation of the net sediment transport.

9. Conclusions and recommendations

The main objective of this research was; to increase the understanding of the nearshore sediment transport processes occurring under irregular non-breaking wave conditions, with the use of the boundary layer model of Kranenburg (2013). The second objective of this research was: to develop, or to approach, a representative regular wave for an irregular wave signal. Six sub research questions were formulated as a guideline to reach the main research objectives and thereby, answering the main research question: "*What are the main differences between irregular and regular waves in terms of sediment transport and what processes can explain the differences?*" This section summarizes the answers to the six sub research questions (section 9.1), followed by recommendations for further research (section 9.2).

9.1 Conclusions

S1: Which hydrodynamic and sediment transport related processes are known for regular waves and when irregularity is involved; which models are developed that incorporate these processes?

Studies on behalf of regular waves showed that there are several hydrodynamic processes related to sediment transport in the water column. Wave propagation is the main reason waves approach the coast, however, in the top part of the water column the orbital motion of water particles, caused by progressive waves, result in a net onshore-directed flow. Closer towards the seabed the orbital motion has less influence and due to bed roughness and emerging shear forces a boundary layer occurs. For the boundary layer, the interaction with current, wave (progressive wave streaming and wave-shape streaming) and a conjunction of current and wave, are of importance of the boundary layer flow.

For the sediment transport processes near the bed, the mobilizing forces on sediment grains, bed shear stress (due to orbital motions) and friction are the main cause sediment starts to move and is brought into suspension (on-and offshore). However, when a certain amount of wave skewness and asymmetry is involved, sediment may not equally be move on- and offshore. The finer the sediment, the less sediment settles down completely (due to fall velocity) after the peaking crest brought the sediment into suspension (onshore). The remaining suspended sediment (phase lag effect) is subsequently brought offshore during the longer trough period (compared to the crest) (velocity skewness).

When irregularity is involved, research of Dibajnia and Watanabe (1998) and Grasso et al. (2011) showed that the importance of phase lag effects increases. With a small amount of velocity skewness included, the net sediment transport will still be onshore, however, when the velocity skewness increases, and subsequently more high wave are involved, the net sediment transport might reverse in direction. For wave groups (with single irregular waves) experiments with coarse sediment, Sato (1992) showed that there is an onshore net sediment transport, however, Shi & Larsen (1984) showed that bound long waves under irregular wave groups may also contribute to an offshore flow and transport. The unsteady behaviour of irregular waves shows that it is hard to distinquish the importance of the occuring processes.

Different regular wave studies resulted in a better understanding of processes causing sediment to be transported and resulted in different sediment transport models. To simulate the reality different quasi-steady, unsteady and semi-unsteady sediment transport models/formulas were formulated, for which the latter model included the coping of phase lag effect. However, since these models/formulas were based on the assumption that the instantaneous transport rate is directly related to some power of the instantaneous near-bed oscillatory velocity or bed-shear stress, Uittenbogaard et al. (2001), Ruessink et al. (2009) and Kranenburg (2013) developed a *numerical* sediment transport model, which aims to eventually include irregular waves and wave-induced streaming to determine the net sediment transport of more *realistic* coastal conditions.

S2: How is the numerical boundary layer model of Kranenburg (2013) specified; and how can it be used to simulate net sediment transport rates?

The boundary layer model is a (quasi-) single-phase wave model, where (horizontal) flow velocities (in the vertical profile of the boundary layer) are solved from Reynolds averaged Navier-Stokes equations and sediment concentrations are solved from an advection-diffusion equation. The input of the model can either consist of (horizontal velocity) spectral input to create a regular wave for input or a timeseries consisting of a horizontal velocity from within the boundary layer or just above (free stream).

With the oscillatory flow tunnel version of the model, there is the posibility to simulate near-bed flow with prototype flow velocities and oscillation periods. The vertical component of the orbital velocity is absent, related wave-induced currents are not reproduced and difficulties and uncertainties related to scaling of turbulence and sediment related process are disabled, which gives the ability to relate observations to transport processes directly. The wave flume version however, does include these restrictions and allows for a more complete representation of the processes in the field. Both models can be forced to either "match" a predefined horizontal velocity (the input) at a certain vertical level (apllicable for i.eg. validation), or to let the unsteady horizontal pressure gradient be determined in advance from a given horizontal free stream velocity (with zero mean), which does not involve a compensation of the arising net current and is therefore allowed to develop "freely".

S3: How well do the boundary layer model results for irregular wave conditions compare with measured data from flume experiments?

With the flume version, and the match forcing, of the boundary layer model, simulations were conducted for irregular wave data from flume experiments of Dohmen-Janssen (2002) and Schretlen (2012). Based on the similarity of the simulated net sediment transports and the measured net sediment transports for both medium and fine sediment conditions, by Dohmen-Janssen (2002) and Schretlen (2012) respectively, it was concluded that the boundary layer model is validated successfully for the use of irregular waves.

S4: How do sediment transport rates for irregular waves and representative regular waves compare, for both flume and oscillatory flow tunnel simulations, with the boundary layer model?

Net sediment transport results of different irregular wave signals and two representative regular waves, created by two imposed representative regular wave approach methods ("full signal influence approach" and "partial signal influence approach" method), showed that for flume simulations with fine sediment, both the representative regular waves have almost equal onshore net sediment transports as their irregular waves, a slight over estimation occurs, which was also seen with the model validation. For the oscillatory flow tunnel simulations with fine sediment however, the irregular waves show an offshore net sediment transport, while both the representative regular waves show onshore net sediment transports. For the latter simulations it was found that in case of irregular waves the net sediment transport encounters a transition from onshore to offshore-directed transport faster than was found by Kranenburg (2013) for regular waves. In conclusion, for the flume simulations the representative regular waves are well comparable with the irregular waves. For the oscillatory flow tunnel simulations the representative regular waves are not comparable.

From the results its was also concluded that the "full signal influence approach" method is a better representation than the "partial signal influence approach" method, since between the two methods the was no significant difference noticeable and the similarity in net sediment transport results with the irregular wave results are better, both for flume and oscillatory flow tunnel simulations. (*Objective* 2)

S5: How can differences in the net sediment transport between irregular and regular waves in oscillatory flow tunnel simulations, and differences in the net sediment transport between oscillatory flow tunnel and flume simulations for irregular waves, be explained in terms of hydrodynamic and sediment transport processes?

Using the "full signal influence approach" method and a new third representative regular wave approaching method, the "high wave, signal influence approach", which is a modification of the "full signal influence approach" method in such a way that only the wave energy of one-third of the highest waves in the irregular wave signal is used to define the velocity amplitudes (u_1 and u_2) and the velocity skewness (*Objective* 2), the origin of the difference between irregular and regular waves (offshore and onshore transport respectively) in oscillatory flow tunnel simulations, for fine sediment, is found in the wave-related component of the intra-wave horizontal sediment flux. This component provides phase lag effects after each single irregular wave and a accumulation of these phase lag effects (pumping effect) in case the irregular wave contains a sequence of high irregular waves.

For the difference in net sediment transport between oscillatory flow tunnel and flume simulations for irregular waves, it is concluded that the vertical momentum advection ($w\partial u/\partial z$) is becoming less important with an increasing wave energy (method three) or when the wave signal is irregular. But the vertical sediment advection ($w\partial c/\partial z$) and the horizontal momentum advection ($u\partial u/\partial x$) do get more important with a regular wave with more wave energy and with an irregular wave (both including phase lag), and decrease the amount of phase lag effect and also the contribution to the pumping effect occurring for irregular waves (amount of sediment concentration due to offshore flow), resulting in more onshore-directed sediment transport.

It was also concluded that the "high wave, signal influence approach" method is a better representation of the irregular wave in a regular wave than the "full signal influence approach" method for the oscillatory flow tunnel, since the higher wave energy resulted in more phase lag effect and an offshore-directed net sediment transport. However, for the flume simulations it was concluded that this method did not represented the irregular wave better than the "full signal influence approach" method, since the higher wave energy allowed more sediment in the higher parts resulting in a/more onshore (net) sediment transport. (*Objective* 2)

S6: To which extent does a skewed wave group, with single irregular velocity skewed waves, has influence on the net sediment transport, for both fine and medium sediment, in oscillatory flow tunnel simulations?

Net sediment transport simulations in the oscillatory flow tunnel version of the boundary layer model showed that for three different skewed wave groups ("normal", waxing and waning), with single irregular waves, there were small differences noticeable between the wave groups for both fine and medium sediment. However, the differences in net sediment transport were of order 10^{-7} m^2/s and therefore, it was concluded that the skewness of the wave group has no influence on (the direction of) the net sediment transport.

Objectives

In conclusion, the boundary layer model is validated for irregular waves and differences in and between irregular and (representative) regular waves, for both flume and oscillatory flow tunnel simulations, are explained according to hydrodynamic and sediment transport related processes.

Furthermore, three representative regular wave-approaching methods are introduced for which it is concluded that the "high wave, signal influence approach" method is the best representation for an irregular wave in oscillatory flow tunnel simulations, but for flume simulations, the "full signal influence approach" method is the best representation for an irregular wave.

9.2 Recommendations

The boundary layer model limits the model input to a horizontal velocity signal. In practice, most of the time there are no horizontal velocities available, but only water level elevation signals. To make the boundary layer model more applicable it is recommended to investigate a combination of a pre-process to convert the water level elevation signal to a horizontal velocity for a demanded vertical height above the seabed.

It would also be interesting to investigate how the net sediment transport rates will behave when different water depths are taken into account with the simulation of irregular waves. For less water depth it would be expected that more sediment is moved with a same irregular wave, for more water depth less sediment movement is expected. However, what would happen with coarser sediment in less water depth? Would there also be influence noticeable of phase lag and pumping effects? And from which (increasing) water depth (in oscillatory flow tunnels) will the phase lag and pumping effects for fine sediments be absent? These propositions indirectly lead to more research on the influences of irregular waves with more variety in the wave (velocity) heights and with variety in the single wave peak periods, as well.

For the irregular, non-breaking, wave flume experiments that are planned for the SINBAD project, carried out in Barcelona, Spain, it would be a recommendation to use the flume version of the boundary layer model first with the irregular wave condition first, to get an indication of the to be expected net sediment transport range. A representative regular wave, according to the “full signal influence approach” method, However, if there are only water level elevation input signals available, and no horizontal velocities, for the wave conditions that will be used for the experiments, it is recommended to first investigate the best way to convert this.

A final recommendation for the SINBAD project large scale experiments, in either the oscillatory flow tunnel in Aberdeen, Scotland, or the wave-flume in Barcelona, Spain, is to not research the influences due to wave group skewness, since in this research it was concluded that there is no significant difference in the net sediment transport result and it would save time. However, if the influence of wave group skewness is necessarily to be done, the suggestion is to investigate a wider range of skewed wave group conditions that have more variety in single wave peak periods and a wider range of the u_{rms} implemented.

References

Abreu, T., Silva, P. A., Sancho, F., & Temperville, A. (2010). Analytical approximate wave form for asymmetric waves. *Coastal Engineering , 57*, 656-667.

Austin, M., Masselink, G., O'Hare, T., & Russell, P. (2009). Onshore sediment transport on a sandy beach under varied wave conditions: Flow velocity skewness, wave asymmetry or bed ventilation? *Marine Geology 259* , 86 - 101.

Bailard, J. (1981). An energetics total load sediment transport model for a plane sloping beach. *Journal of Geophysical Research , Vol. 86* (No. C11), 10938-10954.

Bosboom, J., & Klopman, G. (2000). Intra-wave sediment transport modeling. *Proceedings of 27th International COnference on Coastal Engineering* , 2453-2466.

Bosboom, J., & Stive, M. (2011). *Coastal Dynamics I.* Delft University of Technology.

Camenen, B., & Larson, M. (2006). Phase-lag effects in sheet flow transport. *Coastal Engineering 53* , 531 - 542.

Davies, A., Van Rijn, L., Damgaard, J., Van de Graaff, J., & Ribberink, J. (2002). Intercomparison of research and practical sand transport models. *Coastal Engineering , 46*, 1-23.

Deigaard, R., Borup Jakobsen, J., & Fredsoe, J. (1999). Net sediment transport under wave groups and bound long waves. *Elsevier* , 13,559-13,575.

Dibajnia, M., & Watanabe, A. (1992). Sheet flow under nonlinear waves and currents. *Coastal Engineering Proceedings , 23*, 2015-2028.

Dibajnia, M., & Watanabe, A. (1998). Transport rate under irregular sheet flow conditions. *Coastal Engineering , 35*, 167-183.

Dohmen-Janssen, C. M. (1999). *Grain size influence on sediment transport in oscillatory sheet flow.* Technical University of Delt. Delft, The Netherlands: Febodruk B.V.

Dohmen-Janssen, C. M. (2000). *Sheet flow under monochromatic waves and wave groups.* Datareport, Kust*2000 (RIKZ), Human Capital and Mobility (EU) and NICOP (ONR), Enschede, The Netherlands.

Dohmen-Janssen, C. M., & Hanes, D. M. (2005). Sheet flow and suspended sediment due to wave groups in a large wave flume. *Continental Shelf Research 25* , 333–347.

Dohmen-Janssen, C. M., & Hanes, D. M. (2002). Sheet flow dynamics under monochromatic nonbreaking waves. *Journal of Geophysical Research , 107(C10)*.

Dohmen-Janssen, C. M., Kroekenstoel, D. F., Hassan, W. N., & Ribberink, J. S. (2002). Phase lags in oscillatory sheet flow: experiments and bed load modelling. *Coastal Engineering 46* , 61 - 87.

Grasso, F., Michallet, H., & Barthelemy, E. (2011). Sediment transport associated with morphological beach changes forced by irregular asymmetric, skewed waves. *Journal of Geophysical Research , Vol. 116* (C03020).

Hsu, T.-J., & Hanes, D. (2004). Effects of wave shape on sheet flow sediment transport. *Journal of Geophysical Research , 109* (C05025).

Hulscher, S., & Ribberink, J. (2012). Marine Dynamics. Enschede: University of Twente.

Jonsson, I. G. (1966). Wave boundary layers and friction factors. *Coastal Engineering Proceedings , 1* (10), 127-148.

Klopman, G. (1994). *Vertical structure of the flow due to waves and currents.* Progress report, H 840.30, Part II, Delft Hydraulics, The Netherlands.

Kranenburg, W. M. (2013). *Modeling Sheet-flow sand transport under progressive surface waves.* PhD Thesis, University of Twente, Water Engineering Department, Enschede, The Netherlands.

Kranenburg, W. M., Ribberink, J., Uittenbogaard, R., & Hulscher, S. (2012). Net currents in the wave bottom boundary layer: On wave shape streaming and progressive wave streaming. *Journal of Geophysical Research, 117* .

Malarkey, J. (2008). *A Review of Freestream Descriptions and Velocity and Acceleration Skewness.* Bangor University.

Malarkey, J., & Davies, A. (2012). Free-stream velocity descriptions under waves with skewness and assymmetry. *Coastal Engineering, 68* , 78 - 95.

Meko, D. (2013). *Applied Time Series Analysis, Detrending.* Course notes, University of Arizona, Laboratory of Tree-Ring Research, Tucson, AZ, United Stated of America.

O'Donoghue, T., & Wright, S. (2004). Flow tunnel measurements of velocities and sand flux in oscillatory sheet flow for well-sorted and graded sands. *Coastal Engineering , 51*, 1163-1184.

O'Donoghue, T., Van der A, D., Li, M., Ribberink, J., & Van der Werf, J. (2011). *Sand transport under iregular and breaking wave conditions.* SINBAD Proposal Case, Univeristy of Aberdeen; University of Liverpool; University of Twente.

O'Donoghue, T., van der A, D., Li, M., Ribberink, J., & van der Werf, J. (2011). *Sand transport under irregular and breaking wave conditions.* Proposal case for support, University of Twente; University of Aberdeen; University of Liverpool.

Park, D. (2008). Waves, Tides and Shallow-water Processes. Milton Keynes, United Kingdom: The Open University, ISBN 978-0-7506-4281-1.

Ribberink, J. (1998). Bed-load transport for steady flows and unsteady oscillatory flows. *Coastal Engineering , Vol. 25*, 59-82.

Ribberink, J., & Al-Salem, A. (1995). Sheet flow and suspension of sand in oscillatory boundary layers. *Coastal Engineering , 25(3-4)*, pp. 205-225.

Ribberink, J., Dohmen-Janssen, C., Hanes, D., McLean, S., & Vincent, C. (2000). Near-bed sand transport mechanisms under waves. *Coastal Engineering Proceedings , 27*, 3263-3276.

Ribberink, J., Van der Werf, J., O'Donoghue, T., & Hassan, W. (2008). Sand motion induced by oscillatory flows: Sheet flow and vortex ripples. *Journal of Turbulence , Vol.* 9 (No. 20), 1-32.

Rodi, W. (1984). Turbulence Models and Their Applications in Hydraulics. *A State of the Art Review, 2nd ed* .

Ruessink, B., Van den berg, T., & Van Rijn, L. (2009). Modeling sediment transport beneath skewed asymmetric waves above a plane bed. *Journal of Geophysical Research , Vol. 114* (C11021).

Sato, S. (1992). Sand transport under grouping wave. *23rd International Conference on Coastal Engineering.* Venice.

Schretlen, J. (2012). *Sand transport under full-scale progressive surface waves.* University of Twente, The Netherlands. Enschede, The Netherlands: University of Twente.

Shi, N., & Larsen, L. (1984). Reverse sediment transport induced by amplitude modulated waves. *Marine Geology, 54* .

Shields, A. (1936). *Anwendung der Aehnlichkeitsmechanik und der Turbulenzforschung auf die Geschiebebewegung.* Technical University Berlin. Berlin, Germany: Preussischen Versuchsanstalt für Wasserbau.

Silva , P., Abreu, T., Van der A, D., Sancho, F., Ruessing, B., Van der Werf, J., et al. (2011). Sediment transport in non-linear skewed oscillatory flows: the TRANSKEW experiments. *Journal of Hydraulic Research , Vol. 49* (No. 51), 72-80.

Sleath, J. (1987). Turbulent oscillatory flow over rough beds. *Journal of Fluid Mechanics* (182), 369.

Svendsen, I. (1984). Mass flux and undertow in a surf zone. *Coastal Engineering , 8*, 347-365.

Svendsen, I., Madsen, P., & Buhr Hansen, J. (1978). Wave characteristics in the surf zone. *Proceedings of the 16th International Conference on Coastal Engineering , Vol. 1*, 520-539.

Swart, D. H. (1974). Offshore sediment transport and equilibrium beach profiles. *Delft Hydraulics Labaratory Publication , No. 301*.

Torres-Freyermuth, A., Losada, I., & Lara, J. (2007). Modeling of surf zone processes on a natural beach using Reynolds-averaged Navier-Stokes equations. *Journal of Geophysical Research , 112*.

Uittenbogaard, R., Bosboom, J., & Van Kessel, T. (2001). *Numerical simulation of wave-current driven sand transport: Theoretical background of the beta-release of the Point-Sand model.* Report: Z2899.10, Delft, The Netherlands.

Van der A, D., O'Donoghue, T., & Ribberink, J. (2010). Measurements of sheet flow transport in acceleration-skewed oscillatory flow and comparison with practical formulations. *Coastal Engineering , 57*, pp. 331-342.

Van der A, D., O'Donoghue, T., & Ribberink, J. (2009). Sheet flow sand transport processes in oscillatory flow with acceleration skewness. *Proceedings Coastal Dynamics'09, World Scientific.*

Van der A, D., Ribberink, J., Van der Werf, J., & O'Donoghue, T. (2010). New practical model for sand transport induced by non-breaking waves and currents. *Coastal Engineering , 32*.

Van der A, D., Ribberink, J., Van der Werf, J., O'Donoghue, T., Buijsrogge, R., & Kranenburg, W. (2013). Practical sand transport formula for non-breaking waves and currents. *Coastal Engineering , 76*, pp. 26-42.

Van der Wal, R. (1996). *Grain size influence on sediment transport in sheet flow conditions for combined wave-current flow.* MSc. Thesis, Delft University of Technology, Department of Civil Engineering, Delft, The Netherlands.

Van der Werf, J., Doucette, J., O'Donoghue, T., & Ribberink, J. (2007). Detailed measurements of velocities and suspended sand concentrations over full-scale ripples in regular oscillatory flow. *Journal of Geophysical Research , 112*.

Van der Werf, J., Ribberink, J. S., O'Donoghue, T., & Doucette, J. S. (2006). Modelling and measurement of sand transport processes over full-scale ripples in oscillatory flow. *Coastal Engineering , Vol. 53*.

Van Rijn, L. (1993). *Principles of sediment transport in rivers, estuaries and coastal seas.* Amsterdam, The Netherlands: Aqua Publications.

Vincent, C., & Hanes, D. (2002). The accumulation and decay of nearbed suspended sand concentration due to waves and wave groups. *Continental Shelf Research , 22/14*, pp. 1987–2000.

Yu, X., Hsu, T.-J., & Hanes, D. (2010). Sediment transport under wave groups; Relative importance between nolinear waveshape and nonlinear boundary layer streaming. *Journal of Geophysical Research Vol. 115* , C02013.

Zyserman, J., & Fredsoe, J. (1994). Data analysis of bed concentration of suspended sediment. *Journal of Hydraulic Engineering , 120* (9), 1021-1042.

Appendices

Appendix I: Timeseries in boundary layer model

During research of Kranenburg (2013) the boundary layer model was only used with spectral input. Making it easier to control the input for regular waves. For validation of the model on irregular waves time series of the horizontal velocity u (m/s) will be used. To check if the model can actually handle time series a timeserie for the horizontal velocity u of a regular wave was made with the help of known spectral input. The model was than run with spectral and with a timeserie input to compare the output results on output horizontal velocity u (m/s) and sediment concentration volume (m³/m³), Figure 36 and Figure 37.

For the spectral wave periods (T) 5s, 2.5s, 1.67s, 1.25s and 1s; and for the spectral amplitudes 0.5m, 0.01m, 0.005m, 0.002m and 0.001m were used. These input were also used in combination with $u(t) = u_0 + A_i * \cos\left(\frac{2*\pi}{T_i} * t\right)$ (53) to create a related time serie.

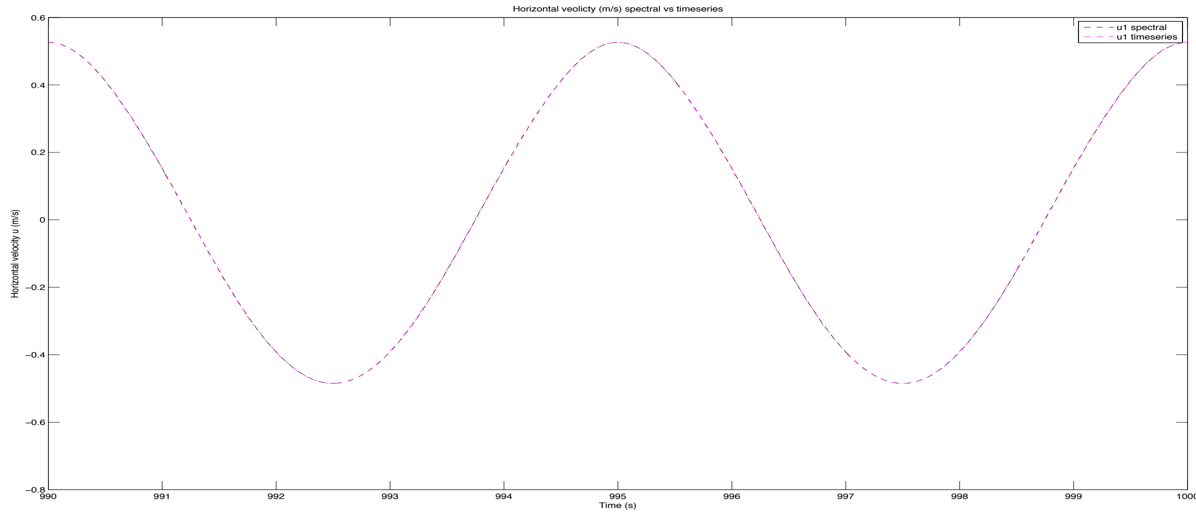

Figure 36: Spectral vs. Time series horizontal velocity u (m/s) BLM output comparison.

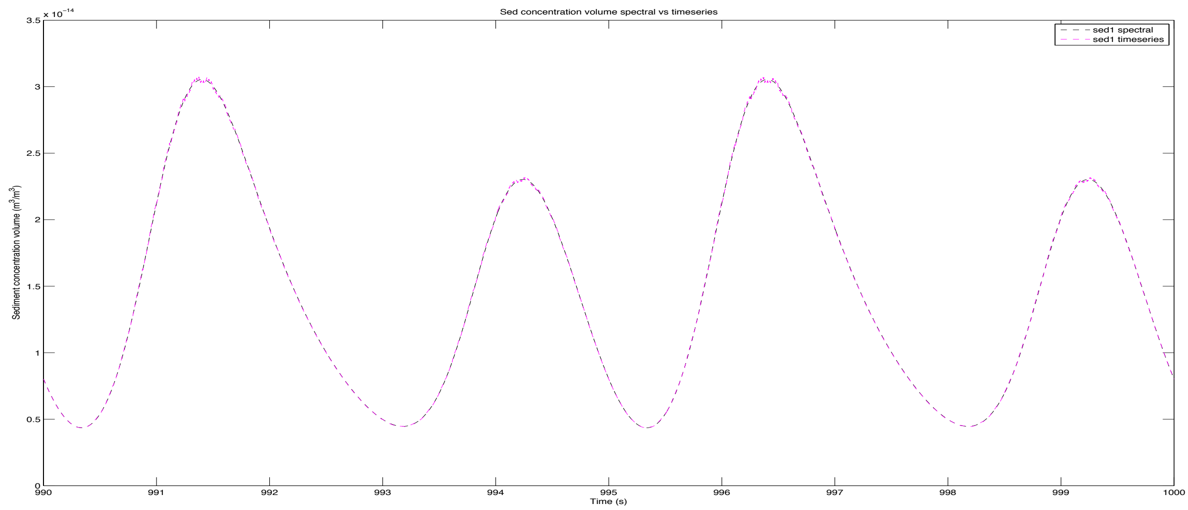

Figure 37: Spectral vs. Time series sediment concentration c (m³/m³) volume BLM output comparison.

Both figures show the boundary layer model output for the last 10 seconds from the 1000s timeserie that was produced. They show that for both the horizontal output velocity u (m/s) and the sediment concentration volume (m³/m³) the model reproduces the same values. Therefor it can be concluded that the boundary layer model can't only be used with spectral input but with timeseries input as well to reproduce wave output properties.

Appendix II: Echosounder profile net sediment transport

Table 15 provides the net sediment transport rates computed for all separate echosounder profiles from the GWK08 experiments. The table is corresponding with the boundary layer model results in Table 16.

Table 15: Net sediment transport rates for all separate echosounder profiles from the GWK08 (Schretlen) experiments.

GWK 08 Run nr.	Echosounder profiles (date_run - date_run)	A $\langle q_s \rangle$ [10^{-6} m2/s]	B $\langle q_s \rangle$ [10^{-6} m2/s]	C $\langle q_s \rangle$ [10^{-6} m2/s]	D $\langle q_s \rangle$ [10^{-6} m2/s]	Average $\langle q_s \rangle$ [10^{-6} m2/s]	Stdv $\langle q_s \rangle$ [10^{-6} m2/s]
1265							
2	300708_run1 - 300708_run2	10.96	13.69	8.53	6.55	9.93	3.09
3	300708_run2 - 300708_run3	8.63	4.71	11.89	2.99	7.05	3.99
4	300708_run3 - 300708_run4HEEN	0.82	19.61	3.79	25.12	12.33	11.86
5	300708_run4TERUG - 310708_run1	16.96	8.49	16.99	7.08	12.38	5.34
	Measured Average					***10.42***	***6.07***
1565							
1	310708_run1 - 310708_run2	13.44	12.15	17.05	14.81	14.36	2.09
2	310708_run2 - 310708_run3	14.43	18.56	19.76	16.62	17.34	2.33
4	310708_run4TERUG - 010808_run1	19.02	8.35	22.74	10.55	15.17	6.83
5	010808_run1 - 010808_run2HEEN	7.39	29.99	11.23	25.61	18.56	10.94
	Measured Average					***16.36***	***5.55***
1575							
1	010808_run2HEEN - 040808_run1	25.76	12.90	23.51	12.38	18.64	6.99
2	040808_run1 - 040808_run2	26.86	14.99	22.16	22.23	21.56	4.90
3	040808_run2 - 040808_run3	18.73	15.25	23.61	21.73	19.83	3.66
4	040808_run3 - 040808_run4TERUG	13.98	27.26	10.39	19.57	17.80	7.35
	Measured Average					***19.46***	***5.73***

Appendix III: Net sediment transport validation result for every condition and every run

Table 16: Net sediment transport results and factors for GWK08 (Schretlen).

Condition	Run	Boundary layer model: BLM: New Original $<q_s>$ [10^{-6} m^2/s]	BLM: Ens. AVG $<q_s>$ [10^{-6} m^2/s]		Factor of equality: Factor New ori avg/Meas avg	Factor EnsAVG avg/Meas avg	Factor (run) EnsAVG/New ori
1265	1	12.67	10.83		0.87	0.80	
	2	10.39	10.42				1.00
	3	12.43	11.38		A:↑|B:↓	A:↑|B:↓	0.92
	4	-0.19	0.03		1.10	1.00	0.16
	5	10.17	9.02				0.89
	AVERAGE	**9.10**	**8.33**	***A***: is ***included*** non matching BLM values			**0.74**
	STDV	5.32	4.72				
	AVERAGE	**11.42**	**10.41**	***B***: is ***excluded*** non matching BLM value (run4). ***Included*** RUN 1			0.93
	STDV	1.32	1.24				
1565	1	11.31	9.55		1.04	0.71	0.85
	2	20.38					--
	4	21.20	14.45				0.68
	5	15.25	10.84				0.71
	AVERAGE	**17.03**	**11.61**				**0.75**
	STDV	4.64	2.54				
1575	1	22.05	20.39		1.24	1.14	0.92
	2	19.95	20.39				1.02
	3	32.75	28.85				0.88
	4	21.82	19.31				0.89
	AVERAGE	**24.14**	**22.24**				**0.93**
	STDV	6.16	4.53				

Table 17: Net sediment transport results and factors for GWK99 (Dohmen-Janssen), including "measured" net sediment transports.

Condition	Run	Boundary layer model: BLM: New original $\langle q_s \rangle$ [10^{-6} m^2/s]	Measured (literature): BLM: New Original average $\langle q_s \rangle$ [10^{-6} m^2/s]	Measured (literature): Literature Method 1* $\langle q_s \rangle$ [10^{-6} m^2/s]	Measured (literature): Literature Method 2** $\langle q_s \rangle$ [10^{-6} m^2/s]	Factor of equality: Factor Lit. AVG/ Ori avg	Factor of equality: Factor Ori AVG/ Lit. AVG
GP (0991) (GWK99)	GPA	18.45	***21.49***	***24.15***	36.23	1.40	**0.89**
	GPB	16.35					
	GPC	20.35					
	GPD	21.21					
	GPE	17.94					
	GPF	33.18					
	GPG	21.46					
	GPH	18.42					
	GPI	22.95					
	GPJ	24.58					
	AVERAGE	**21.49**					
	STDEV	**4.80**					
GI (1065) (GWK99)	GIB	10.59	***12.66***	***12.45***	12.83	1.00	**1.02**
	GIC	7.50					
	GID	16.06					
	GIE	14.65					
	GIF	11.41					
	GIH	15.79					
	AVERAGE	**12.66**					
	STDEV	**3.40**					

	Good similarity to measured.
	Moderate similarity to measured.
	Bad similarity to measured.
	No Ens. AVG possible. --> No repetition time available.

* Measurement 1: Represents the net transport rate calculated on the basis of the survey of the entire sand bed (±45m section along the tank)
**Measurement 2: Represents the net transport rate calculated on the basis of the survey near the test area where the instruments are located (±5m test section)

Appendix IV: Boundary layer model run outputs versus mea

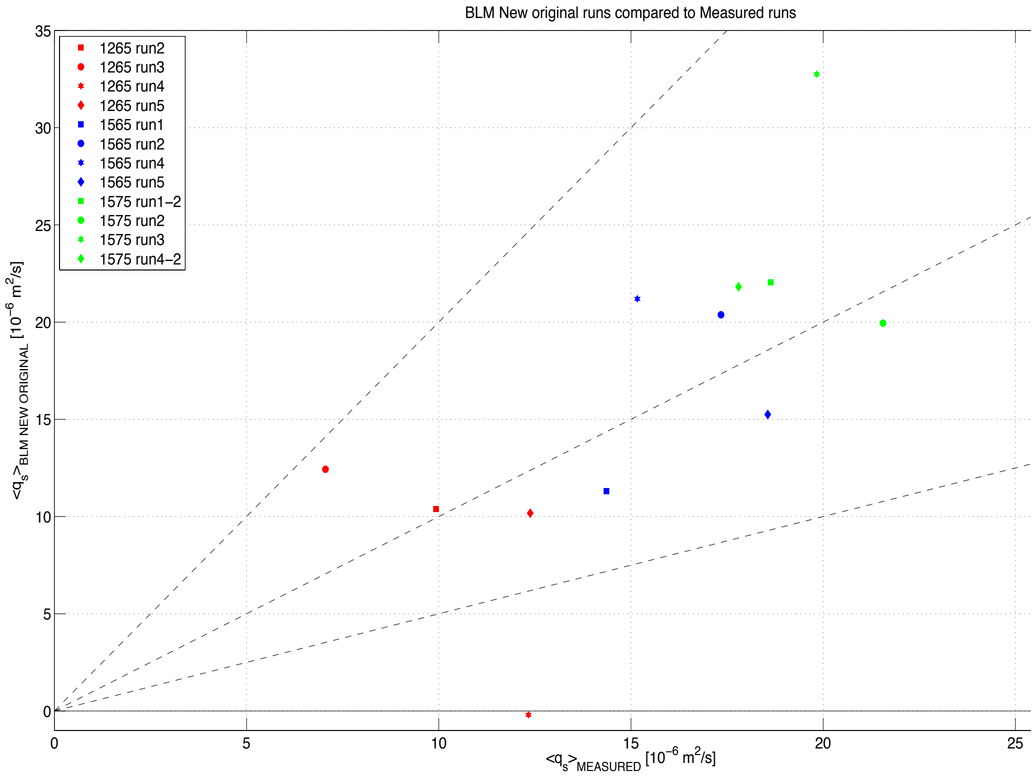

Figure 38: Net sediment transport original timeseries runs vs. measured runs. Dashed gr
factor 0.5, 1, and 2 comparison lines (from bottom to top).

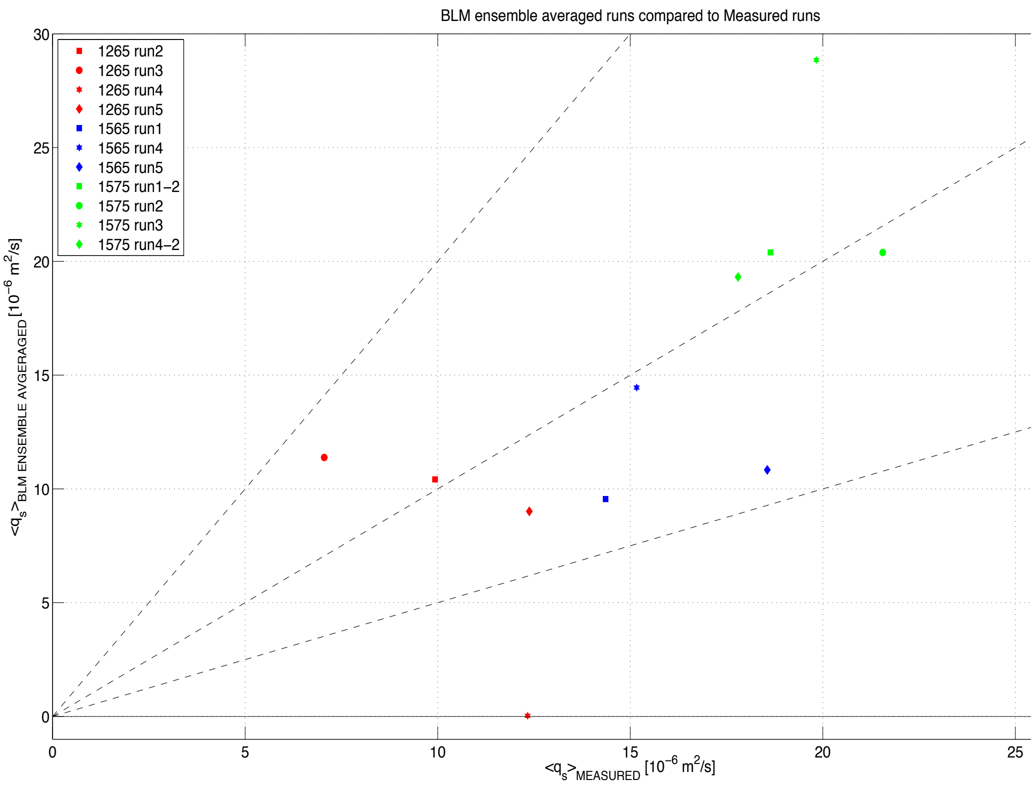

Figure 39: Net sediment transport ensemble average timeseries runs vs. measured run
lines are the factor 0.5, 1, and 2 comparison lines (from bottom to top).

Appendix V: Boundary layer thickness

An input for Kranenburg (2013) Boundary Layer Model is the z_{match}, which is used as a height for the model to be forced to match a predefined horizontal velocity signal. The desired height is closest to 2* δ_s, with δ_s being the boundary layer thickness estimate of (Sleath, 1987):

$$\frac{\delta_s}{k_N} = 0.27\left(\frac{A}{k_N}\right)^{0.67} \qquad (45)$$

,A the orbital excursion ($A = \frac{u_{max}}{\omega}$) and for the Nikuradse roughness height k_N, k_n=2*D_{50} is used.

The domain for each condition used in the boundary layer model is estimated at 2.5 times the boundary layer thickness (2.5* δ_s).

The z_{match} that was chosen for *all validation conditions* is at 40mm above the bed. Allthough in some conditions this is below the prefered two times boundary layer thickness, this is done to prevent the allowance of a large degree of freedom for the net current inside the boundary layer. However, Table 18 shows the estimated z_{match} level when using the indicated desired height.

For all used conditions in this MSc. Thesis the boundary layer thickness, the bed characteristics and the used wave characteristics are shown in Table 18.

Table 18: Boundary layer thicknesses, bed characteristics and wave characteristics for all used conditions in this MSc thesis research.

Condition	Model version: Flume and/or Tunnel	Wave	D_{50} [mm]	T_p [s]	Nikuradse roughness height k_N [m]	Roughness height z_0 [m]	$u_{max, on, red}$ [m/s]	Wave angular frequency w [rad/s]	Orbital excursion A [m]	Boundary layer thickness [m]	Match level [m]	Domain [m]
1265 (GWK08)	Flume/Tunnel	Irregular	0.14	6.5	2.80E-04	9.33E-06	1.27	0.97	1.31	0.02	0.4	0.05
1565 (GWK08)	Flume/Tunnel	Irregular	0.14	6.5	2.80E-04	9.33E-06	1.61	0.97	1.67	0.03	0.4	0.06
1575 (GWK08)	Flume/Tunnel	Irregular	0.14	7.5	2.80E-04	9.33E-06	1.62	0.84	1.93	0.03	0.4	0.07
1265 (GWK08)	Flume/Tunnel	Regular	0.14	6.5	2.80E-04	9.33E-06	0.84	0.97	0.86	0.02	0.4	0.04
1565 (GWK08)	Flume/Tunnel	Regular	0.14	6.5	2.80E-04	9.33E-06	1.03	0.97	1.07	0.02	0.4	0.05
1575 (GWK08)	Flume/Tunnel	Regular	0.14	7.5	2.80E-04	9.33E-06	1.09	0.84	1.30	0.02	0.4	0.05
GI (GWK99)	Flume	Irregular	0.24	6	4.80E-04	1.60E-05	1.65	1.05	1.58	0.03	0.4	0.07
GP (GWK99)	Flume	Irregular	0.24	9.1	4.80E-04	1.60E-05	1.84	0.69	2.67	0.04	0.4	0.10
IRRvSK (SINBAD)	Flume/Tunnel	Irregular	0.14	6	2.80E-04	9.33E-06	1.61	1.05	1.54	0.02		0.06
IRRvSK (SINBAD)	Flume/Tunnel	Regular	0.14	6	2.80E-04	9.33E-06	1.09	1.05	1.04	0.02		0.05
Wave group (SINBAD)	Tunnel	Irregular	0.16	6	3.20E-04	1.07E-05	1.61	1.05	1.54	0.03		0.06
Wave group (SINBAD)	Tunnel	Regular	0.16	6	3.20E-04	1.07E-05	1.09	1.05	1.04	0.02		0.05
Wave group (SINBAD)	Tunnel	Irregular	0.26	6	5.20E-04	1.73E-05	1.61	1.05	1.54	0.03		0.07
Wave group (SINBAD)	Tunnel	Regular	0.26	6	5.20E-04	1.73E-05	1.09	1.05	1.04	0.02		0.06
Wave group (SINBAD)	Tunnel	Irregular	0.46	6	9.20E-04	3.07E-05	1.61	1.05	1.54	0.04		0.09
Wave group (SINBAD)	Tunnel	Regular	0.46	6	9.20E-04	3.07E-05	1.09	1.05	1.04	0.03		0.07
AUKE-PC (Deltares)	Flume/Tunnel	Irregular	0.14	6.5	2.80E-04	9.33E-06	2.73	0.97	2.82	0.04		0.09
AUKE-PC (Deltares)	Flume/Tunnel	Regular M-one	0.14	6.5	2.80E-04	9.33E-06	1.01	0.97	1.05	0.02		0.05
AUKE-PC (Deltares)	Flume/Tunnel	Regular M-three	0.14	6.5	2.80E-04	9.33E-06	1.32	0.97	1.37	0.02		0.06

Appendix VI: Irregular wave and representative regular wave characteristics

Table 19: (Part I, part II on next page): Overview of characteristics for irregular waves and two representative regular waves, method one (M1) and two (M2) of GWK08 (Schretlen, 2008), IRRvSK (SINBAD, 2013) and AUKE-PC (Deltares, 2013). Oscillatory flow tunnel and flume simulations.

Condition	Run	Wave		Periodic characteristics			Velocity characteristics										Velocity skewness		Acceleration skewness	
			D_{50}	T_p	T_s	T_{mean}	U_0	u_{rms}	$u_{max,\ on,\ red}$	$u_{max,\ off,\ red}$	$u_{1/3,\ on,\ red}$	$u_{1/3,\ off,\ red}$	$\langle u^2_{red} \rangle$	$\langle u^3_{red} \rangle$	$\hat{u}_1$	$\hat{u}_2$	R	Sk_u	B	Sk_a
			[mm]	[s]	[s]	[s]	[m/s]	[m/s]	[m/s]	[m/s]	[m/s]	[m/s]	[m^2/s^2]	[m^3/s^3]	[m/s]	[m/s]	[-]	[-]	[-]	[-]
1265 (GWK08)	1	Irregular	0.14	6.3	6.6	6.3	-0.005	0.46	1.20	-0.85	1.14	-0.72	0.211	0.046	0.000	0.000	0.611	0.473	0.475	0.117
		Regular M1	0.14	6.3	6.3	6.3	0.000	0.46	0.79	-0.48	0.79	-0.48	0.211	0.046	0.632	0.153	0.621	0.472	0.500	0.000
		Regular M2	0.14	6.3	6.3	6.3	0.000	0.46	0.78	-0.50	0.78	-0.49	0.211	0.043	0.635	0.141	0.611	0.440	0.500	0.000
	2	Irregular	0.14	6.3	6.8	6.2	-0.005	0.49	1.26	-0.94	1.14	-0.78	0.236	0.047	0.000	0.000	0.596	0.407	0.490	0.116
		Regular M1	0.14	6.3	6.2	6.3	0.000	0.49	0.81	-0.54	0.81	-0.54	0.236	0.047	0.673	0.137	0.602	0.407	0.500	0.000
		Regular M2	0.14	6.3	6.2	6.3	0.000	0.49	0.81	-0.55	0.80	-0.55	0.236	0.044	0.675	0.129	0.595	0.384	0.500	0.000
	3	Irregular	0.14	6.3	6.6	6.6	0.001	0.49	1.27	-0.96	1.15	-0.74	0.236	0.051	0.000	0.000	0.607	0.449	0.488	0.182
		Regular M1	0.14	6.3	6.2	6.3	0.000	0.49	0.84	-0.53	0.82	-0.52	0.236	0.051	0.670	0.153	0.612	0.449	0.500	0.000
		Regular M2	0.14	6.3	6.2	6.3	0.000	0.49	0.83	-0.54	0.82	-0.53	0.236	0.049	0.672	0.144	0.605	0.425	0.500	0.000
	5	Irregular	0.14	6.3	6.6	6.2	-0.014	0.42	1.11	-0.74	1.03	-0.62	0.177	0.044	0.000	0.000	0.625	0.589	0.478	0.017
		Regular M1	0.14	6.3	6.3	6.3	0.000	0.42	0.75	-0.40	0.75	-0.40	0.177	0.044	0.566	0.182	0.649	0.589	0.476	0.000
		Regular M2	0.14	6.3	6.3	6.3	0.000	0.42	0.72	-0.44	0.72	-0.43	0.177	0.036	0.577	0.144	0.624	0.484	0.500	0.000
1565 (GWK08)	1	Irregular	0.14	6.3	7.0	6.2	-0.028	0.62	1.61	-1.07	1.44	-0.94	0.379	0.098	0.000	0.000	0.605	0.420	0.486	0.173
		Regular M1	0.14	6.3	6.2	6.3	0.000	0.62	1.03	-0.68	1.03	-0.67	0.379	0.098	0.852	0.180	0.605	0.420	0.500	0.000
		Regular M2	0.14	6.3	6.2	6.3	0.000	0.62	1.03	-0.68	1.03	-0.67	0.379	0.098	0.852	0.179	0.605	0.419	0.500	0.000
	4	Irregular	0.14	6.7	6.9	6.1	-0.013	0.58	1.49	-1.04	1.36	-0.82	0.342	0.083	0.000	0.000	0.624	0.415	0.464	0.103
		Regular M1	0.14	6.7	6.7	6.7	0.000	0.58	0.98	-0.64	0.98	-0.64	0.342	0.083	0.809	0.169	0.604	0.416	0.500	-0.004
		Regular M2	0.14	6.7	6.6	6.7	0.000	0.58	1.00	-0.61	1.00	-0.60	0.342	0.096	0.803	0.198	0.623	0.481	0.500	-0.004

Table 19: (Part II)

Condition	Run	Wave	D_{50} [mm]	T_p [s]	T_s [s]	T_{mean} [s]	U_0 [m/s]	u_{rms} [m/s]	$u_{max, on, red}$ [m/s]	$u_{max, off, red}$ [m/s]	$u_{1/3, on, red}$ [m/s]	$u_{1/3, off, red}$ [m/s]	$<u^2_{red}>$ [m^2/s^2]	$<u^3_{red}>$ [m^3/s^3]	$\hat{u}_1$ [m/s]	$\hat{u}_2$ [m/s]	R [-]	Sk_u [-]	B [-]	Sk_a [-]
			Periodic characteristics				Velocity characteristics										Velocity skewness		Acceleration skewness	
1565 (GWK08)	5	Irregular	0.14	6.7	6.9	6.2	-0.032	0.55	1.40	-0.93	1.28	-0.75	0.303	0.071	0.000	0.000	0.630	0.428	0.431	0.020
		Regular M1	0.14	6.7	6.7	6.7	0.001	0.55	0.93	-0.60	0.92	-0.60	0.303	0.071	0.761	0.164	0.607	0.429	0.501	-0.005
		Regular M2	0.14	6.7	6.7	6.7	0.001	0.55	0.95	-0.56	0.95	-0.56	0.303	0.084	0.753	0.196	0.629	0.501	0.498	-0.005
1575 (GWK08)	1	Irregular	0.14	7.7	7.4	7.1	-0.030	0.64	1.62	-1.12	1.40	-0.85	0.404	0.090	0.000	0.000	0.623	0.351	0.442	0.384
		Regular M1	0.14	7.7	7.7	7.7	0.000	0.64	1.04	-0.74	1.04	-0.73	0.404	0.090	0.886	0.153	0.586	0.357	0.500	0.000
		Regular M2	0.14	7.7	7.7	7.7	0.000	0.64	1.09	-0.66	1.09	-0.66	0.404	0.123	0.873	0.215	0.622	0.477	0.500	0.000
	2	Irregular	0.14	7.7	6.1	6.7	-0.038	0.63	1.38	-1.17	1.29	-0.91	0.400	0.068	0.000	0.000	0.588	0.270	0.454	-0.380
		Regular M1	0.14	7.7	7.7	7.7	0.000	0.63	1.01	-0.77	1.00	-0.77	0.400	0.068	0.887	0.116	0.565	0.270	0.500	0.000
		Regular M2	0.14	7.7	7.7	7.7	0.000	0.63	1.04	-0.73	1.04	-0.73	0.400	0.090	0.881	0.154	0.587	0.355	0.500	0.000
	3	Irregular	0.14	7.7	7.6	6.5	-0.014	0.65	1.58	-1.11	1.33	-1.01	0.425	0.092	0.000	0.000	0.570	0.333	0.494	0.468
		Regular M1	0.14	7.7	7.7	7.7	0.000	0.65	1.06	-0.76	1.06	-0.76	0.425	0.092	0.910	0.148	0.581	0.333	0.500	0.000
		Regular M2	0.14	7.7	7.7	7.7	0.000	0.65	1.04	-0.79	1.04	-0.78	0.425	0.079	0.913	0.127	0.570	0.287	0.500	0.000
	4	Irregular	0.14	7.7	7.6	7.1	-0.031	0.60	1.27	-1.11	1.12	-0.93	0.364	0.067	0.000	0.000	0.547	0.305	0.463	0.339
		Regular M1	0.14	7.7	7.7	7.7	0.000	0.60	0.97	-0.72	0.97	-0.72	0.364	0.067	0.844	0.125	0.574	0.305	0.500	0.000
		Regular M2	0.14	7.7	7.7	7.7	0.000	0.60	0.93	-0.77	0.93	-0.77	0.364	0.043	0.850	0.080	0.547	0.197	0.500	0.000
IRRvSK (SINBAD)		Irregular	0.14	6.0	6.0	6.0	0.000	0.58	1.47	-1.01	1.40	-0.92	0.399	0.124	0.000	0.000	0.603	0.492	0.501	0.005
		Regular M1	0.14	6.0	6.0	6.0	0.000	0.58	0.99	-0.59	0.99	-0.59	0.399	0.124	0.866	0.221	0.627	0.492	0.500	0.000
		Regular M2	0.14	6.0	6.0	6.0	0.000	0.58	0.96	-0.64	0.96	-0.63	0.399	0.103	0.875	0.180	0.603	0.410	0.500	0.000
AUKE-PC (Deltares)		Irregular	0.14	6.7	6.1	5.2	0.000	0.55	2.73	-1.67	1.32	-0.84	0.304	0.114	0.000	0.000	0.610	0.680	0.406	0.036
		Regular M1	0.14	6.7	6.7	6.7	0.000	0.55	1.01	-0.52	1.01	-0.52	0.304	0.114	0.724	0.290	0.663	0.680	0.500	0.000
		Regular M2	0.14	6.7	6.7	6.7	0.000	0.55	0.93	-0.59	0.93	-0.59	0.304	0.073	0.762	0.168	0.610	0.436	0.500	0.000

Table 20: Overview of characteristics for AUKE-PC (Deltares, 2013) irregular wave and two representative regular waves, method one (M1) and three (M3). Oscillatory flow tunnel and flume simulations.

Condition	Run	Wave	Periodic characteristics				Velocity characteristics										Velocity skewness		Acceleration skewness	
			D_{50}	T_p	T_s	T_{mean}	U_0	u_{rms}	$u_{max, on, red}$	$u_{max, off, red}$	$u_{1/3, on, red}$	$u_{1/3, off, red}$	$<u^2_{red}>$	$<u^3_{red}>$	$\hat{u}_1$	$\hat{u}_2$	R	Sk_u	B	Sk_a
			[mm]	[s]	[s]	[s]	[m/s]	[m/s]	[m/s]	[m/s]	[m/s]	[m/s]	[m²/s²]	[m³/s³]	[m/s]	[m/s]	[-]	[-]	[-]	[-]
AUKE-PC (Deltares)		Irregular	0.14	6.7	6.1	5.2	0.000	0.55	2.73	-1.67	1.32	-0.84	0.304	0.114	0.000	0.000	0.610	0.680	0.406	0.036
		Regular M1	0.14	6.7	6.7	6.7	0.000	0.55	1.01	-0.52	1.01	-0.52	0.304	0.114	0.724	0.290	0.663	0.680	0.500	0.000
		Regular M3	0.14	6.7	6.7	6.7	0.000	0.55	1.32	-0.84	1.32	-0.84	0.304	0.073	1.082	0.239	0.610	0.436	0.500	0.000

Appendix VII: Equation derivatives

$u(t) = \hat{u}_1 \cos\left(\frac{2\pi}{T_1}t\right) + \hat{u}_2 \cos\left(\frac{2\pi}{T_2}t\right)\ with\ \frac{2\pi}{T} = w$

Part VII.A

For $\langle u^2(t)\rangle$:

$\langle u(t)^2\rangle = \hat{u}_1^2\cos^2(wt) + \hat{u}_2^2\cos^2(2wt) + 2(\hat{u}_1\hat{u}_2\cos(wt)\cos(2wt))$

$= \hat{u}_1^2\cos^2(wt) + \hat{u}_2^2\cos^2(2wt) + 2\hat{u}_1\hat{u}_2\cos(wt)\,[2\cos^2(wt) - 1]$

$= \hat{u}_1^2\cos^2(wt) + \hat{u}_2^2\cos^2(2wt) + \cancel{4\hat{u}_1\hat{u}_2\cos^3(wt)} - \cancel{2\hat{u}_1\hat{u}_2\cos(wt)}$

$= \hat{u}_1^2[1/2 + \cancel{1/2\cos(2wt)}] + \hat{u}_2^2[2\cos^2(wt) - 1]$

$= 1/2\,\hat{u}_1^2 + \hat{u}_2^2[4\cos^4(wt) - 4\cos^2(wt) + 1]$

$= 1/2\,\hat{u}_1^2 + \hat{u}_2^2[(1 + \cancel{2\cos(2wt)} + \cos^2(2wt)) - (2 + \cancel{2\cos(2wt)}) + 1]$

$= 1/2\,\hat{u}_1^2 + \hat{u}_2^2\,[1 + \cos^2(2wt) - 2 + 1]$

$= 1/2\,\hat{u}_1^2 + \hat{u}_2^2\cos^2(2wt)$

$= 1/2\,\hat{u}_1^2 + \hat{u}_2^2[4\sin^4(wt) - 2\sin^2(wt) - 2\sin^2(wt) + 1]$

$with\ ([\cos^2(2wt) = (1 - 2\sin^2(wt))^2])$

$= 1/2\,\hat{u}_1^2 + \hat{u}_2^2[4\sin^4(wt) - 4\sin^2(wt) + 1]$

$= 1/2\,\hat{u}_1^2 + \hat{u}_2^2\left[[3/8 - 4/8\cos(2wt) + 4/8\cos(4wt)\right] - [2 - 2\cos(2wt)] + 1\Big]$

$with\ \left(\left[\sin^4(wt) = \frac{3 - 4\cos(2wt) + \cos(4wt)}{8}\right]\right)$

$and\ \left(\left[\sin^2(wt) = 1/2 - 1/2\cos(wt)\right]\right)$

$= 1/2\,\hat{u}_1^2 + \hat{u}_2^2\left[12/8 - \cancel{16/8\cos(2wt)} + \cancel{16/8\cos(4wt)} - 2 + \cancel{2\cos(2wt)} + 1\right]$

$= 1/2\,\hat{u}_1^2 + \hat{u}_2^2[12/8 - 2 + 1]$

$\langle u(t)^2\rangle = 1/2\,\hat{u}_1^2 + 1/2\,\hat{u}_2^2$

Part VII.B

For $\langle u(t)^3\rangle$:

$\langle u(t)^3\rangle = \hat{u}_1^3\cos^3(wt) + \hat{u}_2^3\cos^3(wt) + 3(\hat{u}_1^2\,\hat{u}_2\cos^2(wt)\cos(2wt)) + 3(\hat{u}_2^2\,\hat{u}_1\cos^2(2wt)\cos(wt))$

Read as: $\langle u(t)^3\rangle = A + B + C + D$

With $\frac{1}{T}\int_0^T \cos^n(wt)dt = 0 \quad if\ n = 1, 3, 5, 7, etc.$, *it follows:*

A=0 (*n*=3) and B=0 (*n*=3)

For C:

$= 3(\hat{u}_1^2\,\hat{u}_2\cos^2(wt)\cos(2wt))$

$= 3\hat{u}_1^2\,\hat{u}_2\cos^2(wt)\,[2\cos^2(wt) - 1]$

$with\ ([\cos(2wt) = 2\cos^2(wt) - 1])$

$= 6\hat{u}_1^2\,\hat{u}_2\cos^4(wt) - 3\hat{u}_1^2\,\hat{u}_2\cos^2(wt)$

$= 6\hat{u}_1^2\hat{u}_2[{}^1/_4 + \cancel{{}^1/_2\cos(2wt)} + {}^1/_4\cos^2(2wt)] - 3\hat{u}_1^2\hat{u}_2[{}^1/_2 + \cancel{{}^1/_2\cos(2wt)}]$

$with\ ([\cos^2(wt) = {}^1/_2 + {}^1/_2\cos(2wt)])$
$and\ (\cos^4(wt) = {}^1/_4 + {}^1/_2\cos(2wt) + {}^1/_4\cos^2(2wt))$

$= 6\hat{u}_1^2\hat{u}_2[{}^1/_4 + {}^1/_4({}^1/_2 + \cancel{{}^1/_2\cos(2wt)})] - 3\hat{u}_1^2\hat{u}_2\,{}^1/_2$

$= {}^9/_4\,\hat{u}_1^2\hat{u}_2 - {}^3/_2\,\hat{u}_1^2\hat{u}_2$

$= {}^3/_4\,\hat{u}_1^2\hat{u}_2$

For D:

$= 3(\hat{u}_2^2\,\hat{u}_1\cos^2(2wt)\cos(wt))$

$= 3\hat{u}_2^2\,\hat{u}_1\cos(wt)\,[2\cos^2(wt) - 1]^2$

$= 3\hat{u}_2^2\,\hat{u}_1\cos(wt)\,[4\cos^4(wt) - 4\cos^2(wt) + 1]$

$= \cancel{12\hat{u}_2^2\,\hat{u}_1\cos^5(wt)} - \cancel{12\hat{u}_2^2\,\hat{u}_1\cos^3(wt)} + \cancel{3\hat{u}_2^2\,\hat{u}_1\cos(wt)}$

$= 0$

$\langle u(t)^3\rangle = A + B + C + D$

$\langle u(t)^3\rangle = 0 + 0 + {}^3/_4\,\hat{u}_1^2\hat{u}_2 + 0$

$\langle u(t)^3\rangle = {}^3/_4\,\hat{u}_1^2\hat{u}_2$

Part VII.C

Substitution of Eq. (41) and Eq. (42) to derive $\hat{u}_1$:

$\hat{u}_2 = \sqrt{2\langle u(t)^2\rangle - \hat{u}_1^2}$

$\hat{u}_2 = (2R - 1)\hat{u}_1$

$(2R - 1)\hat{u}_1 = \sqrt{2\langle u(t)^2\rangle - \hat{u}_1^2}$

$(2R - 1)^2\hat{u}_1^2 + \hat{u}_1^2 \ = 2\langle u(t)^2\rangle$

$((2R - 1)^2 + 1)\hat{u}_1^2 \ = 2\langle u(t)^2\rangle$

$with\ \langle u(t)^2\rangle = {u_{rms}}^2$

$$\hat{u}_1 = \sqrt{\frac{2{u_{rms}}^2}{(2R - 1)^2 + 1}}$$

Part VII.D

Substitution of Eq. (44) and (45) to derive $\hat{u}_1$ and $\hat{u}_2$:

$u_{1/3,on,red} = \hat{u}_1 + \hat{u}_2; \qquad \hat{u}_2 = u_{1/3,on,red} - \hat{u}_1$

$|u_{1/3,off,red}| = \hat{u}_1 + \hat{u}_2$

$|u_{1/3,off,red}| = \hat{u}_1 + (u_{1/3,on,red} - \hat{u}_1)$

$|u_{1/3,off,red}| = \hat{u}_1 + u_{1/3,on,red} + \hat{u}_1$

$2\hat{u}_1 = |u_{1/3,off,red}| + u_{1/3,on,red}$

$\hat{u}_1 = \frac{1}{2}|u_{1/3,off,red}| + \frac{1}{2}u_{1/3,on,red}$

$u_{1/3,on,red} = \frac{1}{2}|u_{1/3,off,red}| + \frac{1}{2}u_{1/3,on,red} + \hat{u}_2$

$\hat{u}_2 = u_{1/3,on,red} - \frac{1}{2}|u_{1/3,off,red}| - \frac{1}{2}u_{1/3,on,red}$

$\hat{u}_2 = \frac{1}{2}u_{1/3,on,red} - \frac{1}{2}|u_{1/3,off,red}|$

Appendix VIII: Wave group skewness with coarse sediment conditions

The SINBAD department in Aberdeen, Scotland asked to simulate the wave averaged horizontal velocity (U_0) for coarse sediment conditions for eight different wave group signals, including previous described wave conditions from section 7.1. Next to the three different skewed wave groups with single irregular velocity skewed waves and the regular single wave velocity skewed wave group, wave groups with irregular and regular sine oscillations and irregular and regular acceleration skewed oscillation where simulated with the oscillatory flow tunnel version of the boundary layer model (Table 21)

Table 21: Wave conditions and wave characteristics, SINBAD, Aberdeen.

Wave	Type/ method	u_{rms} [m/s]	T_p [s]	T_{gr} [s]	r	phi	M	N	R	Sk
Irregular Sine	**SINBAD/ Tunnel**	0.52	6	60	0	0	1.02	10		
Irregular Acc. SK	**SINBAD/ Tunnel**	0.525	6	60	0.28	0	1.02	10		
Irregular Vel. SK	**SINBAD/ Tunnel**	0.577	6	60	0.36	-1.57	1.55	10	0.6027	0.4922
Irregular Vel. SK WAXING	**SINBAD/ Tunnel**	0.632	6	60	0.374	-1.57	1.55	10	0.6027	0.4922
Irregular Vel. SK WANING	**SINBAD/ Tunnel**	0.632	6	60	0.355	-1.57	1.55	10	0.6028	0.4734
Regular Sine	**SINBAD/ Tunnel**	0.632	6	60	0	0				
Regular Acc. SK	**SINBAD/ Tunnel**	0.632	6	60	0.375	0				
Regular Vel. SK	**SINBAD/ Tunnel**	0.632	6	60	0.431	-1.57				

The input settings of the boundary layer model are shown in Table 22 and the model was set to not pick up sediment (no sediment flux). It will therefore not produce a net sediment transport result.

Table 22: Flow and bed characteristics, and boundary layer model input settings, SINBAD, Aberdeen.

Condition	Wave peak period T_p [s]	Grain size D_{50} [mm]	Roughness height k_s [m]	Max hor. velocity u_{max} [m/s]	Max. orbital excursion A [m]	Boundary layer thickness δs [m]	Roughness height z_o [m]	Domain [m]	Water-depth h [m]
Coarse	6	0.46	9.20E-04	1.54	1.61	0.04	3.07E-05	0.08	Tunnel-free

Wave averaged horizontal velocity U_0

The horizontal averaged velocity (U_0) profiles are the averages of the oscillating horizontal velocities of the implemented wave group signals; see Figure 40 and Figure 41.

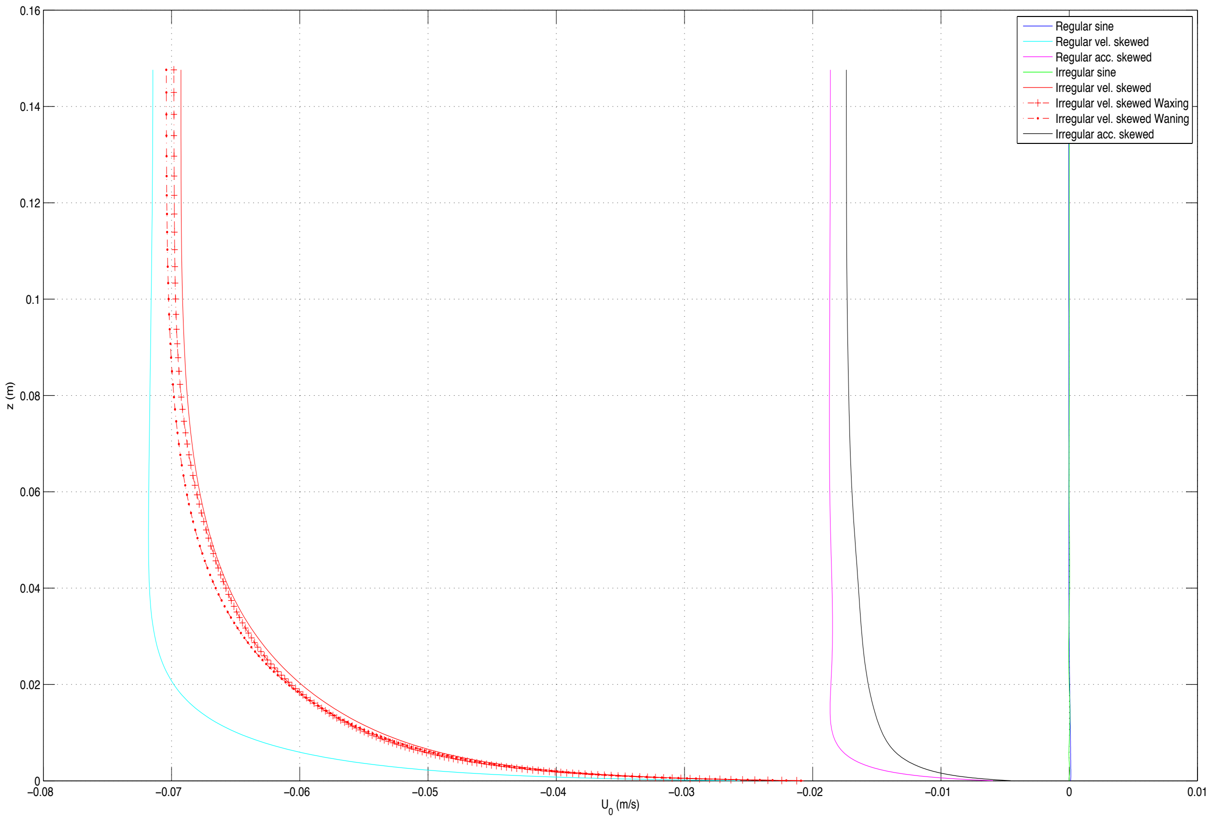

Figure 40: Wave averaged horizontal velocity profiles (U_0) for the eight wave group conditions, fixed bed, coarse sediment condition.

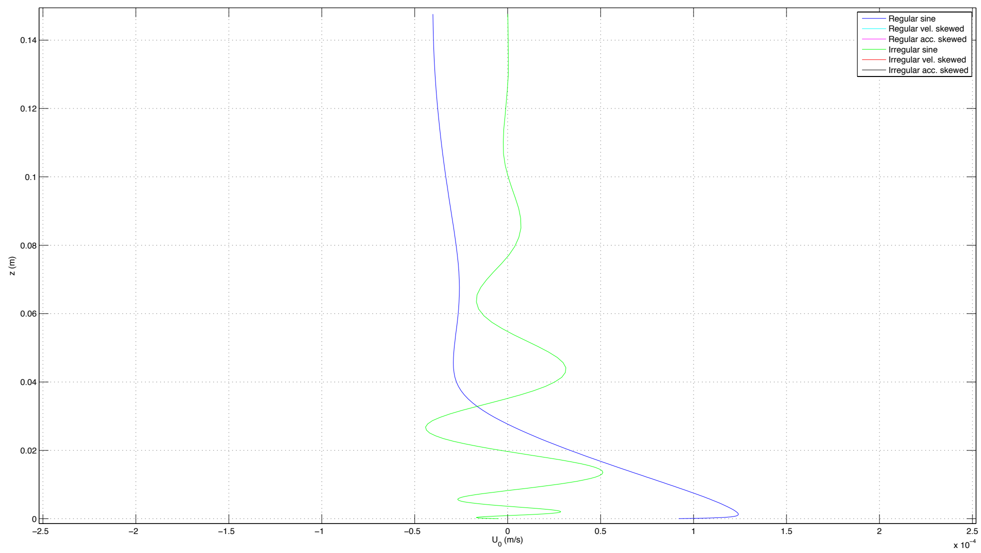

Figure 41: Zoom for the wave averaged horizontal velocities (U_0) of the regular and irregular sine conditions, fixed bed.

In Figure 40 *all* velocity- and acceleration skewed oscillations have a negative U_0, and the three velocity-skewed oscillations are even more negative than the acceleration skewed ones. These results are corresponding with test cases in earlier research of Kranenburg et al. (2013) (i.e. Campbell and Van der A) and in research of Van der A et al. (2011).

Figure 40 also shows the different boundary layer thicknesses. However, for both sine conditions these are also visible (Figure 41) but differ from the velocity- and acceleration skewed oscillations. The regular sine still has a "normal" (rapidly increasing) known (from

Kranenburg, 2013) horizontal wave averaged velocity shape in the lower part of the boundary layer, but the irregular sine already starts to act in a strange way from the top of the boundary layer. The averaged horizontal velocity is changing back and forth between negative and positive. This observation might be important since it differs from the results of regular wave oscillations and it might have effect on the sediment behavior within the entire boundary layer. The rapidly increasing and then decreasing of the maximum horizontal velocity of the wave group (see Figure 34) might cause the U_0 to act this way. However, both velocity- and acceleration skewed conditions do not show this behavior, which might be caused by the dominance of the wave shape streaming.

For the irregular velocity skewed, irregular velocity skewed waxing and irregular velocity skewed waning wave groups the difference between the averaged horizontal velocities is of no significance. Although the waning variant shows the most negative averaged horizontal velocity the height of the boundary layer thickness can be visually estimated at the same height as the normal and waxing irregular velocity skewed wave, approximately 0.1m above the bed. This however is almost twice the Sleath (1987) estimate of 0.04m for the coarse sediment condition, Appendix V.

For all simulations contour figures of the horizontal wave velocity above the bed have been produced as well, see Figure 42. In these figures the phase lead and overshoot (darker color/higher velocity within a vertical color strip) characteristic of oscillatory boundary flow are apparent.

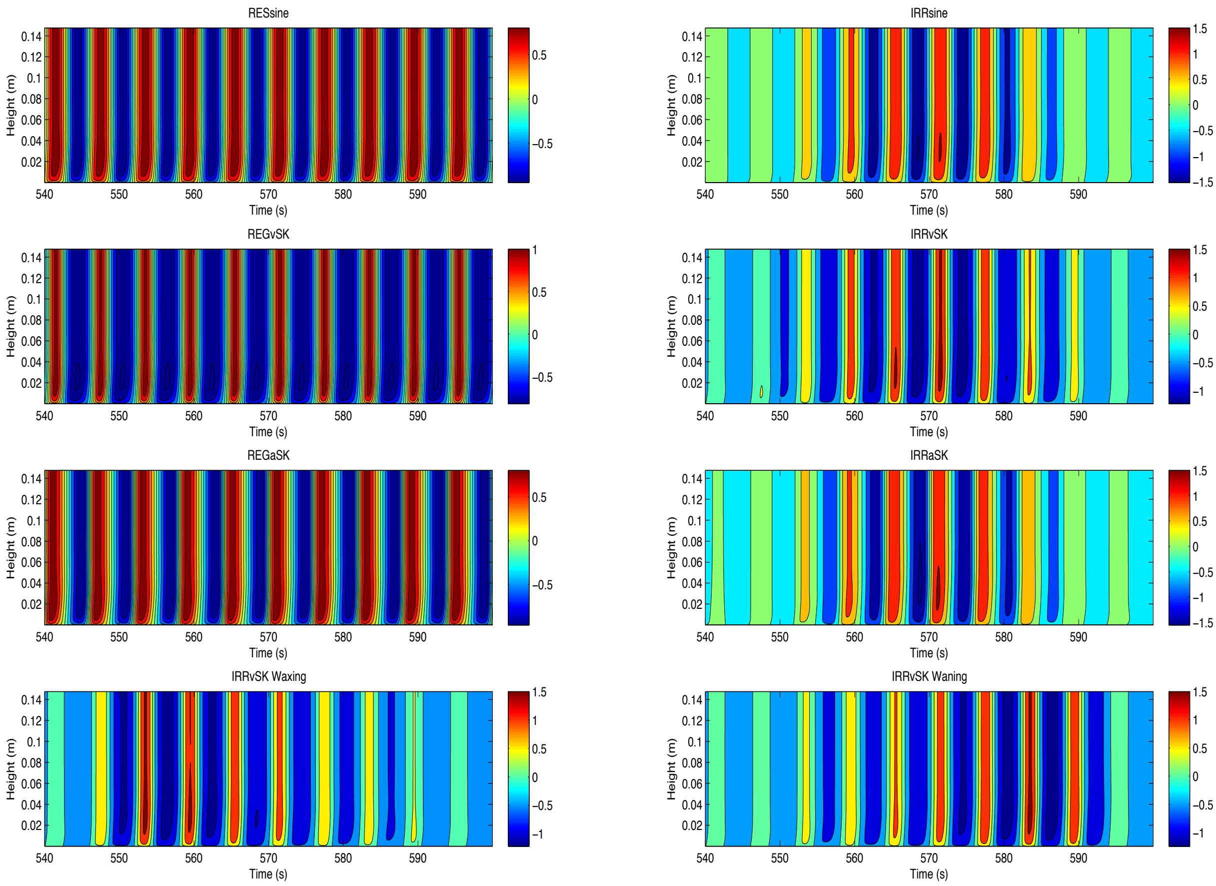

Figure 42: Contour figure of all wave group conditions, fixed bed.

Appendix IX: Flume simulations SINBAD, Aberdeen, Scotland

On request of the Aberdeen department of the SINBAD project, for several flume wave conditions the net sediment transport rates are produced with the help of Kranenburg (2013) boundary layer model, flume version.

Boundary layer model input conditions

With a provided Matlab script, which includes Malarkey & Davies (2012) GSAW, saw tooth function, to produce water level elevations, and wave conditions (see Table 23) four (IG3, 4, 5, 6) water level *elevation* timeseries were produced.

Table 23: SINBAD flume simulations wave characteristics (IG3, 4, 5, 6).

	type	$T_{(p)}$	H_m	H_{rms}	H_s	$H_{1/10}$	H_{max}	$U_{max1/10}$	δ_s	δ	T_g	M	β	n
ID		(s)	(m)	(m)	(m)	(m)	(m)	(m/s)	(mm)	(mm)	(s)			
IM1	mono	4.40			0.91			1.20	6.3	32				
IM2	mono	4.40			1.00			1.30	8.8	39				
IG3	group	4.40	0.53	0.62	0.90	1.00	1.00	1.30	8.8	39	44	0.90	0.25	10
IG4	group	4.40	0.53	0.63	0.91	1.00	1.00	1.30	8.8	39	44	0.90	0.50	10
IG5	group	4.40	0.53	0.62	0.90	1.00	1.00	1.30	8.8	39	44	0.90	0.75	10
IG6	group	4.40	0.53	0.63	0.92	1.00	1.00	1.30	8.8	39	88	0.90	0.50	20
IR7	random	4.40	0.53	0.63	0.92	1.00	1.00	1.30	8.8	39	based on IG condition			
IR8	random	4.40			0.63	0.77		1.00	2.5	14	JONSWAP			

Within the table for the IG tests it is listed that the time series consist of a group wave. Within this group of irregular waves the peak period (T_p), the wave height characteristics, the U_{max} (based on the average of the highest one tenth wave velocities), boundary layer thickness and Malarkey & Davies (2012) amplitude parameter of the modeling signal (M) are kept constant. The group wave period of the IG6 test differs from the other (IG) test since the amount of waves (n) within the group is larger. The skewness of the envelope is indicated with the β and differs for each test.

The originally produced time series consisted of three irregular wave groups (Figure 43). To be able to run the boundary layer model to run properly the three wave groups were repeated ten times for conditions IG3, 4 and 5, which makes a time series of 1320s instead of 132s (3x T_{gr}= 3x 44s). For condition IG6 a repetition of five is maintained, which also creates a timeserie of 1320s.

However, Kranenburg (2013) boundary layer model needs a horizontal *velocity* timeseries within or near the boundary layer as an input. To transform a "spacing" timeseries to a "velocity" timeseries, one can take the derivative, which was done as a method A, however this will not become a *horizontal* velocity. Another method, method B, is to include more complicated theories such as the linear wave theory or the use of Abreu et al. (2010) (horizontal velocity). The latter is used, since it is also included in the provided script.

Figure 43 shows the water level velocity profile of method A and its associated water level elevations, and the horizontal velocity computed with method B for one of the four wave conditions (IG3).

Note that for method B only one horizontal velocity was produced. Which is caused by the fact that within Abreu et al. (2010) equation the Bèta, which is used in the original provided script to make multiple irregular wave tests (IG), is not included. The used U_{rms} for the Abreu equation is 1m/s.

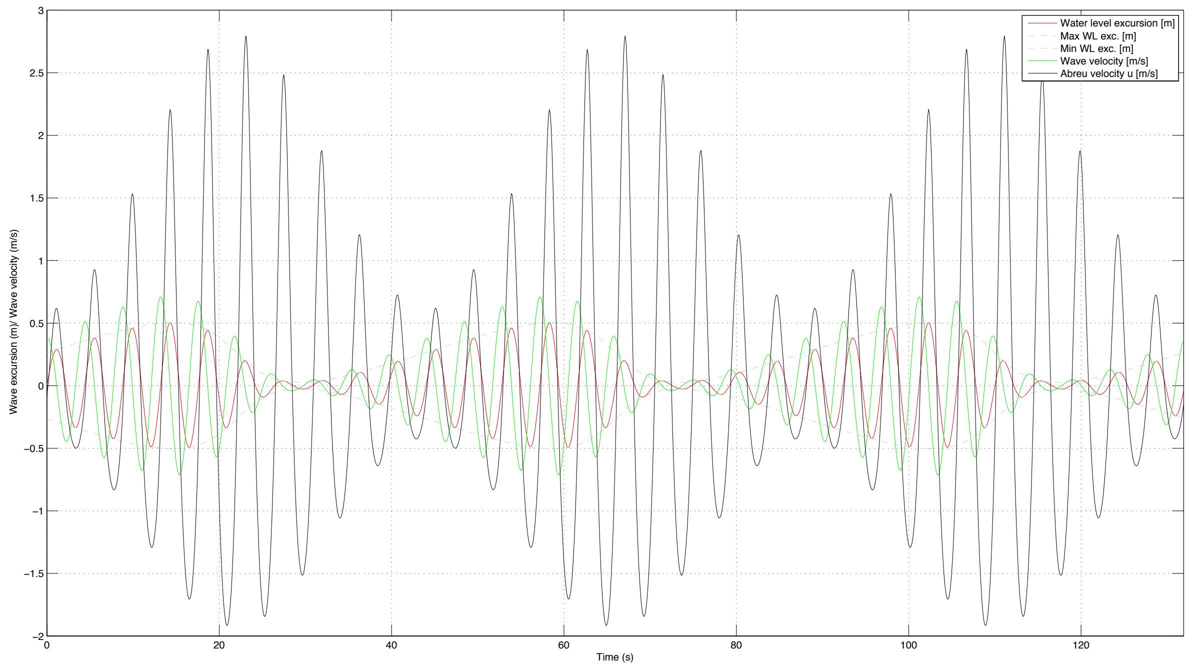

Figure 43: Water level elevation and water level wave velocity for condition IG3, method A. And Tiago's horizontal velocity, by method B.

The net sediment transport runs were done for fine sediment (D_{50}=0.15mm) and medium sediment (D_{50}=0.25mm) conditions. The flow and bed characteristics and the boundary layer model input settings are listed in Table 24. The used forcing method of the model is "free".

Table 24: Flow and bed characteristics and boundary layer model settings.

Condition	Wave peak period T_p [s]	Grain size D_{50} [mm]	Roughness height k_s [m]	Max hor. velocity u_{max} [m/s]	Max. orbital excursion A [m]	Boundary layer thickness δs [m]	Roughness height z_o [m]	Domain [m]	Water-depth h [m]
Fine	4.4	0.15	3.00E-04	0.72	0.50	0.01	1.00E-05	0.03	Flume-free
Medium	4.4	0.25	5.00E-04	0.72	0.50	0.01	1.67E-05	0.03	Flume-free

Net sediment transport

The net sediment transport results of the four test conditions for the two different grain sizes are listed in Table 25.

Table 25: Net sediment transport rates, flume simulations.

Flume: $<q_s>$ is in $10^{-6}\ m^2/s$				
	Method A		**Method B**	
D50	0.15mm	0.25mm	0.15mm	0.25mm
Bed	Mobile	Mobile	Mobile	Mobile
IG3	1.457	0.563	305.134	147.057
IG4	1.493	0.577		
IG5	1.452	0.559		
IG6	1.581	0.613		

For both sediment conditions of method A the results of all wave conditions tests do not have a significant difference. When comparing method A and B with each other it can be seen that method B gives results that are much higher. Which is caused by the velocity differences between the two methods, as can be seen in Figure 43.

For both methods the model does compute differences for fine or medium sediment conditions. The lower net sediment transport results for medium sediment conditions indicate that less sediment is set into motion (Shields parameter).

Discussion

Since for method A the used velocity profiles are computed of the water level elevations by taking the derivative it suggests that the resulting velocity profile is the vertical velocity (since elevation is going up en down). When a theory as used in method B is applied and matched to a height of 30mm above the bed the net sediment transport results turn out to be really high and doubtful. The reason for this might be the large U_{rms} input and the large horizontal velocities as can be seen in Figure 43, caused by the fact that the horizontal velocity of the waves at the surface is used as input for waves near the seabed. In section 2 it was shown that with the orbital motions, the horizontal directed velocity near the seabed is (very) low compared to the surface.

To be able to get a more realistic net sediment transport a more complex theory might have to be applied to convert the water level elevation for the first method (which include the different Beta's) to horizontal velocities near or within the boundary layer. Than there will be a more realistic horizontal velocity for the free stream velocity, which can be used in the boundary layer model to compute a more reliable net sediment transport.